Markus Eder, B.Sc.

“Origin of arsenic concentration in spring waters of relict rock glacier springs in alpine headwaters of the Seckauer Tauern Range (Austria)”

Master’s Thesis

to achieve the university degree of

Master of Sience

Master’s degree programme: Earth Siences

Submitted to

Graz University of Technology

Supervisor

Assoz.-Prof. Mag. Dr.rer.nat. Gerfried Winkler

Institute of Earth Sciences, Karl Franzens University

Ao.Univ.-Prof. Dr.rer.nat. Christoph Hauzenberger

Institute of Earth Sciences, Karl Franzens University

Graz, March 2019

AFFIDAVIT

I declare that I have authored this thesis independently, that I have not used other than the declared sources/resources, and that I have explicitly indicated all material which has been quoted either literally or by content from the sources used. The text document uploaded to TUGRAZonline is identical to the present master‘s thesis dissertation.

Danksagung

Ich möchte mich bei allen bedanken, die mir dieses Studium ermöglicht haben und mich in all den Jahren sowie auch bei dieser Masterarbeit unterstützt haben.

Zuerst möchte meinem Betreuer dieser Masterarbeit Prof. Gerfried Winkler danken, für die Möglichkeit diese Arbeit zu verfassen, für die zahlreichen Erlebnisse im Gelände und die unkomplizierte Hilfe, wenn ich Sie nötig hatte. Sowie für Motivation und Unterstützung ohne die, diese Arbeit nicht so zustande gekommen wäre.

Danke möchte ich auch zu meinen Eltern sagen, die mich immer unterstützt haben auf meinem Weg und mir dieses Studium überhaupt erst ermöglicht haben.

Vielen Dank an meinen Zweitbetreuer Prof. Hauzenberger der sich für meine Anliegen immer Zeit genommen hat und mir einen tieferen Einblick in die Geochemie ermöglicht hat.

Dankeschön möchte ich auch sagen zu Prof. Goessler für all die durchgeführten Messungen und seine Hilfe. Ebenfalls danken möchte ich Prof. Martin Dietzel für die Benutzung des Hydrochemielabors und die zahlreichen Tipps für diese Arbeit. Einen großen Dank auch an Albrecht Leis für seine Unterstützung mit PhreeqC, die mir sehr geholfen haben. Mein Dank gilt auch noch Prof. Böttcher für die unkomplizierte Messung meiner Sulfatprobe. Bei vielen kleinen und großen Fragen war mir Thomas Wagner eine große Hilfe danke dafür.

Zu guter Letzt möchte ich noch allen meinen Helfern im Gelände und auf der Universität Danken, Maria Schweighart, Thomas Knoll, Veronika Ehrenhauser, Mathias Stabler, Rita Pleschberger, Lisa Brückner, Kajetan Heigert, Simon Kainz, und Wedenig Michael. Ohne euch wäre diese Arbeit nicht möglich gewesen.

Abbrevations

Ab	Albite
As	Arsenic
As(III)	Arsenite
As(V)	Arsenate
BGBI	Bundesgesetzblatt
BSE	Back scatter electrons
BSQ1	Brandstätterkar Quelle (spring)
BSTQ1	Brandstätterthörl Quelle (spring)
BTQ1	Bärental Ost Quelle (spring)
BTQ2	Bärental West Quelle (spring)
Compo	Composite
dis	dissolute
DOQ1	Donnerofen Quelle (spring)
DTQ1	Dürrtal Quelle (spring)
EC	Electrical Conductivity
EDX	Energy dispersive x-ray spectroscopy
FLQ1	Finsterliesingtal Quelle (spring)
fm	Formation
GLQ1	Goldlacke Quelle (spring)
GMS	Glaneck Metamorphic suite
GMWL	Global Meteoric Water Line
GP	Griesstein Pluton
Grt	Granate
HFO	Iron Hydroxides
HKAQ1	Hühnerkaralm Quelle (spring)
HKQ1	Hirschkarl spring
HPS	Hochreichhart Plutonic Suite
HRQ1	Hochreichhartschutzhaus Quelle 1 (spring)
HTQ1	Hölltal Quelle (spring)
i.d.g.F	in der geltenden Fassung
ICP MS	Inductive Coupled Plasma Mass Spectrometry
ICP OES	Inductive Coupled Plasma Optical Emission Spectrometry
Ilm	Ilmenite
Kfs	Kali-Feldspar
KTQ1	Kettentörl Quelle (spring)
LA-MC-ICP MS	Laser Ablation Multi Collector
LMWL	Local Meteoric Water Line
LOI	Loss on Ignition
m.a.s.l.	meter above sea level
Mag	Magnetite
Ms	Muscovite
N1	Weigth of annealed empty ceramic pod
N2	Weigth of ceramic pod with ca. 1g sample
N3	Weight of ceramic pod and sample after burning
NW	North-West
PP	Pletzen Pluton
prec	precipitate
Qtz	Quartz
RG	Rock Glacier
Rt	Rutile
SBQ1	Siebenbründl
SE	Secondary electrons
SEQ	Schöneben Quelle (spring)
SRG	Schöneben Rock Glacier
TAS	Total Alkalis vs Silika
TDS	Total dissolved Solids
temp	Temperature
Ti-Mag	Titano-magnetite
UTM	Universal Transversal Mercator
VCDT	Vienna Canon Diablo Troilite
VSMOW	Vienna standard mean ocean water
VSMOW	Vienna standard mean ocean water
VSQ1	Vorwitzsattel
XRF	X-Ray Fluorescence
Zrn	Zircony

Abstract

Arsenic mobilization in groundwater is a worldwide problem. The influencing factors for a contamination of water are widespread and for most locations individual. Four dominant mechanisms are known, two are associated with adsorption processes on metal oxides or clay under an alkaline environment or a reductive environment. The others are sulphide oxidation and evaporation of geothermal waters. Sediment basins and geothermal springs were of special interest in recent years due to high arsenic contamination and thus related serious health problems in these areas. However, low contaminated areas are more widespread and are less investigated. This work aims to understand the processes of arsenic mobilization in such low contaminated settings bound to periglacial landforms such as rock glaciers in alpine regions. Recent research in the Seckauer Tauern Range led to new questions related to arsenic contamination of spring water bound to these landforms. What is the arsenic source, how the geographical distribution is and which dissolution/retention processes are active. Water temperatures between 2-4°C, relatively short retention times (hours – several months) and neutral pH values are in general not very favourable conditions for dissolution and mobilization of arsenic. Furthermore, the overall total cation concentration of these spring waters is less than 13,8 mg/l, where Ca^{+2}, Si^{4+}, Mg^{2+}, Na^{+1} and K^{+1} dominates. Anions such as SO_4^{-2}, NO_3^-, NO_2^-, Cl^- and PO_4^{3-} are also extremely low concentrated ($\sum$< 7,2 mg/l). Nevertheless, the arsenic concentration in some spring waters exceeds 10 µg/l, which is the recommended threshold (parameter value) for drinking water according to the WHO. Therefore, seasonal water sampling for isotopic and hydrogeochemical analysis as well as rock sampling for geochemistry was applied. These investigations revealed no distinct spatial distribution of higher As concentrations in the Seckauer Tauern Range and no significant correlation with other elements which reveal a common source. However, petrographic analysis of samples within the Schöneben spring catchment showed locally occurring ore rich carbonates bound to quartz dikes, which are rich in As. This leads to the assumption that the As occurrence is bound to locally occurring As deposits (e.g. As bearing ores) within different lithologies of the catchment areas. Most probably the important water rock interactions take place in an oxidizing environment in the fine grained base layer of the Schöneben rock glacier. Within the Schöneben spring catchment the occurrence of As bearing sulphide minerals is confirmed by the detection of arsenical tetrahedrite. In addition, near neutral sulphur isotopic values in the dissolved SO_4 support the theory of dissolved sulphides. Accompanied with this dissolution, Fe got mobilized, but precipitated very fast as iron hydroxides, which is able to adsorb significant amounts of As. Adsorption processes can be inhibited to a certain extent by alkali desorption, which is possible in the carbonate dissolution areas. Therefore, the predominant dissolution processes were identified as sulphide dissolution and in addition, but of less importance, alkali desorption. Finally, this work contributes to a better understanding of the origin and fundamental process of low concentration arsenic mobilisation in crystalline basement areas.

Table of content

Research Question and Objective

Previous hydro(geo)chemical investigations within the project "Wasserwirtschaftliche Aspekte von Blockgletschern in Kristallingebieten der Ostalpen - Speicherverhalten, Abflussdynamik und Hydrochemie mit Schwerpunkt Schwermetallbelastungen (RGHeavyMetal)" revealed unexpected arsenic (As) concentrations in several relict rock glacier spring waters in the Seckauer Tauern Range. The unfavorable environmental conditions for dissolution of minerals like nearly neutral pH value, weathering resistant rock, low water temperatures and an oxidizing environment in this area, led to the question of the source and mechanism of As mobilization. Related to this general question, the distribution of the As occurrence in the studied area is of interest, as well as possible transport mechanism within such aquifers.

To answer the questions this work is separated into several parts.

- The theoretical part contains the literature research regarding As behaviour in aquatic systems and all applied methods.

- The first practical part includes localization and sampling of springs in the investigation area, between Hammerkogel and Goldkogel, with the aim to detect the occurrence and distribution of As concentrations. The samples were analysed for anion and cation content, in addition isotopic samples were taken.

- In the second step a detailed investigation of one spring with the highest As concentration was accomplished, including rock sampling from nearby lithological formations in the catchment and river sediments. These samples were investigated by applying geochemical and mineralogical methods to determine the general elemental composition and mineral phases, with special respect to As.

- The collected data was finally used to build up a conceptual model of the internal water rock interaction processes by using PHREEQC and the literature. Finally, this conceptual model should be able to describe the dissolution and transport mechanism of the high As concentration in the spring water.

1. Introduction

Arsenic (As) is one of the most widespread elements in the earth´s crust, in fact it counts to the 20th most abundant elements worldwide (Herath et al. 2016). It indicates a ubiquitous distribution of small concentration, however can be classified as rare earth element. In elemental form it exists in three different modifications: most important as grey As, which is a durable, semimetal of shining steel grey colour, or as yellow As which is not durable and non-metallic or as black As which is amorphous and nonmetallic (Wemhöner et al. 2012). In most cases As occurs naturally, as major constituent in more than 200 different minerals, which are mainly sulphide or oxide ores (Mandal 2002). Erosion and alteration processes lead to mobilization, mostly bound to natural groundwater, but also the transport by wind through As enriched dust is possible. The main natural processes for a mobilization in groundwater are typically water rock/soil interactions. The toxicity of As for the human health is a wide discussed topic since the last decades. Even the consumption of low concentrations from tens of microgram to milligrams of inorganic As in drinking water can lead to arsenicosis, which is associated with skin cancer, mutations and deformities (Zhang et al. 2017; Chakraborti et al. 2017). Due to its distribution it has a serious effect on the health of millions of people around the world. Regarding to this the WHO lowered 1993 the parameter value of As in drinking water provisionally from 50 to 10 µg/l (World Health Organization 2011). Austria has according to the "Qualitätszielverordnung Chemie Grundwasser" ("BGBl. II Nr. 98/2010 i.d.g.F.") an even lower threshold value for drinking water of 9 µg/l (Wemhöner et al. 2012). In fact it is listed as one of the most serious inorganic contaminants for drinking water worldwide (Smedley and Kinniburgh 2002).

Even if anthropogenic induced contamination of As (e.g. mining and industrial activities) is a serious problem, the main contamination is bound to geogenic sources. Concentrated in minerals, As occur in sulphides, oxides, arsenates, arsenites and as elemental As. The highest contaminations are in most cases associated with ore minerals or alteration products and as an accompanying element of heavy metal elements. In general, arsenic sulphides like arsenopyrite, realgar and orpiment are the most widespread arsenic minerals. The major As minerals are listed in Table 1.

In addition to typical As minerals sources, also common rock forming minerals like pyrite are of importance (Table 2). This is caused in chemical similarities of sulphur and As, due to that many sulphide minerals contain As as an substitute for sulphur. Because pyrite precipitates in a very common reducing, low temperature environment, it is part of a great variety of ores and sediments. In fact, it is the most common As bearing mineral which indicate this process. Additionally adsorption processes can cause also higher As concentrations, regarding to that also oxides, silicates, carbonates, sulphides and other minerals are able to contain As (Smedley and Kinniburgh 2002) (Table 2). According to Ure and Berrow 1982 the general concentration in As of igneous rocks is about 1.5 mg/kg. Metamorphic rocks indicate a slightly higher concentration of < 5 mg/kg and sedimentary rocks 5 – 10 mg/kg (Webster 1999).

1.1 Natural occurrence of As

As mentioned above As occurs worldwide on every continent, in the atmosphere, water and in soils or rocks. Within rocks it is widely distributed in all rock types, typically highest in sediments followed by igneous-, and metamorphic rocks.

In Asia the Bengal basin and several places in China are hotspots of As contaminated areas, as well as the southwest part of the United States in North America. In Mexico, Argentina and Chile high As concentrations are also found. Africa shows serious contaminations in the west, east and south of the continent. In Australia and Oceania areas with a smaller As contamination are located (Ravenscroft et al. 2009; Smedley and Kinniburgh 2002; Amini et al. 2008). In some of these places As contaminations have serious effects on the health of the people. Bangladesh is the most famous negative example for such high level contaminated spots.

The most affected area in Europe is the Pannonia basin located in the countries Hungaria, Romania, Slovakia and Croatia. To summarize more than 0.5 million people are living in areas with a serious influence of As on their health. But, most countries in Europe indicate arsenic contaminations of lower risk. Compared to the rest of Europe, Austria has only few As contaminated areas (Ravenscroft et al. 2009), but low level As concentrations are frequent, especially in the alp region.

Typically, in Austria As occurs in volcano-sedimentary sulphide deposits or within hydrothermal ore mineralization. The associated elements indicate a wide elemental range from Au, Cu, Ni, U, Co, Mo, Sn, Hg up to Sb (Thalmann 1989). In general, most areas of Austria indicate As values in ground or river waters below 10 µg/l. High contaminations are very localized and bound to specific ore veins or sedimentary deposits. This is also shown in the Austro-Alpine (Eastern Alps) ore province where As is a characteristic element (Thalmann 1989; Wemhöner et al. 2012). Arsenic anomalies (> 50 µg/l) of river sediments were investigated and indicate that the main hotspots are distributed within the central zone of the Alps (Figure 1). Smaller areas with cumulated As anomalies are in Tyrol at “Matrei am Brenner”, Schwaz, Kitzbühel and the Dientener mountains.

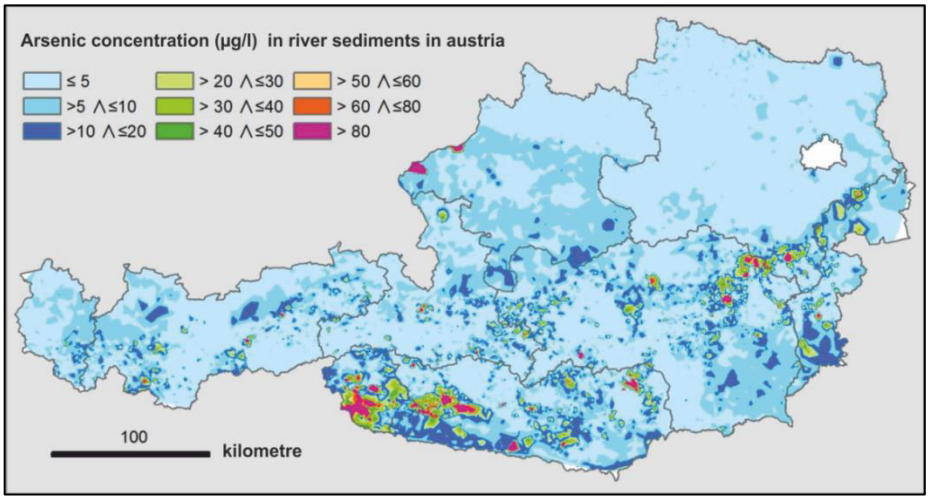

Figure 1: Map of arsenic concentrations in river sediments in Austria (Wemhöner et al. 2012).

The areas from Kapfenberg to Neunkirchen and around the Saualpe show an increased number of anomalies. The highest amount of concentrated As waters are found in the south of Austria, within the Defregger Alps and the Kreuzeckgruppe (Figure 1) (Wemhöner et al. 2012). According to the "Grundwasserkörper Stammdatenblatt" (GK 100116) the general As concentration in the Seckauer Tauern range is about 4 µg/l (GBA 2015). Localized ore bearing areas show a As concentration of > 10 µg/l. In general, the As hotspots in waters indicate a good correlation with locations of ore mineralization and mineral finds. In the case of the nearby situated Schladminger Tauern the As contamination is bound to Cu-Ag- and Ni-Co-ore mineralization (Thalmann 1989). Close to the investigation area at the Ingering valley, As bearing minerals were already found in 1860 (Alker A. 1972). According to the GIS Steiermark service "Digitaler Atlas", a copper-pyrite-deposit also exists within the investigation area.

1.2 Theoretical basics

The main occurrence of As in groundwater is in inorganic form, where different oxidation states (-3, 0, +5 and +5) are known (Ma et al. 2014). Different species exist and depend mostly on the redox potential and pH value of the surrounding water. In groundwater As occurs as oxyanion/oxyacid and the most common species are As(III) (arsenite), which exists mainly in reducing conditions in the form of H_3AsO_3, and the As(V) (arsenate) under oxidizing conditions in the form of $H_2AsO_4^-$ and $HAsO_4^{2-}$, normally both exist simultaneously (Sharma and Sohn 2009; Yan et al. 2000).These species show a high variety of ratios, due to redox active solids, the activity of microorganisms, convection and diffusion of O_2 from the atmosphere. As(III) indicates the highest toxicity followed by As(V) and organic species (Cullen and Reimer 1989).

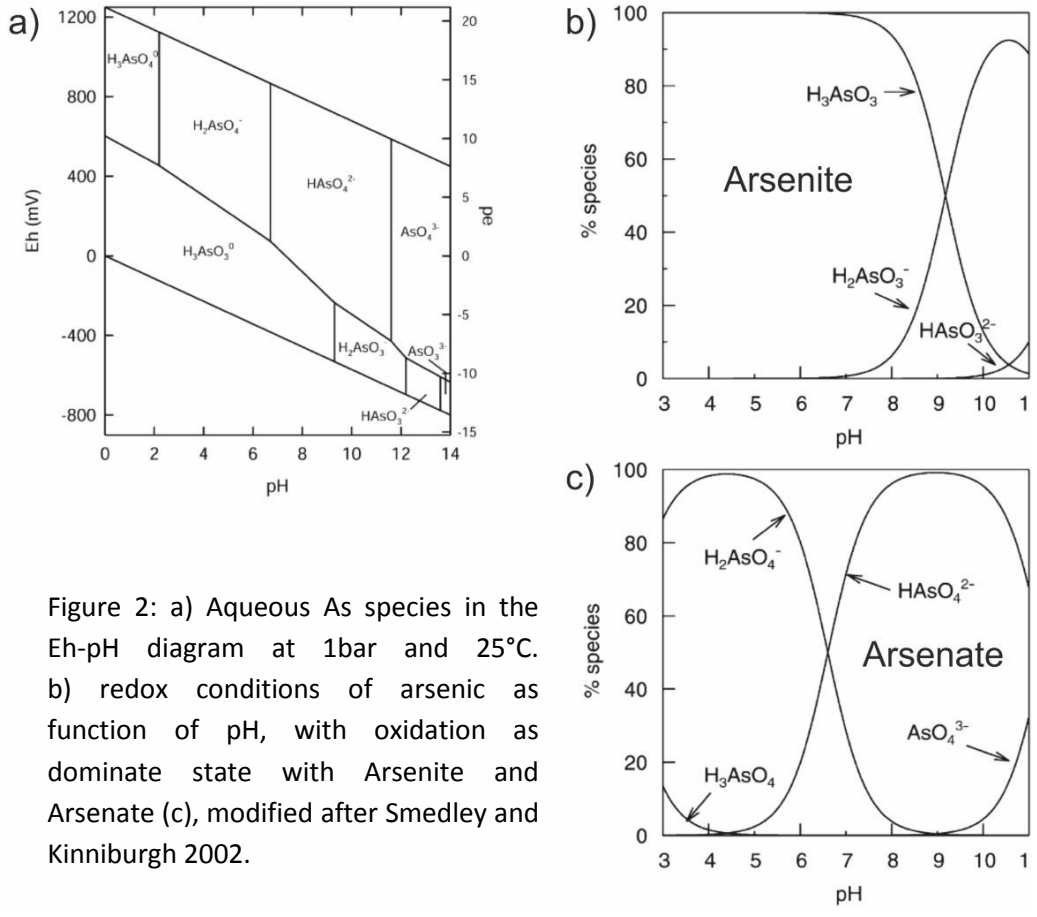

Figure 2: a) Aqueous As species in the Eh-pH diagram at 1bar and 25°C. b) redox conditions of arsenic as function of pH, with oxidation as dominate state with Arsenite and Arsenate (c), modified after Smedley and Kinniburgh 2002.

The geogen sources could be minerals which contain As within their mineral structure or minerals with a high specific surface which adsorb As on their surface. Important As bearing minerals for this thesis are Arsenopyrite, Orpiment, Realgar and As bearing Tetrahedrite. Further As minerals are listed in Table 1 and rock forming minerals with As content are in Table 2.

- **Arsenopyrite**
  The reaction of arsenopyrite with an alkaline solution results in the precipitation of Fe^{3+} hydroxide surface layers and an oxidation of As(III) to As(V). In addition, sulphur oxidizes to sulphate and gets transported with the solution. In acidic solutions no sulphate but elemental sulphur or iron sulphur covers the surface. Typically, arsenopyrite can be found in hydrothermal mineral deposits, like high temperature gold-quartz or also tin veins. Less important are low temperature hydrothermal veins. Generally associated minerals are pyrite, pyrrhotite, chalcopyrite, galena, gold, scheelite, and cassiterite (Lengke et al. 2009).

- **Orpiment and Realgar**
  These yellow and red minerals commonly occur within low-temperature-hydrothermal veins which are associated with As-Sb minerals, carbonates and barite or gypsum (Lengke et al. 2009). Dissolution rates depend on the dissolved oxygen content in the solution, more oxygen leads to a higher dissolution rate (Walker et al. 2006).

- **Tetrahedrite**
  Studies of dissolution reactions at oxidizing conditions with potassium hydroxide indicate the development of various reaction layers. These layers can contain metal oxide/hydroxide species from copper, antimony, arsenic, zinc and silver (Mielczarski et al. 1996), partially also iron can occur (Andreasen et al. 2008). During this oxidation As is enriched in the oxidation layers either as phase or as adsorbent, again the remobilization of As at high bicarbonate concentrations is possible.

Mineral	Composition	Occurrence
Orpiment	As_2S_3	veins, hot springs, volcanic sublimation products
Cobaltite	CoAsS	High-temperature deposits, metamorphic rocks
Arsenopyrite	FeAsS	The most abundant As mineral, dominantly in mineral veins
Tennantite	$(Cu,Fe)_{12}As4S_{13}$	Hydrothermal veins
Enargite	Cu_3AsS4	Hydrothermal veins
Arsenolite	As_2O_3	Secondary mineral formed by oxidation of arsenopyrite, native arsenic and other As minerals
Claudetite	As_2O_3	Secondary mineral formed by oxidation of realgar, arsenopyrite and other As minerals
Scorodite	$FeAsO_4.2H_2O$	Secondary mineral
Annabergite	$(Ni,Co)_3(AsO_4)_2.8H_2O$	Secondary mineral
Hoernesite	$Mg_3(AsO_4)_2.8H_2O$	Secondary mineral; smelter wastes
Haematolite	$(Mn,Mg)_4Al(AsO_4)(OH)_8$	

Table 1: Major As minerals occurring in nature modified after Smedley and Kinniburgh 2002; Mandal 2002.

Important minerals with high adsorbent capacities for As are Fe-, Mn- and Al-oxides, further carbonates, silicates and other minerals like apatite or clay minerals show this effect (Smedley and Kinniburgh 2002). Detailed information about these minerals and their As content are shown in Table 2.

Mineral	As concentration range (mg kg^{-1})	References
Sulphide minerals		
Pyrite	100–77,000	Baur and Onishi (1969); Arehart et al. (1993); Fleet and Mumin (1997)
Pyrrhotite	5–100	Boyle and Jonasson (1973);
Marcasite	20–126,000	Dudas (1984); Fleet and Mumin (1997)
Galena	5–10,000	Baur and Onishi (1969)
Sphalerite	5–17,000	Baur and Onishi (1969)
Chalcopyrite	10–5000	Baur and Onishi (1969)
Oxide minerals		
Haematite	up to 160	Baur and Onishi (1969)
Fe oxide (undifferentiated)	up to 2000	Boyle and Jonasson (1973)
Fe(III) oxyhydroxide	up to 76,000	Pichler et al. (1999)
Magnetite	2.7–41	Baur and Onishi(1969)
Silicate minerals		
Quartz	0.4–1.3	Baur and Onishi (1969)
Feldspar	<0.1–2.1	Baur and Onishi (1969)
Biotite	1.4	Baur and Onishi (1969)
Amphibole	1.1–2.3	Baur and Onishi (1969)
Olivine	0.08–0.17	Baur and Onishi (1969)
Pyroxene	0.05–0.8	Baur and Onishi (1969)
Carbonate minerals		
Jarosite	34–1000	Boyle and Jonasson (1973)
Other minerals		
Apatite	<1–1000	Baur and Onishi (1969), Boyle and Jonasson (1973)

Table 2: Major rock forming minerals with As content, the oxide, silicate, carbonate and other minerals mainly contain As in adsorbed form, modified after Smedley and Kinniburgh 2002.

1.3 Environmental conditions for occurrence of As

Depending on the As source and the environmental conditions, different dissolution mechanisms are possible. The main environmental factors are the pH value, the oxygen content (redox potential) and associated dissolved minerals. Redox reactions are the most important water-rock interaction processes for As release (Gulens et al. 1979). The four most common environmental conditions for As release are:

- **At near neutral pH values and strongly reducing conditions:**
  This water is enriched in bicarbonate, iron and manganese. However, it contains just very small amounts of oxidised species. The dominant process is **reductive dissolution**, which releases mainly As(III) from iron/manganese hydroxides (Ravenscroft et al. 2009).

- **At higher pH values ≥ 8 and oxidizing conditions:**
  Water types with these conditions contain dissolved oxygen, sulphates and nitrates. Constituents like Fe and Mn which oxidise in contact with dissolved oxygen are mainly removed from the solution. These so called Alkali-Oxic waters contain mainly As(V), the associated mechanism is **alkali desorption** (Ravenscroft et al. 2009).

- **At lower pH values of <1 – 6 and oxidizing conditions:**
  Dissolution of sulphides leads to low pH values, due to the release of SO_4. In most cases high concentrations of iron occur, additionally different heavy metals can be dissolved. The dominant mechanism is **sulphide oxidation**, with As(V) as major species (Ravenscroft et al. 2009).

- **High temperature conditions:**
  Geothermal influenced springs can indicate extreme high As concentrations (up to 27 mg). A relation between As and salinity seems to be probable (Smedley and Kinniburgh 2002; Ravenscroft et al. 2009).

- **Influence of Bacteria and organic matter**
  Bacteria are able to increase the mobility of most toxic As species (As(III)) by the reduction of metals and As itself (Islam et al. 2004; Zobrist et al. 2000). Above all this mechanism is important in areas around the Bengal delta basin. Dissolved organic matter in Pleistocene and Holocene aquifers is also able to accelerate the process of reductive dissolution of As (Kulkarni et al. 2017).

1.4 Mobilization of As

As described above the environmental conditions of an aquifer control the dissolution and transport mechanisms of As in groundwater. Summarized lead this observation to four main dissolution mechanisms.

- **Reductive dissolution**
  The reductive dissolution process is the most common mechanism for high level contaminations. Remarkable is the fact that the As sources in this case are not As-minerals, but adsorbed As. The preferable adsorbents are iron oxides, iron hydroxides (HFOs) (Dixit and Hering 2003) and manganese oxides (Table 2). These “adsorbing” minerals precipitate under oxidizing conditions and indicate a very high specific surface. Other minerals like phosphates, clay minerals, carbonates or aluminium oxides are also able to adsorb As but in much smaller quantities (up to 5 orders of magnitude smaller) (Smedley and

Kinniburgh 2002). If dissolved As ($H_2AsO_4^-$ and/or $HAsO_4^{2-}$) reaches this surface it got adsorbed and bound to the surfaces, the quantity of the capture strongly depends on the pH of the solution. The different As species indicate not the same adsorption affinity, due to that more As(V) got adsorbed than As(III). This process could be stabile for a long time, until the environmental conditions change, e.g by bacterial activities, which lead to a change from oxidation to reduction (Nickson et al. 2000). This is possible if organic matter will be deposited into the aquifer (e.g. river delta) and covered from fine grained sediments, which are able to decrease the flux of oxygen to organic material. Under a reductive environment the iron oxides and HFO phases start to dissolute (Equation 1), simultaneously the adsorbed As got released. An example for this mechanism is the Bengal basin in Bangladesh, with very high As contaminations (Smedley and Kinniburgh 2002).

$$\mathbf{8FeOOH + CH_3COOH + 14H_2CO_3 => 8Fe^{2+} + 16HCO_3^- + 12H_2O}$$

Equation 1: Example for reduction of HFO by organic matter (Ravenscroft et al. 2009).

- **Alkali desorption**

  A lot of As influenced waters indicate high pH values and oxidizing conditions. Due to this the alkali desorption is defined as possible mechanism for these waters (Ravenscroft et al. 2009). Experiments from Dzombak and Morel 1990 showed that the adsorption rate of HFOs, which are the most important adsorbing minerals, strongly depends on the pH value. Neutral to slightly acidic waters indicate a strong adsorption, however pH values at ≥ 8 and particularly above 8.5 have a much smaller adsorption capacity. This leads to desorption of As from the HFOs and an increase of the As concentration in the solution. These experiments do not include competitive ions, which are able to reduce the adsorption capacity of HFOs for As. Solutes with this effect in natural waters are phosphate, bicarbonate and less importantly silicate. Due to this the As adsorption capacity of HFOs will be reduced, additionally to the smaller adsorption capacity at high pH values. With regard to that the concentration of As in the solution increases significantly (Gao et al. 2011). It should be noted that also other factors like evaporation, weathering and residence time influence the As concentration and pH value in the water, and it is difficult to distinguish between alkali desorption or other not well known processes (Ravenscroft et al. 2009).

- **Sulphide oxidation**

  Some iron sulphides like pyrite (FeS_2), chalcopyrite ($CuFeS_2$), arsenopyrite (FeAsS) or other sulphides like orpiment (As_2S_3), realgar (As_4S_4), stibnite (Sb_2S_3), tennantite ($Cu_6[Cu_4(Fe,Zn)_2]As_4S_{13}$) or arsenical tetrahedrite ($Cu_6[Cu_4(Fe,Zn)_2](Sb,As)_4S_{13}$) are able to contain significant amounts of As (Table 1). Preferentially they develop in reducing environments and dissolute under oxidizing conditions in water. When exposed to an aqueous solution with dissolved oxygen these minerals dissolute relatively fast and release sulphate, iron, copper and antimony. Due to the oxidizing conditions most of the iron,

copper and antimony precipitate immediately in form of secondary minerals or get adsorbed on existing or newly precipitated phases. This effect applies also for As, i.e. it is removed from the solution and mainly “stored” on HFOs. Regarding to this the mechanism of sulphide oxidation decreases the potential for the dissolution of As significantly (Ravenscroft et al. 2009). As mentioned above other mechanisms also influence the adsorption process and could increase the As concentrations in the solution (competitive ions). Normally, if sulphides dissolute the pH value will decrease due to the release of SO4. However, if carbonates are associated they act as a “buffer” and the pH value can be neutral or even basic (Lengke et al. 2009). According to (Anawar et al. 2004) surface complexations of bicarbonate onto HFOs are also able to remobilize previously adsorbed As.

- **Geothermal As**
  Areas with a high geothermal gradient and circulating groundwater are usually situated at active and former continental-volcanic settings. Some spots indicate very high As concentrations in the groundwater. According to (Webster and Nordstrom 2003) there are three typical tectonic settings for geothermal As. One setting is characterized by colliding plates with and without subduction zones, another is associated with intraplate “hot spots” like Hawaii or Yellowstone and the last one is associated with rift zones. As mentioned before the As concentrations can reach very high values and range over three orders of magnitude. In most cases As(III) occurs and is correlated with Cl, for high temperatures an association with precipitating pyrite seems to be likely. Low temperature conditions favour As(III) and As(V) appearance. When the solutions cool down elemental As is stable in some cases. For oxidizing conditions realgar and orpiment are likely to occur (Ravenscroft et al. 2009).

2 Investigation area

2.1 Geographical overview

The investigated area is located in the upper part of Styria in Austria. In more detail, it is situated in the Seckauer Tauern Range, which is part of the Central Alps. This mountain range belongs to the Niedere Tauern Range and is bordered in the west by the Rottenmanner and Wölzer Tauern Range, in the north by the Liesing valley and in the south by the Mur valley (Figure 3) (Lieb 1991).

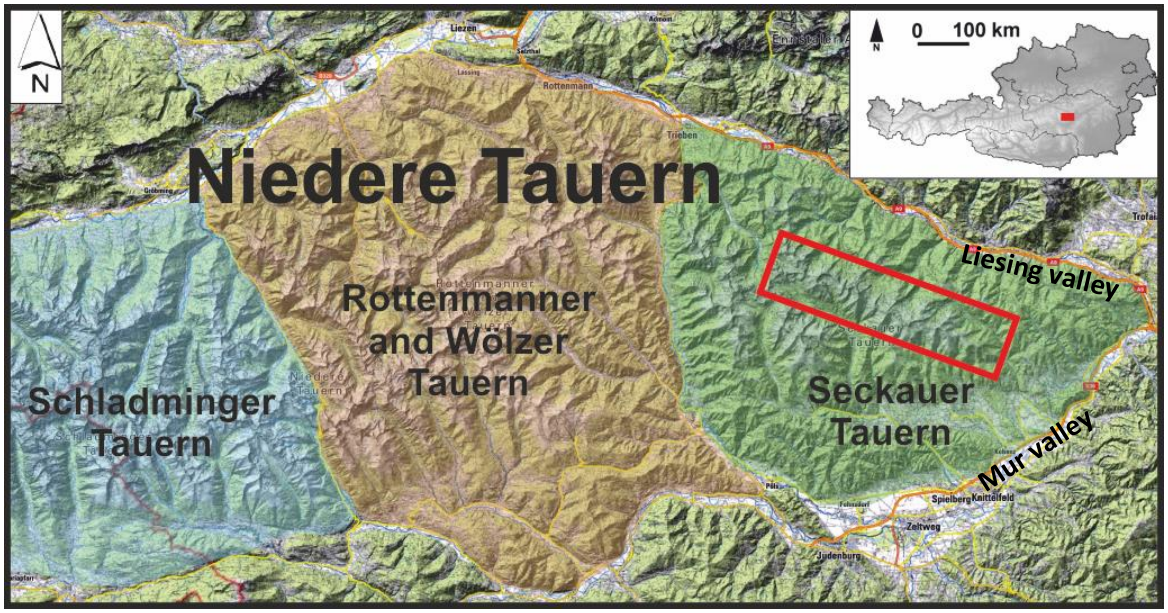

Figure 3: Geographical overview of the investigation area, detailed map without scale. The red frame indicates the exact position of the study area, map modified after bergfex open street map (www.bergfex.at).

Within the Seckauer Tauern Range the study area extends north and south along a mountain crest from the Hämmerkogel in the east to the Goldkogel in the west. The important mountains within this area are the Seckauer Zinken, the Maierangerkogel, the Hochreichhart and the Geierhaupt (Figure 4). Several valleys and cols were taken into account: Bärenkar, Brandstätterkar, Bärental, Ingeringtal, Hölltal, Hirschkarl, Dürrtal, Hirschfeld, Donnerofen, Finsterliesing and Hühnerkar. The elevation of investigated springs and geological features ranges from approximately 1500 m to nearly 2000 m a.s.l..

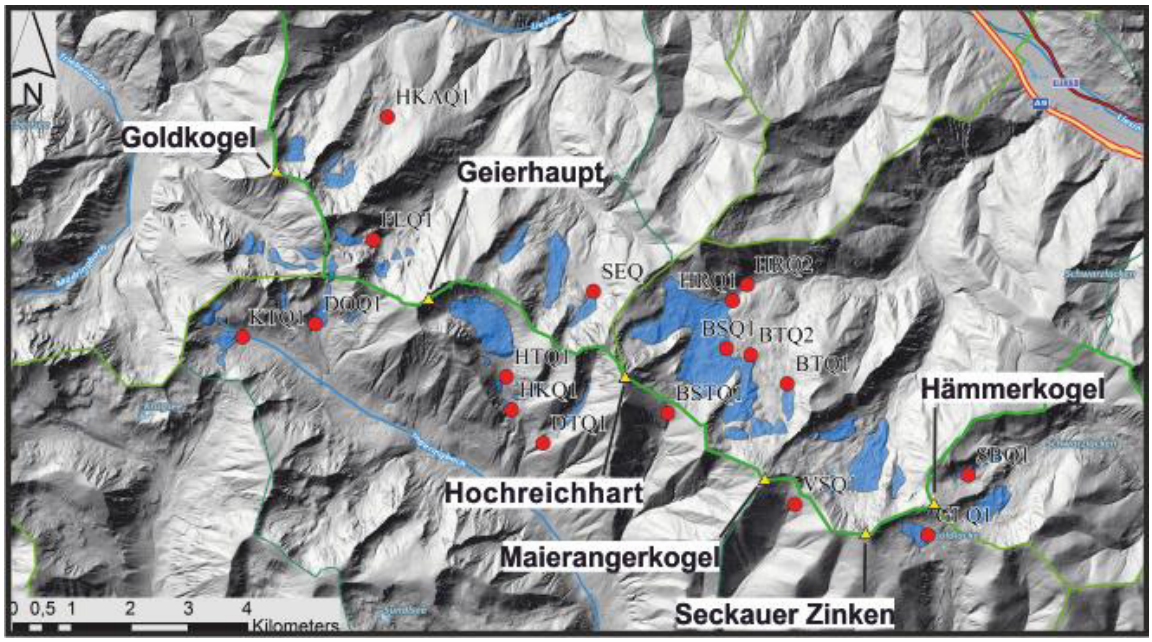

Figure 4: Study area with the investigated springs within the Seckauer Tauern Range. The green line highlights the central mountain ridge. The blue areas are relict rock glaciers.

2.2 Geological overview

The Seckauer Tauern Range is part of the crystalline basement unit of the Silvretta Seckau Nappe, which is situated within the Upper Austro Alpine unit. This unit can be assigned to the eastern Alps (Gasser et al. 2009).

The Alps are a product of the collision of the African and European continent. In detail, the subduction induced collision of the European and the Apulian tectonic plate was the main process. Accompanying this collision several oceans and small continental areas have occurred and disappeared since the Palaeozoic until now, which led to a very complex orogeny genesis (Schuster 2015).

According to Schuster 2015 the general structure of the Alps can be classified into four major units:

i) The Helvetic unit, which represents the European plate, is divided in a late Devonian – Carboniferous continental basement and a late Carboniferous – Cretaceous sedimental cover. This unit is mainly represented in the western Alps.

ii) The Penninic unit, which includes two oceans (Piemont ligurian and Valais) and a micro continent (Iberia – Briançonnais). Through transport processes different nappes of Variscian metamorphic crystalline rocks and permo – carboniferous clastic sediments were created. Additionally, in the Triassic and lower Jurassic shallow water sediments and deep water sediments were deposited. Main parts of this unit are located in the western Alps, exceptions are the Tauern and Engardiner Window and the Flysch zone in the north of the Alps.

iii) The Austro Alpine unit, which originally represents the northern part of the Apulian plate and which can be characterised as continental plate with Cadomian influence and Palaeozoic metasedimentary and magmatic rocks. A metamorphic overprint and the development of different nappe structures are characteristic features. This unit forms the central basement part of the eastern Alps.

iv) The South Alpine unit, which has the same origin as the Austro Alpine unit, but did not experience a development of nappes. This unit is separated from the Austro Alpine unit by the Periadriatic line.

2.2.1 Austro Alpine unit

The Austro Alpine unit is the most important part of the Central Alps and also contains the study area (Gasser et al. 2009). As mentioned before pre Alpine basement builds up the main parts of this unit (Schmid et al. 2004). This basement was influenced in the Ordovician until the Carbon by phases of intensive magmatic activities. Subsequently, the Variscian orogeny induced metamorphism and further synorogenic magmatic activities. After the erosion and deposition of the orogenic material in depressions, an extension of the lithosphere in the Perm again induced magmatic activities and high temperature metamorphism. Due to the subsidence, a shallow marine environment developed and induced the deposition of a massive stack of marine sediments, today these are the South Alpine and the Northern Calcareous Alps. During the Eoalpine Event in the Cretaceous this unit was separated from the mantel and the lower crust. This process led to the development of nappes, which were transported northwards on top of the Penninic nappes. However, the South Alpine shows no further developments. As a result of the transport processes the nappes can be separated in a Lower and Upper Austro Alpine unit (Schuster 2015).

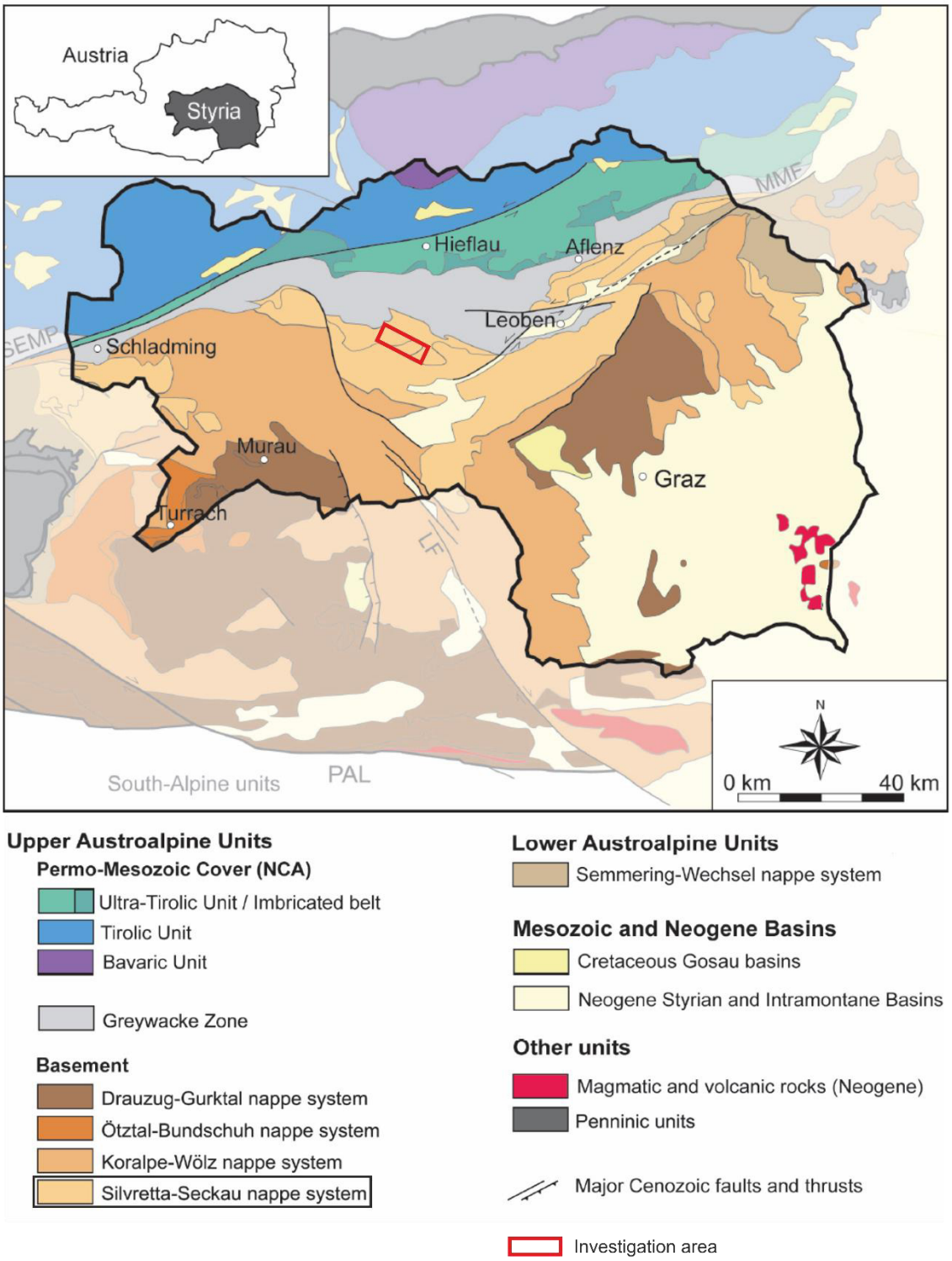

Figure 5: Tectonic overview of Styria, the investigation area is situated in the Silvretta-Seckau nappe system, modified after Gasser et al. 2009; Frisch and Gawlick 2003; Schmid et al. 2004.

The Lower Austro Alpine unit was the passive continental margin between the Apulian plate and the Penninic Ocean. It was affected by extension processes in the Jurassic. During the Eoalpine Event (higher cretaceous) the nappe stacking was formed and due to subduction processes green schist facies metamorphic grade was reached. The lithology is dominated by continental crust material, which is overlaid by Permo-Mesozoic Meta sediments. In the Eastern Alps, only the Semmering-Wechsel nappe system represents this unit (Figure 5).

The Upper Austro Alpine unit was created between the lower and the middle cretaceous, with the Silvretta-Seckau nappe system as lowest unit. Variscian and Eoalpine metamorphic events influenced this unit and reached sub green schist to amphibolite facies in the end. In Permo-Triassic times, transgressive metasediments overlaid the Silvretta-Seckau nappe, today remnants of this event are still visible (Rannach fm.).

The “Grauwackenzone” borders the Silvretta-Seckau nappe system in the north and is overlaid by the “Northern Calcareous Alps” (Schuster 2015).

Most of the area of the Seckauer Tauern Range is represented by the Silvretta-Seckau nappe. The Silvretta-Seckau nappe system can be subdivided into the basement units: Seckau, Speik and Amering Complex, and in the cover unit which is represented by Permomesozoic sediments, for this thesis only the Seckau Complex is of relevance.

The origin of the Seckau Complex is interpreted as a magmatic island arc which was created at the end of the Neoproterozoic. It represents the basement and extends over a triangle shaped area from the Bösenstein massif and the Seckauer Tauern in the northwest to the Fischbacher Alps in the east (Pfingstl et al. 2015). It can be separated into the Bösenstein nappe, the Pletzen nappe, the Mugel-Rennfeldzug of the Troiseck-Floning nappe and the Seckau nappe. In general, the lithology is described as orthogneisses, paragneisses and magmatic paragneisses (Metz 1976). In smaller quantities the occurrence of amphibolites, quartzites and micaschist are described (Neubauer 2002).

The cover is characterised by Permomesozoic sediments which are generally represented by the Rannach formation (Pfingstl et al. 2015). This formation also called “Alpine Verrucano” includes quartz conglomerates, sericite quartzite and phyllites. Additionally, sericite schist and crystalline limestone are present (Metz 1976).

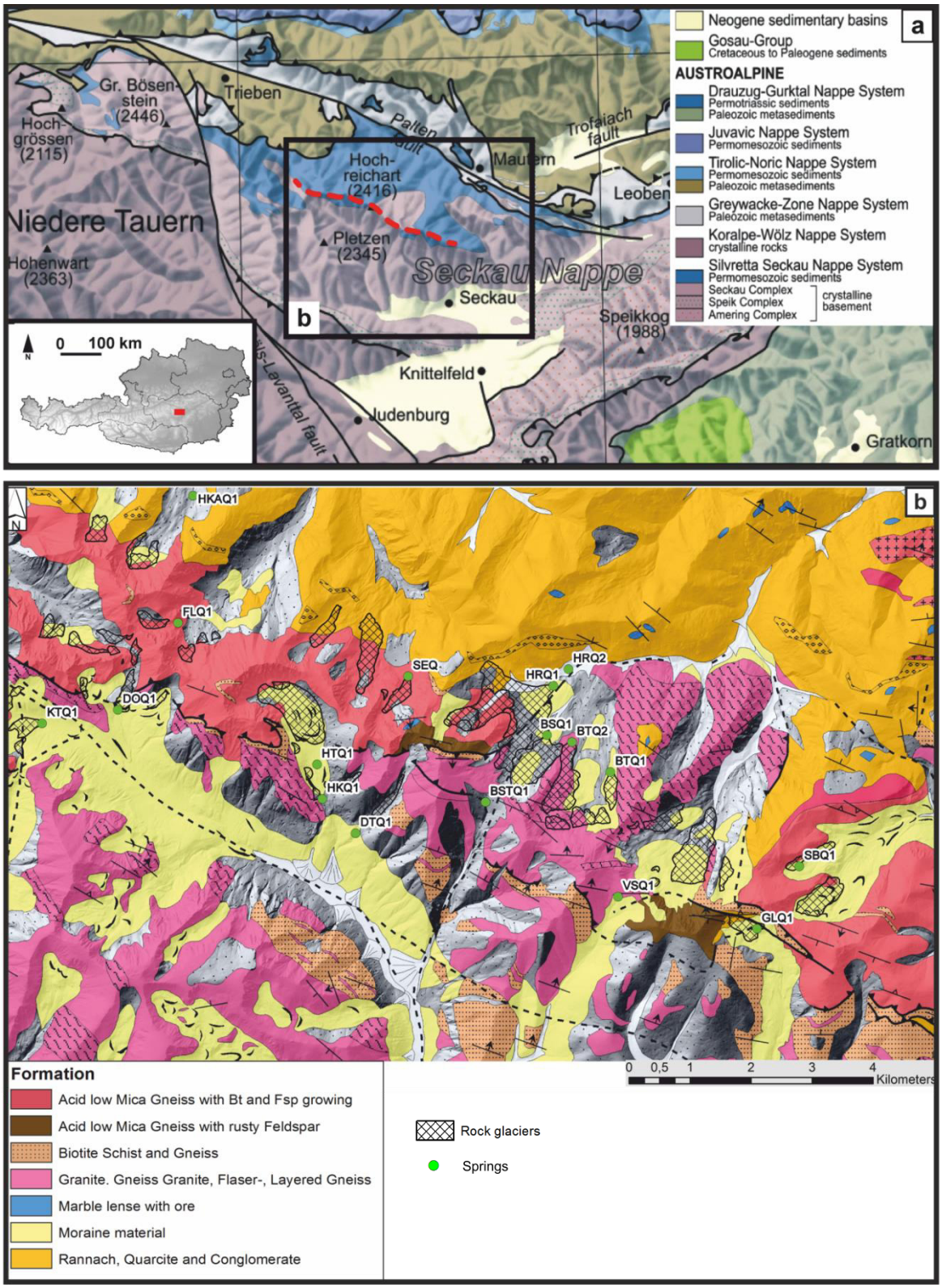

Figure 6: a) Geological overview of the investigation area modified after Pfingstl et al. 2015, b) detailed geological map according to Metz 1976. The lines mark tectonic borders; dashed lines are assumed positions of tectonic borders.

2.2.2 Geology of the investigation area

The study area is situated near the contact of the Seckau complex and the Permomesozoic cover (Figure 6 a, b). According to recent research (Mandl et al. 2018), this area represents mainly the basement and contains four different units named Glaneck Metamorphic suit (GMS), Hochreichhart Plutonic suite (HPS), Pletzen Pluton (PP) and Griessstein Pluton (GP). The GMS represents the initial host rock and the other units intruded in the Cambrian into the host rock. The study area extends around the contact area between the HPS, the PP and the GMS. Most of the investigation area is predominated by the HPS, which can be classified as S type metagranitoids. Smaller parts are also represented by the GMS, the Rannach formation (Permomesozoic cover) and the GP. The lithology of this area is dominated by a low biotite bearing flaser gneiss with a sericite-quartzite matrix (Metz 1976). Additionally, slightly rusty button shaped feldspar clasts are associated with this matrix and thin biotite minerals are visible around the quartzitic lenses. If the biotite growing continues it is possible that as already mentioned flaser gneisses occur. This type of gneiss is represented at the top of the Hochreichhart Mountain and also shows the sericite-quartzite matrix (Metz 1976). Furthermore, quarzitic dikes in the shape of lenses with several tens of meters in length and few meters in height, as well as related contact metamorphic rocks exist in the catchment area of SEQ.

After (Metz 1976) north-east striking thrusts separate the different lithologies / plutonic suites which are the product of the alpine orogeny with the indenter tectonic development. Accompanied by this development, deformation zones with mylonitized granitoids occur (Böcher H. 1927). Scalar fabric data measurements were applied in the catchment area of the relict rock glacier spring Schöneben around a quarzitic dike (Figure 7). With a general direction to the NW and a dip angle of around 30° to 40° they fit to the data of previous works in the Seckauer Tauern Range (Schönegger 2015; Pfingstl 2013).

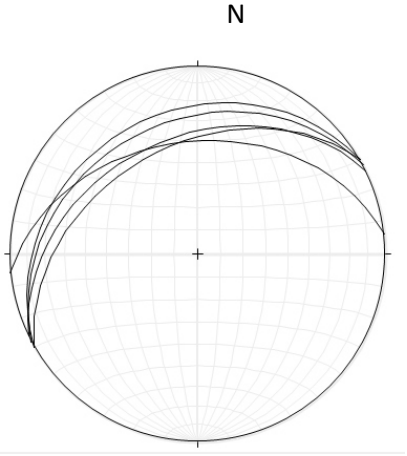

Figure 7: Stereonet of the measured scalar fabric values near the sampling point P1 within the catchment area of the Schöneben glacier, the general dip direction is NW.

The Seckauer Tauern Range was not totally glaciated during the last glacial phase (Würm, 100.000 to 10.000 years b.c.), because it was situated on the eastern edge of the alpine glaciation. Nevertheless, this glacial activity was the dominant factor for the development of the actual geomorphological shape of this area. The impact of strong erosion processes is still visible in some valleys and moraine sediments were produced, which are widely distributed in the Seckauer Tauern Range. Nearest to the

investigation area is the glacial influenced Ingering valley, situated in the South. Between the Ingering valley and the Feistritzgraben are several small, north-south oriented valleys, which are all glacially influenced. This is made visible by typical glacial formations like cols and U shaped valleys. Erosional processes, which produced a lot of blocky material, also led to the development of rock glaciers. These stone-ice-structures developed in the periglacial (late Würm) and still shaped the area after the common glaciers had disappeared (Nagl 1976). Important for this work are the today ice free relict rock glaciers and the debris talus formations because they act as effective catchment area for rain water and most of the springs in this area are related to such formations.

2.2.3 Hydrology / hydrogeology

Catchment areas along the mountain ridge of the study area are predominated by scree slopes which consist of moraine, talus or landslide material. A high number of episodic springs (Wechmann 1968) are bound on the widespread heterogeneous distribution of moraine material, which results in a spatially heterogeneous distributed permeability of the surface near layers. This resulted in many small aquifers instead of one big aquifer as e.g. in river influenced valleys. But there are also permanent springs, which are mostly associated with periglacial landforms such as relict rock glaciers. Therefore, relict rock glaciers represent the most important aquifers in the study area. The surface of these periglacial landforms acts as very effective catchment area and the internally highly conductive, porous and layered structure is characterised by a high flow rate and short retention time (Pauritsch et al. 2017). In fact, two different discharge conditions characterise the rock glaciers: i) the first one is a fast component, where the infiltrated water flows through the top layer which consists of course blocky material with a very short retention time of hours to days; ii) the second component is much slower and represents the flow through the fine grained base material (basal moraine) with retention times up to several months. Thereby the base material acts as storage and buffers the discharge over several months (Winkler et al. 2016).

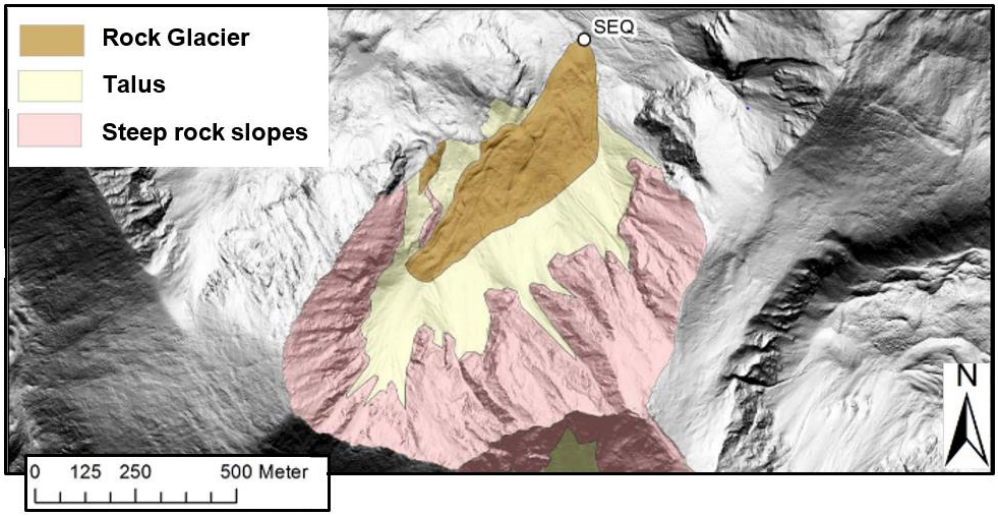

Figure 8: Catchment area of the SEQ with a differentiation into steep rock slopes in the upper part, overlaid by talus material and finally the Schöneben rock glacier, modified after Winkler et al. 2016.

The climatic conditions in the investigation area are cold and wet with annual mean air temperatures of 1.5 to 2.4°C and precipitation rates of nearly 2100 mm/a (ZAMG 2004). Due to these factors the duration of the vegetation period ranges from 150 to 50 days (Pilger and Prettenthaler 2012) depending on the elevation level. This affects the thickness of the soil which influences the infiltrating rain water with respect to the amount of dissolved carbonic acid. Steep slopes, a very thin to missing soil layer and generally lower temperatures also lead to reduced evapotranspiration rates (Wagner et al. 2016).

Within the study area 17 springs were chosen for further investigation. Most of these springs are related to relict rock glaciers, exceptions are the Hochreichhart-schutzhaus 2, Brandstätterthörl and Vorwitzsattel springs. These springs have catchment areas which contain beside rock cliffs just scree slopes but no relict rock glacier. Detailed information about the internal structure of the scee slope aquifers does not exist. The coordinates based on GPS measurements are given in the Appendix 1. Continuative detailed investigations were conducted at the Schöneben spring (SEQ).

The SEQ is related to the relict Schöneben rock glacier (SRG) which is located southwest of the "Schöneben" (Appendix 1), in a height of 1715 m a.s.l.. The catchment area (0.67 km²) is characterised by steep slopes and talus formations in the transition between steep slopes and the relict rock glacier (Figure 8). In general, most of the catchment area is free of vegetation and soil, only few parts indicate thin soil coverage. The spring is situated at the front of the RG, which expands over an area of approximately 0.17 km². An automatized gauging station is a few tens of meters below the spring. The discharge ranges from approximately 10 to more than 100 l/s. The present hydrogeological behaviour has developed after the disappearance of the internal ice. Now the coarse blocky layer on the top indicates a k_f value of ~ 10^{-2} - 10^{-3} and the fine grained base shows a maximum k_f value of about 7×10^{-5} m/s (Winkler et al. 2016).

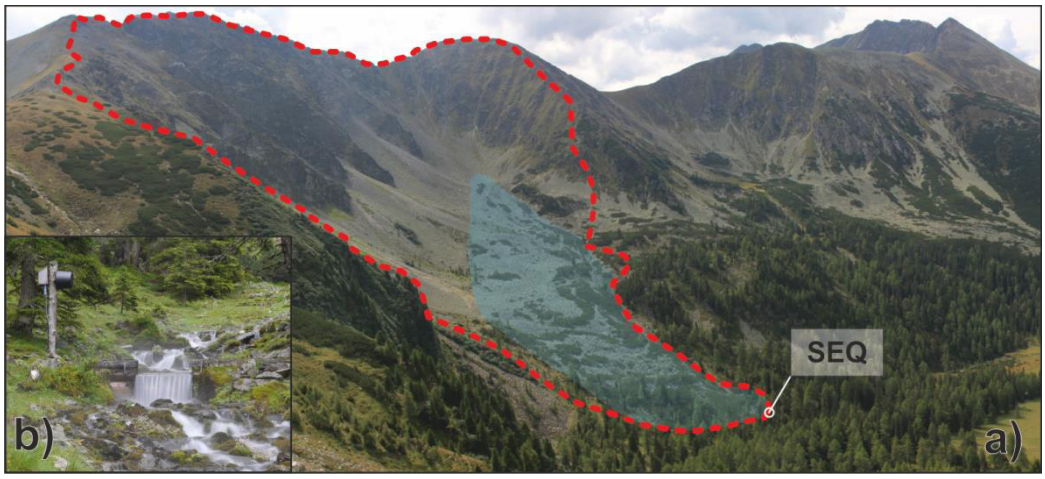

Figure 9: a) Overview picture of the SRG (blue area) and the associated catchment area (red dashed line), modified after Winkler et al. 2016. b) Gauging station at the river Schöneben, positioned several tens of meters downstream the spring.

3 Methods

The simplified scheme in Figure 10 gives an overview of the applied methods and materials which were used to produce the dataset for the analysis and interpretation.

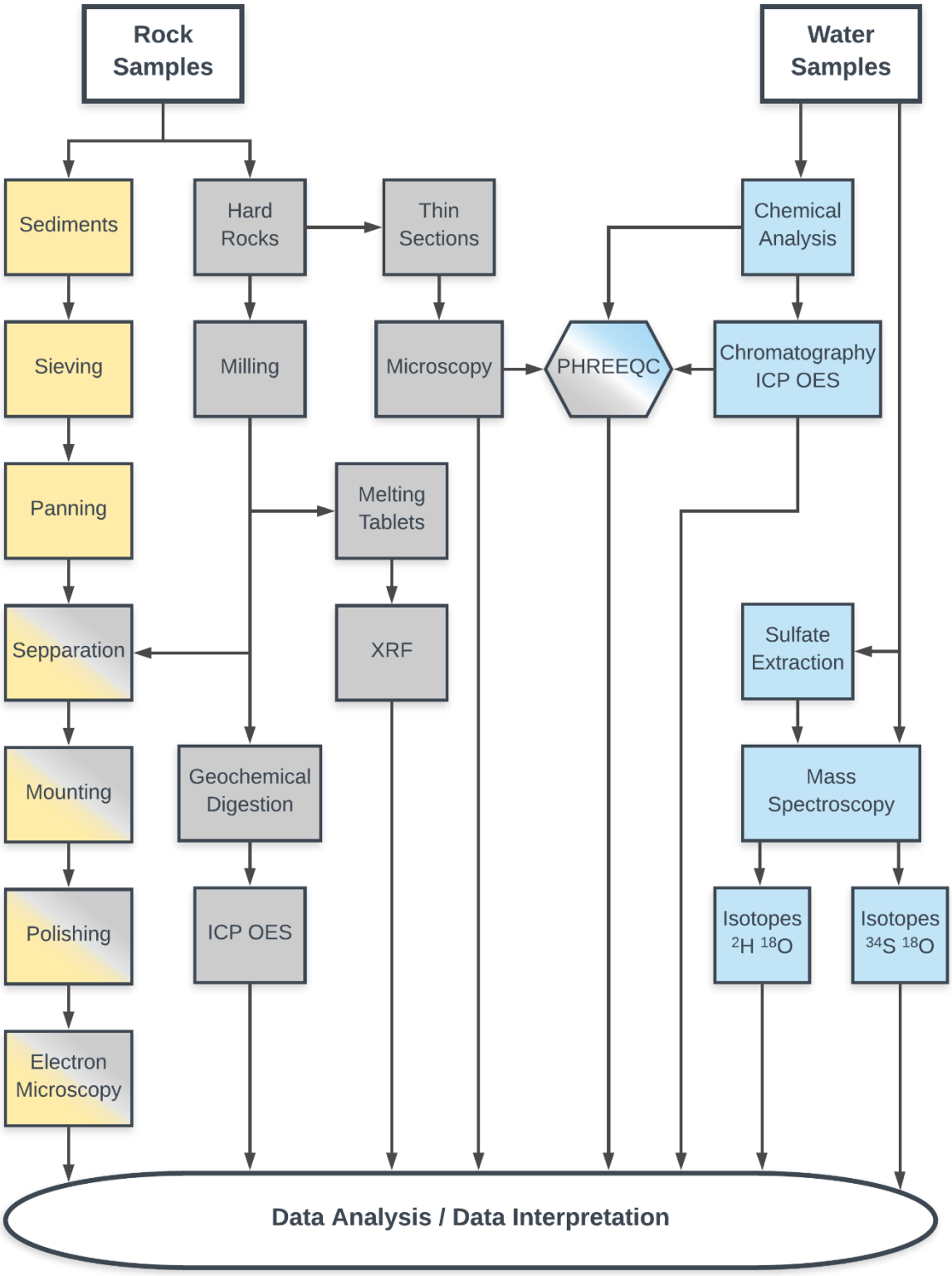

Figure 10: Simplified scheme of the applied methods.

Field, laboratory and modelling work was done to generate the dataset for answering the scientific question. Therefore, taking water and rock samples, measuring in situ parameters and analysing the samples in the laboratory were accomplished. Data sets from previous projects delivered fundamental knowledge about the hydrogeochemical behaviour of the springs and the geology in the Seckauer Tauern Range and thus, they were necessary to choose the sampling points for water and rock samples.

3.1 Field work

Two sampling campaigns were completed to investigate the hydrogeochemical behaviour. In total 17 springs were sampled for their hydrochemical content and partially of their isotopic composition (^{2}H, ^{18}O). Additionally, in situ measurements of pH, electrical conductivity, water temperature and oxygen content were applied. All samples were taken in summer and autumn of 2017, campaign one contains all 17 springs, but campaign two only contains five selected springs. The river sample Hochreichhartschutzhaus 2 was sampled in addition, though it is not important for this project and therefore not included in the following chapters. The weather conditions at the sampling campaigns were very different and ranged from hot dry summer to snowfall conditions. Samples were taken for the anion, cation analysis and isotopes, altogether 36 different elements were measured (Table 3). On-site cation samples were acidified with HNO_3 in order to avoid precipitation processes. All samples were cooled during the transport to the laboratory. A WTW Multi 3320 (multimeter) was used to measure the pH value, electric conductivity, water temperature and O_2 content. Additionally, the electric conductivity was checked with a conductivity pen (ULTRAPEN PT1).

Locations of the rock samples were chosen according to the findings of the water sample analysis. The highest As concentrations were detected at the Schöneben spring. Therefore, this spring was chosen for further detailed investigations. Within the catchment area of the Schöneben spring, six in situ samples from outcrops were taken (P1 - P5) and one fragment of bedrock (P9) with high ore content at the position of P1. The selection of the sample locations was based on the combination of the catchment area with the geological map after Metz 1976 (Figure 11, b and Figure 6). In the field special respect was given to areas with ore content. It must be taken into account that recent research in this area resulted in a less differentiated geological map (Figure 11, a) in relation to the work of Metz 1976 (Figure 11, b, Figure 6, b). Two block samples were taken at the Schöneben creek in the area around the spring (P7, P8), one sample near the weather station within the Rannach formation (P6). And additionally, one sediment sample (S1) at the gauging station (Figure 9, b). The sediment sample mainly indicates a grain size of rocks and sand, only small parts of the sample were of the silt fraction. This grain size distribution resulted from the fact that the sediment transport from the spring to the sampling point is only a few metres in length. Coordinates are given in Appendix 1.

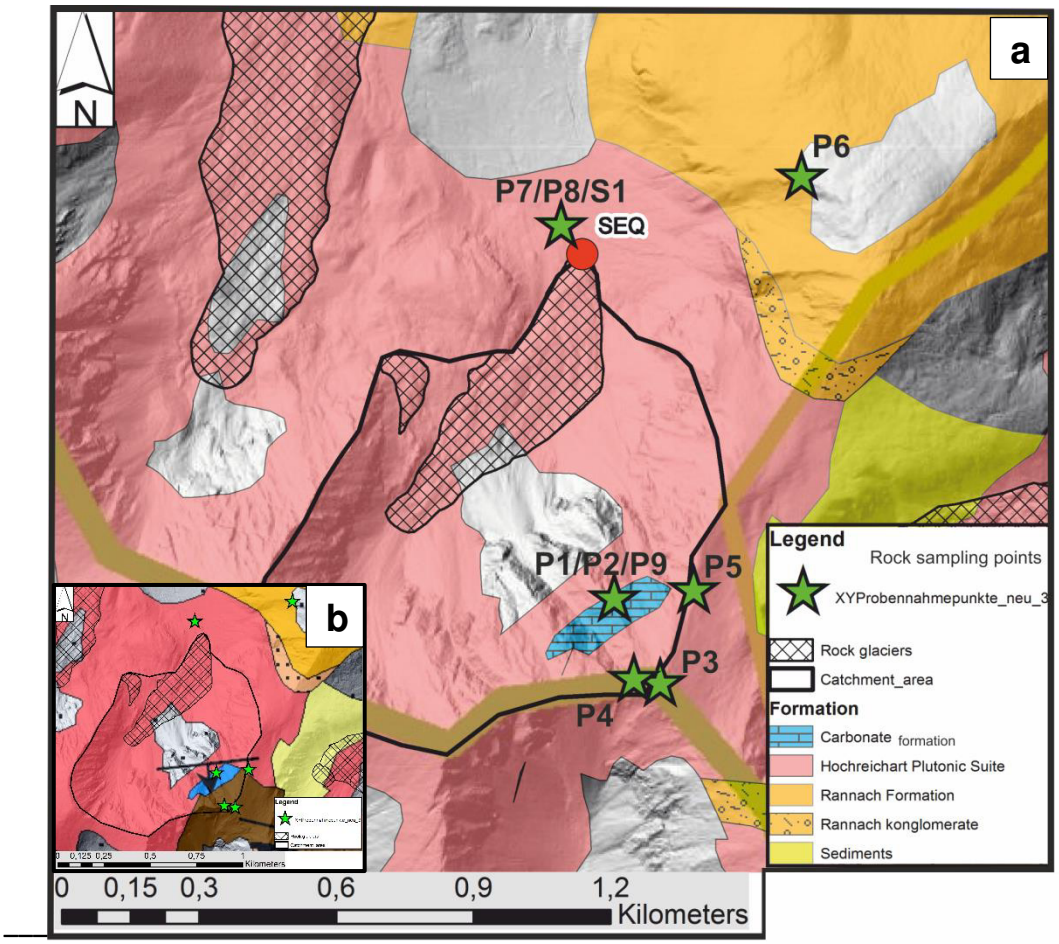

Figure 11: a) Sampling points in the area around the Schöneben spring geological map after Mandl et al. 2018, b) geological map after Metz 1976 (Figure 6). The brown area is a lithological variation within the HPS.

3.2 Hydrogeochemistry

The water samples were analysed in respect of their cation and anion content. 29 different cations were taken into account, including the major elements, minor elements and heavy metal elements. Additionally the seven most important anions were analysed (Table 3). The measurement of the cations was performed by ICP MS (Agilent 7700x) and the evaluation of the anions were completed by an Ionic Chromatograph (Dionex ICS 5000), both at the Chemical institute Graz. Previous measurements were applied at the “Umweltlaboratorium Land Steiermark” according to the norm: DIN EN ISO 10523, DIN 38409-7, ÖNORM EN ISO 103404-1, ÖNORM EN 26777, and the ÖNORM EN ISO 17294-2.

Every measured element had its own detection limit, which depends on its element specific properties, the used method and the involved laboratory. Values below the detection limit were not used for further data interpretation. Note arsenic as an exception for two measurements, if the result is less than 1 µg/l the value was set to zero to show the differences between “high” As waters to “low” As waters in the further interpretation. Due to the different sampling campaigns from 2014 to 2017 also two laboratories with different measurement uncertainties analysed the water samples (Table 3).

Laboratory		Institute of chemistry		"Umweltlaboratorium Land Steiermark"	
		Main SD		Measurement Uncertainty*	
Element	unit	lowest	highest	lowest	highest
Ca	[µg/l]	10	330	200	500
Na	[µg/l]	1	34	100	100
Mg	[µg/l]	1	12	100	300
K	[µg/l]	1	21	100	100
P	[µg/l]	-	-	-	-
Si	[µg/l]	3	130	-	-
Be	[µg/l]	-	-	-	-
B	[µg/l]	0.01	0.1	-	-
Al	[µg/l]	0.1	1	-	-
Ti	[µg/l]	0.001	0.1	-	-
V	[µg/l]	0.001	0.01	-	-
Cr	[µg/l]	0.001	0.023	-	-
Mn	[µg/l]	0.001	0.014	-	-
Fe	[µg/l]	0.1	1.1	-	-
Co	[µg/l]	0.001	0.002	-	-
Ni	[µg/l]	-	-	-	-
Cu	[µg/l]	0.002	0.01	-	-
Zn	[µg/l]	0.01	0.2	-	-
As	[µg/l]	0.002	0.4	0.6	1.9
Se	[µg/l]	0.001	0.007	-	-
Sr	[µg/l]	0.1	0.2	-	-
Mo	[µg/l]	0.003	0.1	-	-
Ag	[µg/l]	-	-	-	-
Cd	[µg/l]	-	-	-	-
Sb	[µg/l]	0.001	0.01	-	-
Ba	[µg/l]	0.01	0.04	-	-
Hg	[µg/l]	-	-	-	-
Pb	[µg/l]	0.001	0.01	-	-
U	[µg/l]	0.01	0.1	-	-
Cl	[mg/l]	-	-	-	-
NO_2	[mg/l]	-	-	-	-
SO_4	[mg/l]	0.03	0.31	0.3	0.5
NO3	[mg/l]	0.04	0.2	0.4	0.5
PO_4	[mg/l]	-	-	-	-
HCO_3	[mg/l]	-	-	7.2	7.3
NH_4	[mg/l]	-	-	0.003	0.003

- no value available

*extended measurement uncertainty for 95 % of all cases

Table 3: Measurement uncertainties for the different elements combined for all samples.

3.2.1 Data visualisation

A common way to visualize data sets is the usage of scatter plots with two axes, where different elements are plotted as a point cloud against each other. The aim is to detect correlations (like linear, exponential,..) or similarities within the data. The software Grapher 11 was used for the projection of the scatter plots.

As a standard tool in the hydrogeochemistry a Piper plot was used. This plot shows a two dimensional visualisation of the seven major constituents (anions and cations) of the water hydrochemistry. First the data is plotted in ternary diagrams which lead to the plot in the central prism (Piper 1944). Finally this projection was used to determine the hydrochemical type of water, according to the method of Back 1966 (Figure 12). The software Grapher 11 was used to create the plots.

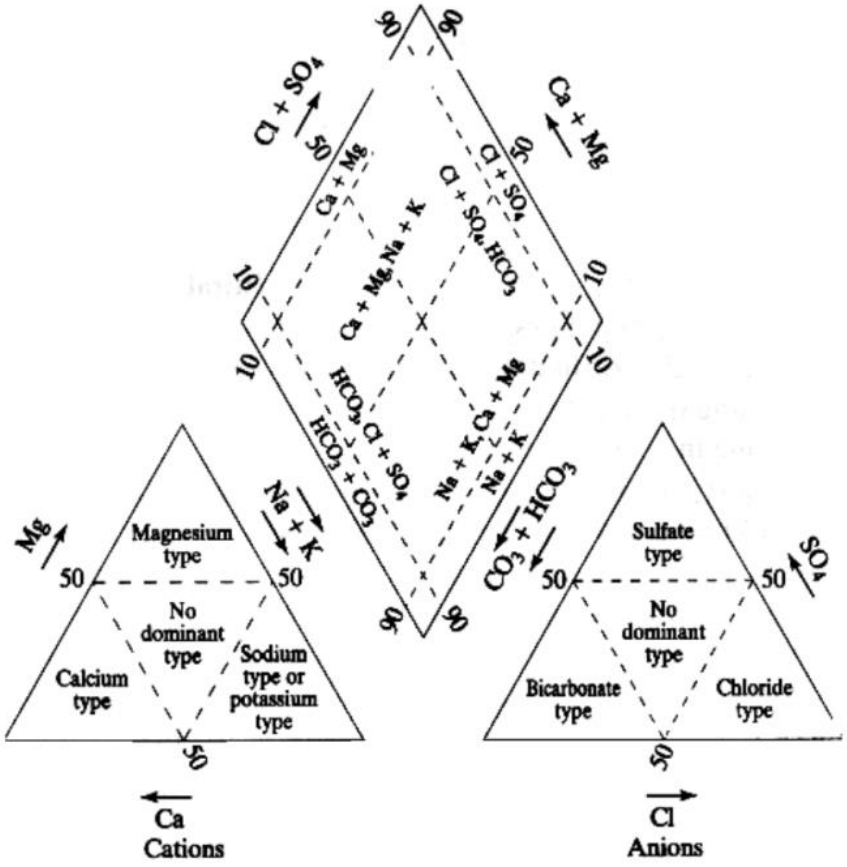

Figure 12: Interpretation of Piper diagrams after Back 1966.

Additionally, a Schoeller diagram was used. This diagram gives an overview of the compositional differences between the collected samples. It represents a semi logarithmic plot of major anions and cations from different samples. As important elements and ions for the comparison Mg, K, Na, Si, Ca, HCO_3, SO_4 and NO_3 were chosen. The diagram was created with Grapher 11.

3.2.2 Isotopes

^{2}H, ^{18}O

Some geological processes are visible in the stable isotopic ratio of ^{2}H, ^{18}O, hence isotopic samples from different springs were taken and analysed.

The investigation of stable isotope fractionation is a very common method in the water analysis. The main concept is to use the mass ratio of two isotopes of the same element (e.g. $^{2}H/^{1}H$ or $^{18}O/^{16}O$) and compare this ratio with an internationally accepted standard (Table 4). By applying a simple calculation (Equation 2) this newly calculated value is lower or higher than the standard and the difference δ (in ‰) gives information about the related processes which influenced the water. This ratio is called delta notation (δ). Therefore, either the heavier or the lighter isotope is accumulated. If δ is positive, the water sample is enriched with the heavier isotope and vice versa is the case for negative δ values. By using mass spectrometry the ratios of the isotopes can be determined (Fetter 1990).

$$\delta = \frac{R_{Sample} - R_{Standard}}{R_{Standard}} * 10^3$$

Equation 2: Delta notation for stable isotopes.

The used standard for these samples is the standard mean ocean water (SMOW), the exact calculation for ^{2}H, ^{18}O with this standard is shown in Equation and Equation .

$$\delta\ ^{18}O(‰) = \left[\frac{^{18}O/^{16}O_{sample}}{^{18}O/^{16}O_{SMOW}} - 1\right] 10^3$$

Equation 3: Delta notation for oxygen.

$$\delta\ ^{2}H(‰) = \left[\frac{^{2}H/\ ^{1}H_{sample}}{^{2}H/\ ^{1}H_{SMOW}} - 1\right] 10^3$$

Equation 4: Delta notation for hydrogen.

Finally, the δ ^{2}H can be plotted as a function of δ ^{18}O. When this is done for water from a wide range of climatic regions from all over the world, a linear relationship can be seen. The global relationship can be described by the equation (Equation) by Mayo et al. 1985.

$$\delta\ ^{2}H = 8\,\delta\ ^{18}O + 10$$

Equation 5: Linear function of the global meteoric water line.

This linear relationship is known as the global meteoric water line (GMWL). In a worldwide dataset it is possible to identify warm, cold, dry and wet areas. Reasons for various positions of the isotopic data on the GMWL are the different evaporation and precipitation conditions which result in different isotopic ratios (Figure 13).

δ D_{H2O} and δ $^{18}O_{H2O}$ of the waters were analysed by wavelength-scanned cavity ring-down spectroscopy (WS-CRDS) using a Picarro L2120-I system (Brand et al. 2009; Gupta et al. 2009). Measurements were done in the high precision (standard) mode at the isotope laboratory of Joanneum Research / JR-AquaConSol in Graz. The analytical precision for stable isotope measurements in water is ±0.8 ‰ for δD and ±0.08 ‰ for $\delta^{18}O$, respectively.

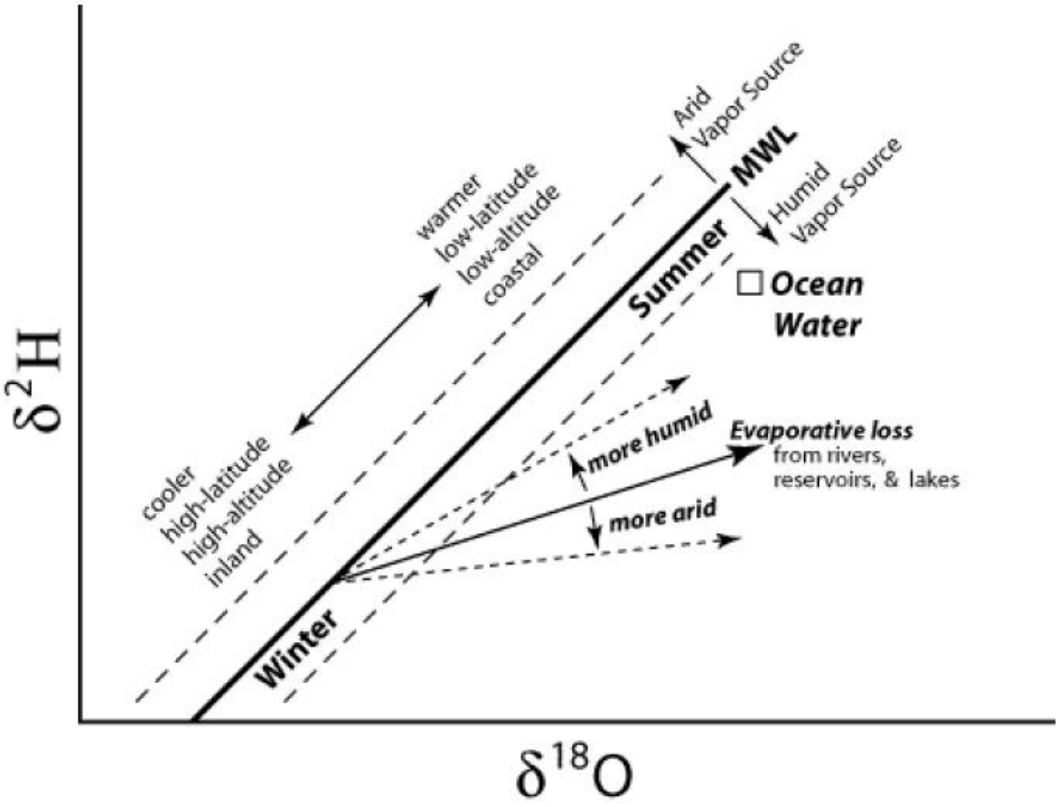

Figure 13: Influence of different environmental conditions on the position of the meteoric water line (MWL) (Clark and Fritz 1997).

^{34}S

Besides the standard stable isotopic systems several other systems exist. For this work the sulphur isotopic system was of particular interest. Due to the low mineralisation of the water in the investigation area dissolution processes of sulphide minerals were not obviously visible in the pH value. Because As is often bound to sulphide minerals, this could be one possible source for the contamination. With sulphur isotopic data it is possible to deduce the source of the dissolved sulphate in the spring water and possibly reveal some hidden dissolution processes.

For the isotopic analysis, all the sulphate has to be extracted out of the water sample. Due to the low mineralisation ten litres of sample water were needed to get a measurable amount of sulphate.

Several steps were performed for this extraction process which was run at the Institute of Applied Geosiences at the Technical University Graz:

First, the sample was acidified until a pH value of 1.5 – 2 was reached by adding HCl in one ml steps and filtered. Then, the solution was heated up to 70 – 80°C on a heating plate and 0.3 ml/l BaCl were added to produce $BaSO_4$ crystals. Furthermore, the solution was tempered overnight to increase the size of the crystals. At the next day a drop of BaCl was added again and the solution was cooled down and filtered with a blue ribbon filter which can be burned residue-free. Then the filter was put in a ceramic pot and dried in an oven at 100 °C for the night. After the drying a muffle furnace was used to burn the filter, therefore the temperature was slowly increased every hour for

100 °C to avoid sample loss. Starting temperature was 200°C and in the end 600°C where held overnight. Finally, the sample was weighted and the residual $BaSO_4$ was prepared for the mass spectroscopy.

Mass spectroscopy was done by Professor Böttcher at the Leibniz Institute for Baltic Sea Research at Warnemünde, Germany.

Isotope ratio	International reference	
$^{2}H/^{1}H$	VSMOW	Vienna standard mean ocean water
$^{18}O/^{16}O$	VSMOW	Vienna standard mean ocean water
$^{34}S/^{32}S$	VCDT	Vienna Canon Diablo Troilite

Table 4: International reference standards for stable isotope ratios ($^{2}H/^{1}H$; $^{18}O/^{16}O$; $^{34}S/^{32}S$) (Werner and Brand 2001).

3.3 Geochemistry

Optical microscopy
Out of every piece of sampled rock two to five polished thin sections were produced. These thin sections were analysed by polarisation microscopy to determine the mineral content. For oxides and sulphides reflective microscopy was used by applying the "Olympus SZX12" and "Zeiss Discovery V8" microscope.

X-Ray Fluorescence Spectroscopy (XRF)
This method provides a geochemical bulk dataset. For the analysis the samples have to be prepared in the shape of melting tablets. Additionally, the loss of ignition has to be determined to reduce the systematic error.

For the grinding unaltered parts of the samples were cut out, washed and dried in the oven at 105°C. In the next step the produced pieces were crushed by hand and then grinded to a fine powder. For the grinding a vibrating disc mill machine (Retsch RS200), with tungsten carbide grinding tool was used.

The fine sample powder was then again dried in the oven and afterwards cooled in the desiccator. For the melting tablets 1 g of fine sample powder was mixed with 7 g of Dilitiumtetraborate which acts as flux. This mixture was then melted with the Vulcan 2M (VAA 2M) machine. In this process a platinum crucible was filled with the mixture, melted and then poured off into a platinum plate. The melting tablet is finished after a short cooling time. For every following melting process, it is necessary to clean the platinum crucible first with deionised water and then in an ultrasonic bath filled with HCl (37%) acid to avoid contamination.

To include also the organic content of a sample it is necessary to determine the loss on ignition (LOI).

First of all, ceramic pots had to be annealed until the weight constancy was reached, for cooling a desiccator was used. The powdered sample was prepared by drying it in an oven at 105°C for two hours. In the next step the ceramic pots were weighted (N1), then approximately 1 g of the powdered samples were added to the ceramic pots and again weighted (N2). Now the ceramic ovens were heated up to 1000°C and then the ceramic pots with the samples annealed for one hour. The last steps were cooling of the samples in a desiccator, first with slightly open lid (15 min) then with closed lid for one hour and finally the samples were weighted again (N3). The LOI was calculated by using Equation 6.

$$LOI(Weight\ \%) = 100 \cdot [(N_2 - N_3)/(N_2 - N_1)]$$

Equation 6: Calculation of the loss on ignition.

The physical principal of the XRF is based on a specific energy release from elements if they were radiated with x-rays of a specific wavelength. The x-rays “lift” the electrons in a higher state of energy, in the next step they “fall back” to their lower state of energy and emit an element specific radiation which can be detected. By comparison of the measured signals with a standard the element can be determined (Markl 2015).

Sediment preparation

The taken sediment sample (around 2 – 3 kg) was prepared in several steps to detect possible cumulated sulphides or heavy metals which contain As.

First, the coarse components were separated by using a sieving stack, particles > 0.63 mm dropped out of the further preparation. The remaining particles ≤ 0,63 mm were than filled into a panning tray and reduced by washing out of the light weight components. This process was continued until the amount of the heavy mineral components was strongly increased. In the next step these particles were dried in an oven at 40°C for several days and then again separated by using a magnetic separator (Isodynamic L1). The separator used a sliding plane which was vibrating, through the adjustment of the steepness angle (5°) and the magnetic field intensity (1,2 Amps) the separation can be specified to separate especially sulphides. This separation was done several times to concentrate the sample.

One part of the concentrated sample was then used to produce a strewn slide. For this preparation the inner side of a plastic ring was rubbed with Vaseline and the ring was placed on an adhesive film. Then epoxy resin was warmed up and mixed with a hardener. The sample was poured into the ring until it covered the adhesive film and the ring was filled up by the epoxy-hardener-mixture. After a slow cooling phase first without heating plate (1h) and then overnight on the heating plate the ring and adhesive film could be removed and the strewn slide was ready to be polished.

The polishing was done first with the 800 granulation, then with 1200 granulation and finally in three steps (6, 3, 1 microns) for the fine tuning.

With the same concentrated sample again a mounted strewn slide was produced. Therefore, special grains were manually separated by using an incident light

microscope and a needle to pick the grains of interest out of the concentrated sample. The chosen grains were then mounted on a conductive, adhesive film.

Electron microscopy

The used microscope was a Jeol Field Electron Emission Microprobe JXA-8530 F Plus (LA-ICPMS/LA-MC-ICPMS) situated and operated at the Department of Petrology and Mineralogy of the Karl Franzens University. Parameters of interest were the chemical composition of the grains, the mineralogy and their relative quantity. In general, the results give a qualitative statement of the chemical composition. To increase the conductivity on the surface for all samples carbon coatings were used.

Measurements were applied for two sediment samples, polished strewn slide and mounted grains, and for two polished ore samples. The used settings for the analysis were:

- Acceleration voltage: 15 kV
- Electrical current: 10nA
- Electron source: tungsten tip

In the analysis the used imaging methods were Back Scatter Electrons (BSE) (also named COMPO), Secondary Electrons (SE) and Energy dispersive x-ray (EDX). In all investigations special respect was given to high density mineral phases, with the aim to detect As within ore. Therefore, mainly BSE pictures were used where phases with a bright contrast give a clue for a high density. SE was mainly used to visualize structures of the sediment grains.

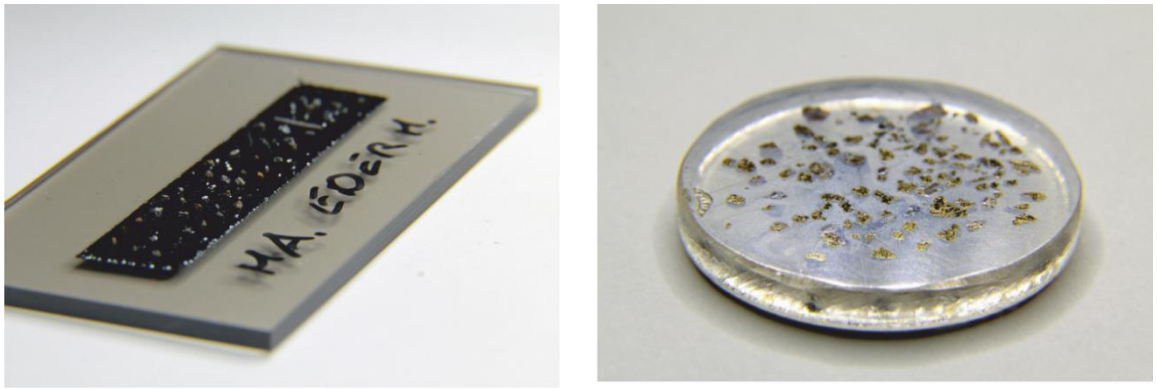

Figure 14: Prepared samples for the electron microscopy. Left: mounted strewn slide; Right: polished ore sample embedded in epoxy resin.

Geochemical digestion

To determine the chemical composition of the sampled rocks a geochemical digestion was performed. Then the digested samples were measured at the Chemical Institute at the Karl Franzens University with a mass spectrometer. Following steps were accomplished for the sample preparation:

First of all, unaltered parts of the samples were cut out, washed and dried in the oven over night at 105°C. In the next step the produced pieces were crushed by hand and then grinded to a fine powder. For the grinding a vibrating disc mill machine (Retsch RS200) with tungsten carbide grinding tool was used. The gathered fine sample powder was then dried again in the oven over night (105°C) and afterwards cooled in the desiccator.

All further steps were done in a clean room at the institute of Mineralogy and Petrology at the Karl Franzens University. First, 50 mg of each sample were weighted, filled into Teflon beakers and mixed with 1 ml HNO_3. During this process sample P2 showed foam reaction at the mixing process, all other samples did not show any reaction. In the next step 2 ml of suprapur fluorhydric were added. The samples were then placed on a heating plate at 50°C, first for 30 minutes with an open lid and then at 180°C with closed lid for two nights. Within this time the Teflon beakers with the samples were slightly moved in the morning and in the evening to avoid a separation of the acid through evaporation and condensation on the lid. As the next step, the beakers were opened and the inside wall and the lids were flushed with ultrapure water. This solution was then again heated up to 110°C with the heating plates until the whole acid solution evaporated. On the next day 1 ml suprapur HNO_3 acid was added and again evaporated, this process was done two times. Then 1 ml suprapur HCl was added and all samples were closed and positioned in an ultrasonic bath for five minutes. After that the samples were again placed on heating plate to evaporate the acid and then refilled with 1 ml of 7 mol HNO_3 acid to dilute the solution. In the last step the samples were diluted with pure water and filled into new plastic vials. The measurement was done at the Institute of Chemistry at the Karl Franzens University Graz by Prof. Goessler. The used device was an ICP-MS (Agilent 7700x).

Data analysis

For the final data interpretation of the geochemical analysis the software GeoChemical Data Toolkit (GCDkit 5.0) after JANOUŠEK et al. 2006 was used. This software is based on the statistic tool R (version 3.4.3) and is able to plot geochemical data from XRF and ICP MS measurements into different available classification diagrams. This software was used for all plots in geochemical analysis.

3.4 PhreeqC

The free hydrogeochemical modelling software PhreeqC was used for modelling the rock water interaction processes within the rock glacier Schöneben. Therefore, the hydrogeochemical, mineralogical and geochemical data was combined in an inverse PhreeqC model.

Inverse Modelling
For an inverse model the initial and final solutions must be known as well as the mineralogy of the rock which is in contact with the flow through water. By using these parameters PhreeqC calculates all possible combinations of dissolution and precipitation of minerals along the flow path, which leads to the development from the initial to the final solution. All possible minerals have to be chosen manually. The final models have to be verified if they are realistic or not (D.L. Parkhurst and C.A.J. Appelo).

Model setup
Solution 1 represents the start solution, in this case an synthetic rain water which was equilibrated with the CO_2 and O_2 partial pressure of the atmosphere (CO_2 = - 3.5; O_2 = - 0.7). Due to low ion concentrations within the rain water it is suggested that synthetic rain water is permissible to use. In the suggested simplified model rain water can easily infiltrate into the rock glacier and the talus formations in the catchment. However, due to the lack of soil most of the rain water at the top of the bare cliffs provide an overland flow, but just till the top of the scree slopes, and then one can assume some kind of interflow as a very fast groundwater flow component till the water infiltrates into the rock glacier. Based on the very short retention time the sparsely occurring soil and the scree slopes have a negligible impact on the alkalinity and the pH value. Thus, it is permissible to use rain water as solution 1. Solution 2 represents the measured hydrogeochemical data of SEQ (SEQ_4, SEQ_5) (Table 5). For the calculation uncertainty limits are necessary, the general limit was 2,5 % and element specific limits were: 2.5 % for Ca, 2 % for As, 2.5 % for Na and 5% for S(6).

SOLUTION 1	
	Synthetic rain water
temp [°C]	2.5
pH	7
pe	4
units	mmol/l
Na	0.007
K	0.01
Mg	0.013
Ca	0.033
Si [SiO_2]	0.006
S(6) [SO_4]	0.033 as SO_4
C(4)	0.06
Cl	0.007

SOLUTION 2		
	SEQ_4	SEQ_5
temp [°C]	2.5	2.4
pH	7.878	7.771
pe	4	4
units	mg/l	mg/l
Na	0.626	0.68
K	0.369	0.4
Mg	0.896	0.954
Ca	10.364	10.825
Si [SiO_2]	1.4	1.517
S(6) [SO_4]	3.8	3.6
C(4)	22	22
As	0.0114	0.0124

Table 5: Solution 1 and 2 of the PhreeqC inverse modelling.

Mineral dissolution/precipitation

The results of the mineralogical investigation were used to determine the reaction phases within the rock glacier. Beside the main phases quartz, feldspar (mainly plagioclase, K-feldspar) and mica (biotite, muscovite), special attention was given to the ore phases. Main ore phases are goethite and chalcopyrite. The main As bearing minerals are arsenical tetrahedrite and arsenopyrite. Because arsenical tetrahedrite is not part of any thermodynamic database in PhreeqC, arsenopyrite was used as arsenic source. Sb was neglected due to its very low concentrations in the water analysis of SEQ_4 and SEQ_5. Simultaneously to As also Fe dissolute, but it does not remain as dissolution component in the water. Due to an oxidizing environment, Fe oxidizes immediately and Fe-hydroxides precipitate. These Fe hydroxides can be ferrihydrite, lepidocrocite or goethite and they indicate a high specific surface, where dissolute As can be adsorbed (Blowes et al. 2003). These adsorption processes cannot be integrated into the inverse model. To compensate the adsorption effect, other mineral phases which were not determined in the mineralogical analysis and probably not occur were integrated in the model to "buffer" the surplus. The chosen "buffer" phase for As is arsenolite (As_4O_6), for S gypsum ($CaSO_4 \cdot 2H_2O$) and for Cu cuprit (Cu_2O). Kaolinite was used as a substitute for probable aluminosilicate precipitations, which are weathering products of feldspar. These dissolution processes release SiO_2 which is precipitated along the flow path as SiO_2 (am-gel) or chalcedony.

Calcite dissolute congruent and as a result CO_2 is degassing. Plagioclase and biotite dissolute incongruent, because of that the Ca and Fe concentration rises. Again Fe precipitates immediately, as well as aluminosilicates similar to allophanes and SiO_2 (am-gel) (Malmström et al. 1996). Chalcopyrite dissolute incongruent and releases sulphur which oxidizes immediately to SO_4 (Lengke et al. 2009).

Initially, the phases in Table 6 were included into the model, in addition some phases were forced only to precipitate or dissolute. The other phases are free for both processes.

Initial Phases	
Phases	**dissolute / precipitate**
CO_2(g)	
As-pyrite	dis
Calcite	
Biotite	dis
SiO_2 (am-gel)	
Chalcopyrite	
Ferrihydrite	
Arsenolite	prec
Plagioclase	dis
Kaolinite	prec
Cuprite	
Chalcedony	
Gypsum	
Muscovite	

Table 6: Initial phases for the PhreeqC inverse modelling.

The "buffer" phases are carbon dioxide (g), gypsum, arsenolite, cuprite and SiO_2 (am-gel). A representation of the complete code is attached at Appendix 4.

4 Results

4.1 Hydrogeochemistry

Regional distribution of As concentrations

Arsenic concentrations of the spring waters in the study area indicate a range from 0.065 to 12.7 µg/l (Table 7). The results show that the highest As concentrations occur at the Schöneben spring, which is situated within the HPS. Other springs with slightly elevated As concentrations, but also springs with no indication for an increased As value are situated within the HPS. However, the Goldlacke spring, which indicates the second highest measured As values also show values above 10 µg/l. But this spring is situated in an area where four different units (Hochreichhart plutonic suite, Rannach formation, Glaneck metamorphic suite and Griesstein Pluton) intersect within the catchment area. Despite the similarities in the As concentration this spring indicates some significant differences in the hydrogeochemical composition (Figure 20). According to the Piper and Schoeller diagrams the water chemistry of all investigated springs is in a hydrogeochemical way quite similar. Nevertheless, the geographical position of high or low As contaminations is not bound to a distinct pattern and occur very locally (Figure 15), also no correlations to specific lithological units or formations are significant (Figure 6). The springs HKAQ1 and KTQ1 indicates very low As concentrations, but first one is situated within the permomesozoic cover (Rannach fm) and, second one is situated in the influence area of the HPS.

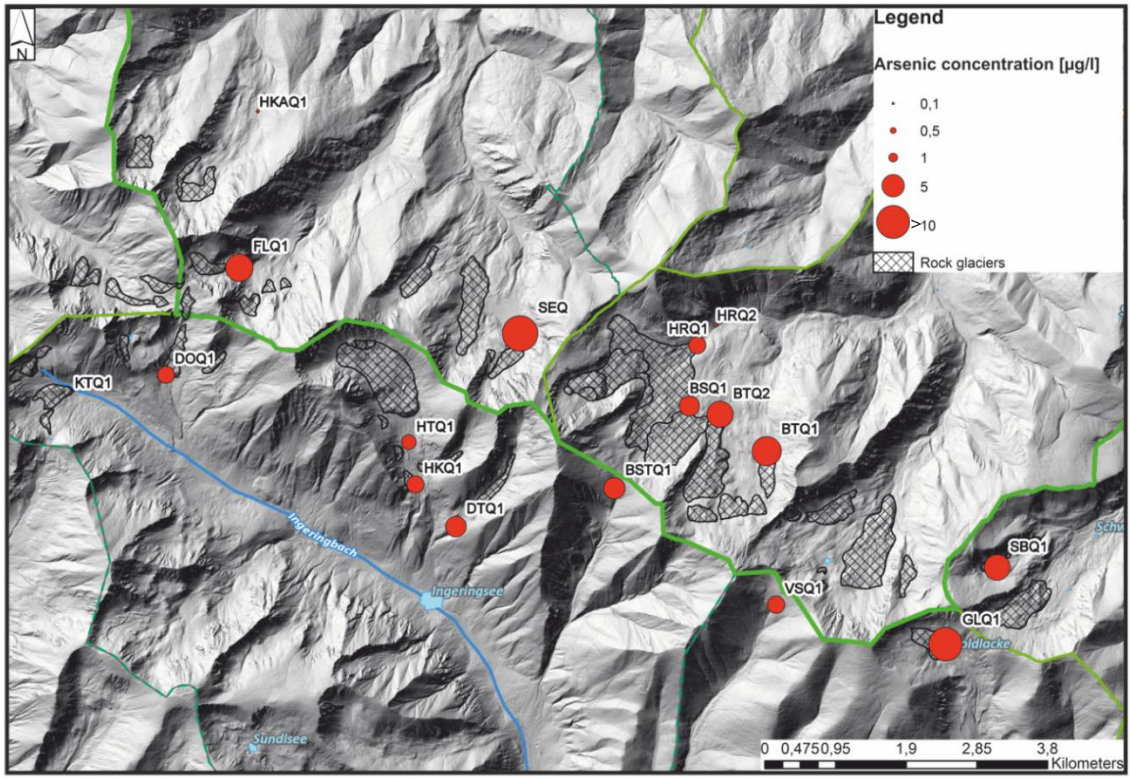

Figure 15**:** Distribution of As concentrations (red dots) at the sampled springs in the investigation area with associated rock glaciers, SEQ and GLQ1 indicates the highest concentrations above 10 µg/l.

Water analysis

The final dataset also includes measurements from previous measuring campaigns, which tracked fewer trace elements. In general, the mineralization is very low, the TDS ranges only from 13.7 to 61.6 mg/l, HCO_3 and Ca indicate the highest element concentrations in all samples. The O_2 content for all samples was at the saturation level.

Spring-ID	Sample-ID	pH	W. T.	LF	Ca	Na	Mg	K	SO_4	Alkalinity	As	TDS
			[°C]	[µS/cm]	[µg/l]							[mg/l]
BSQ1	BSQ1_1	7.21	4.2	41.2	5901	585	161	430	1700	12761.2*	4,2	24.54
	BSQ1_2	7.90	2.3	39.4	6468	587	175	455	1500	15268.3*	4	27.30
BSTQ1	BSTQ1_1	7.24	2.5	27.5	3951	745	157	302	2000	7106.5*	4,7	17.30
BTQ1	BTQ1_1	7.08	4.3	48.8	7780	613	250	606	3700	18056*	8	33.74
	BTQ1_2	7.02	3.9	51.7	8510	679	292	708	4000	19971.4*	7,1	37.01
BTQ2	BTQ2_1	7.25	4.6	48.5	7673	800	266	515	3500	19251.6*	6,6	34.77
	BTQ2_2	7.44	4.4	48.5	8007	788	302	506	4100	18769.7*	6,4	35.57
DOQ1	DOQ1_1a	7.70	3.4	43	7100	500	400	500	3800	17400	4,4	31.71
	DOQ1_2a	7.50	5.4	34	5700	500	400	500	3100	13100	3,8	25.03
	DOQ1_3	7.34	4.4	25.5	3776	448	135	363	1600	9272*	3,1	17.86
DTQ1	DTQ1_1a	7.60	2.7	52	8300	700	400	600	3300	-	5,2	-
	DTQ1_2a	7.50	2.9	45	7800	600	400	500	2900	20000	5,3	34.12
	DTQ1_3	6.95	2.9	51.8	8437	600	348	583	3300	18794.1*	4,5	35.14
	DTQ1_4	7.61	2.9	56.6	9041	597	371	578	3300	22014.9*	4,4	38.63
FLQ1	FLQ1_1a	7.90	2.5	29	5200	400	400	400	1900	12200	7,3	22.44
	FLQ1_2a	7.50	7.4	38	5500	500	400	400	2000	13800	7,9	24.11
	FLQ1_3	7.54	3.2	35.7	5926	465	157	313	2000	12389.1*	7,3	23.86
GLQ1	GLQ1_1	7.59	2.6	35.7	5768	634	176	578	1500	15402.5*	**10,3**	26.54
HKAQ1	HKAQ1_1a	7.70	3.8	78	8800	500	4200	400	1400	42900	0	60.70
	HKAQ1_2	7.92	2.6	36.3	9126	541	4378	145	1300	43261.2*	0,17	61.57
HKQ1	HKQ1_1	7.39	3.6	33.9	5291	559	247	532	2000	12444*	3,2	23.86
HRQ1	HRQ1_1	7.08	4.3	48.8	6388	719	338	431	2600	15664.8*	3,3	29.20
	HRQ1_2	6.68	4.4	41.8	6901	706	326	430	2300	17037.3*	3,7	30.79
HTQ1	HTQ1_1a	7.50	2.1	45	7800	500	400	500	2700	20000	3,6	34.02
	HTQ1_2	7.67	2.9	42	6719	470	326	438	2300	14658.3*	2,5	27.67
KTQ1	KTQ1_1a	7.20	3.8	19	2400	800	400	400	1700	-	0	-
	KTQ1_2a	7.00	3.7	17	2100	700	400	400	1100	10000	0	16.02
	KTQ1_3	7.88	2.5	64.2	2488	689	145	379	940	6270.8*	0,065	13.68
SBQ1	SBQ1_1	7.18	3.3	37.4	6099	679	234	389	1900	11797.4*	6,5	26.48
SEQ	SEQ_1a	7.90	2.3	58	8800	600	700	400	3800	18977.1*	**12,7**	35.34
	SEQ_2a	7.60	2.4	45	7300	600	600	400	2700	20000	**10,8**	33.83
	SEQ_3a	7.60	2.4	49	7500	500	600	400	3000	21400	**11,6**	35.42
	SEQ_4	7.88	2.5	64.2	10364	626	896	369	3800	27395.1*	**11,5**	46.29
	SEQ_5	7.77	2.4	65.1	10825	680	954	400	3600	29499.6*	**12,4**	48.91
VSQ1	VSQ1_1	6.78	2.4	25.8	3649	745	149	348	2700	7344.4*	3,2	17.69

*values are calculated with PhreeqC

Table 7: Major constituents, As concentration and in situ parameters of the taken samples. The high-lighted values are above the WHO guideline value (10 µg/l). The suffix a means that this sample was taken in a previous sampling campaign and was also measured at another laboratory.

The pH values of all samples are near neutral with a range from 6.7 to 7.9, the temperatures are generally low with 2.4 to 7.4 °C. It must be noticed that only two samples exceeded 5 °C. Due to the low mineralisation the conductivity indicates low values with a range from 17 to 78 µS/cm. The As concentrations range from below the measurement limit (<1 µg/l) up to 12.70 µg/l. The highest As concentrations were measured at SEQ and GLQ1 (Figure 15, Table 7). A detailed table with all measurements is shown in Appendix 2.

Water types can be differentiated through their hydrochemistry. In this thesis Piper plots, a Schoeller diagram and scatter plots were used for the characterisation. The results give an overview of the major cations and anions in the water samples. Later the differences between the samples are represented.

For all spring water samples, a classification of the hydrochemical facies was applied (Figure 16). Regarding to the Piper diagram all investigated spring water samples indicate the calcium-bicarbonate type. The samples KTQ1, HKAQ1 and VSQ1 show a slightly different behaviour (Figure 16).

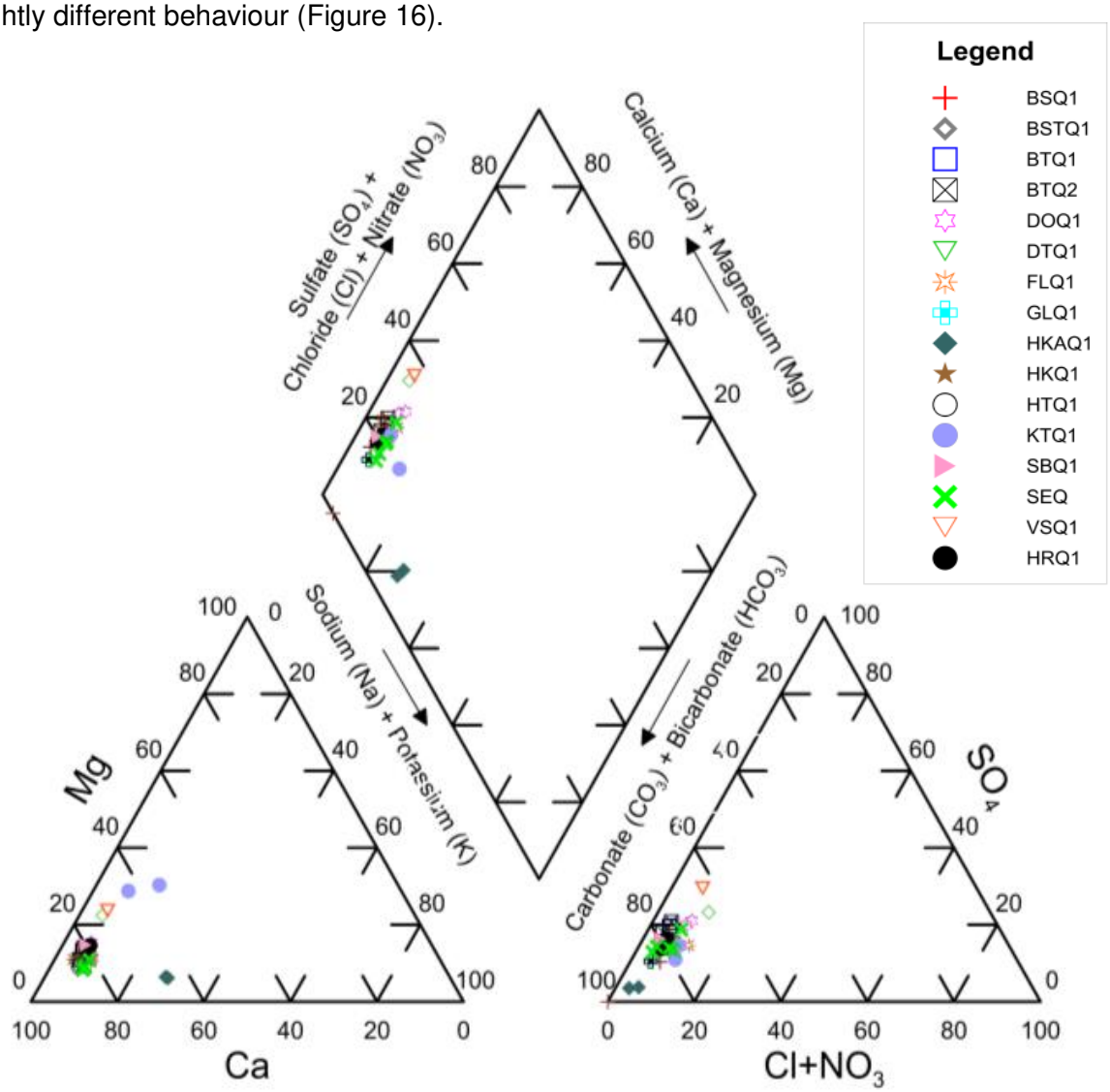

Figure 16: Piper plot of all investigated samples.

The Schoeller diagram for the different spring waters in the Seckauer Tauern Range confirms the previous results that the different samples show a similar hydrochemistry. Exceptions are KTQ1, HKAQ1 and SEQ which indicate differences at Mg, K and Ca. HCO_3 and Ca are dominant in all samples (Figure 17).

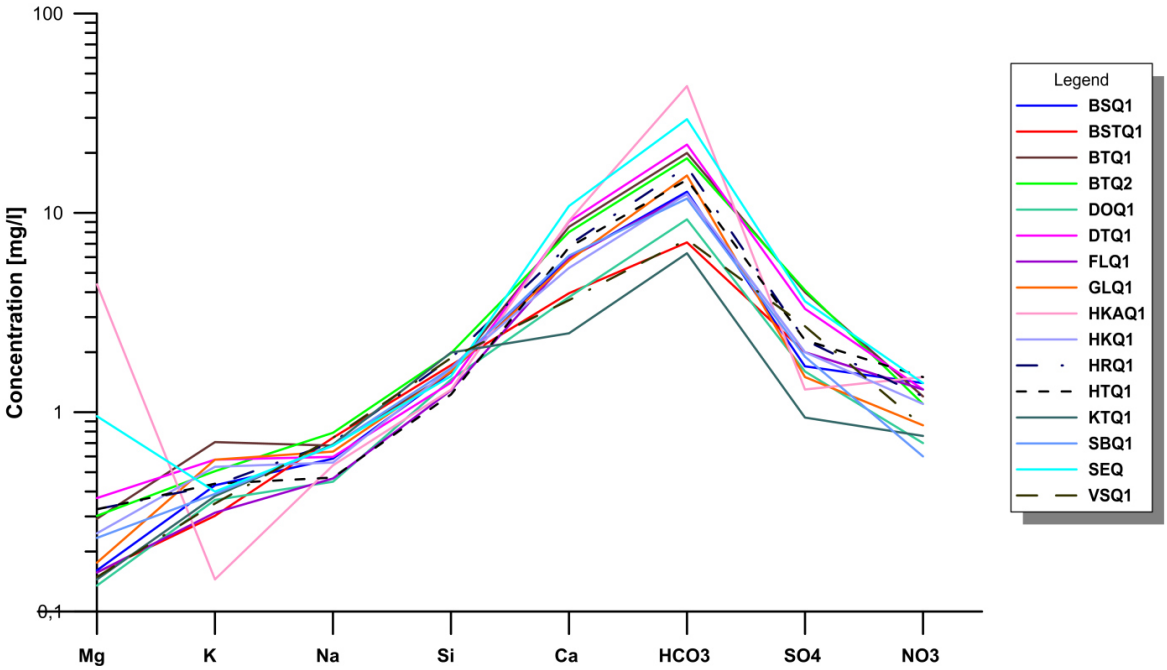

Figure 17: Schoeller diagram of all investigated samples.

Plotting measured elements and field parameters against arsenic indicates only few significant linear correlations. Some trends of minor elements are visible.

Regarding the correlation with in situ parameters and As, the comparison of pH values indicates that “high” As concentrations occurred with higher pH values. However also low As concentrations occur with high pH values, but high As values did not occur with low pH values. All further parameters show no significant correlation (Figure 19). Noteworthy for the major constituents are the samples HKAQ1 and KTQ1, which indicate in general the lowest As concentrations and show a wide range in respect to the major constituents, from the lowest to the highest concentrations. HKAQ1 has the highest concentrations of all samples of Mg, Sr and HCO_3, whereas KTQ1 has the lowest concentrations of Ca, SO_4 and HCO_3. The spring water SEQ indicates the highest As and Ca concentrations. For the Ca and Sr concentrations a weak positive trend is visible.

Within the minor constituents the As concentrations indicate a trend with Mo and Sb concentrations (Figure 21, e,f), except for GLQ1, Fe, Mn, Si and Sr concentrations seem to be not connected to the As concentrations (Figure 21, a - d). Plotting Ca and Mg against HCO_3 and SO_4 revealed that all samples plot near the transition between carbonate to silicate weathering. Nevertheless carbonate weathering could be seen as the dominant process (Figure 18). This indicates an influence form both weathering processes, therefore this spring could be characterized as a crystalline spring with a very low mineralization and an influence from carbonate dissolution.

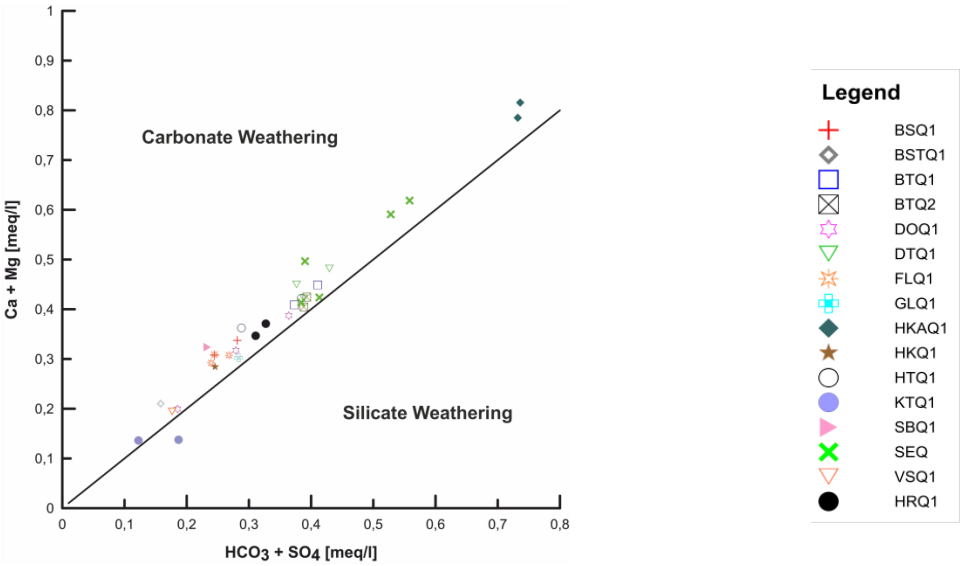

Figure 18: Scatter plot to determine the weathering type.

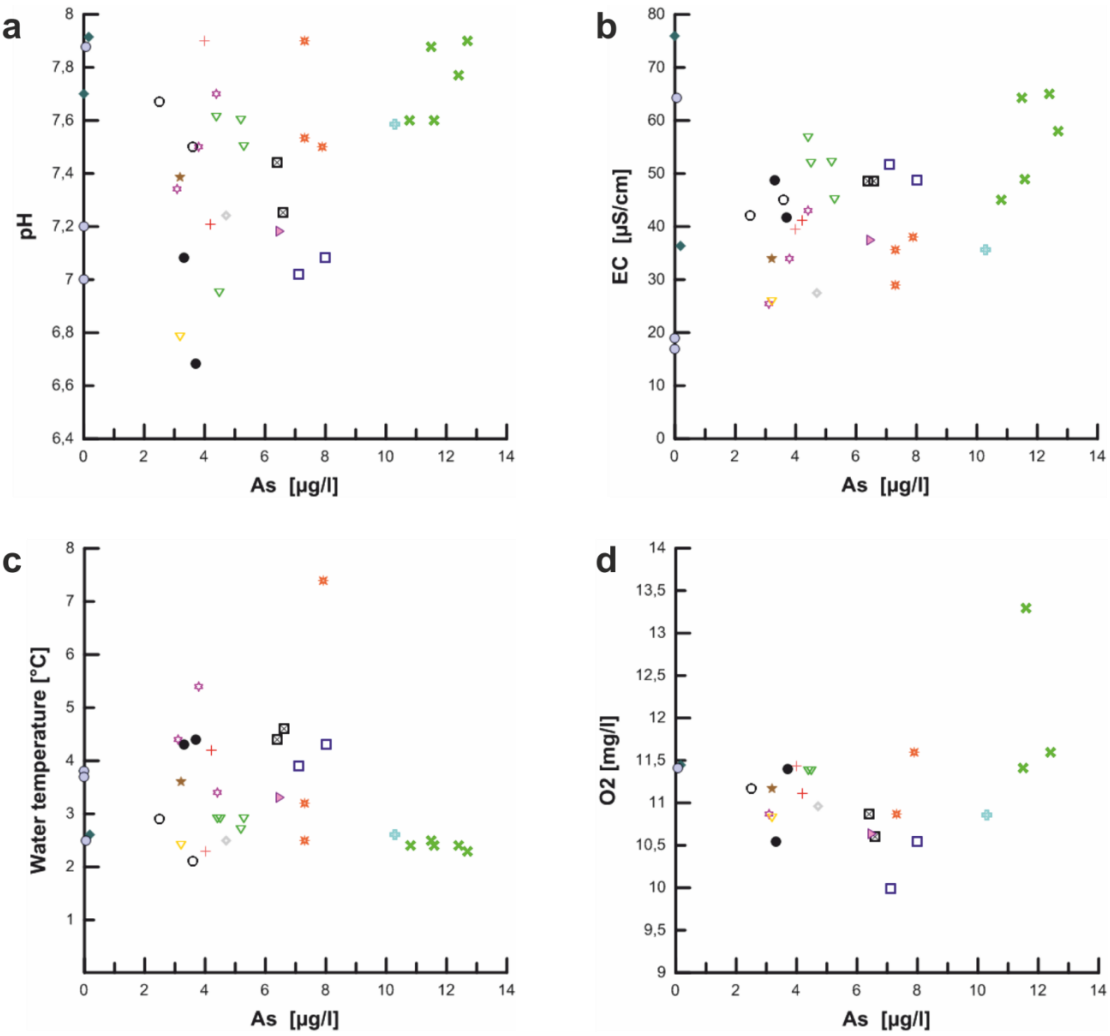

Figure 19: In situ parameters plotted against As concentration.

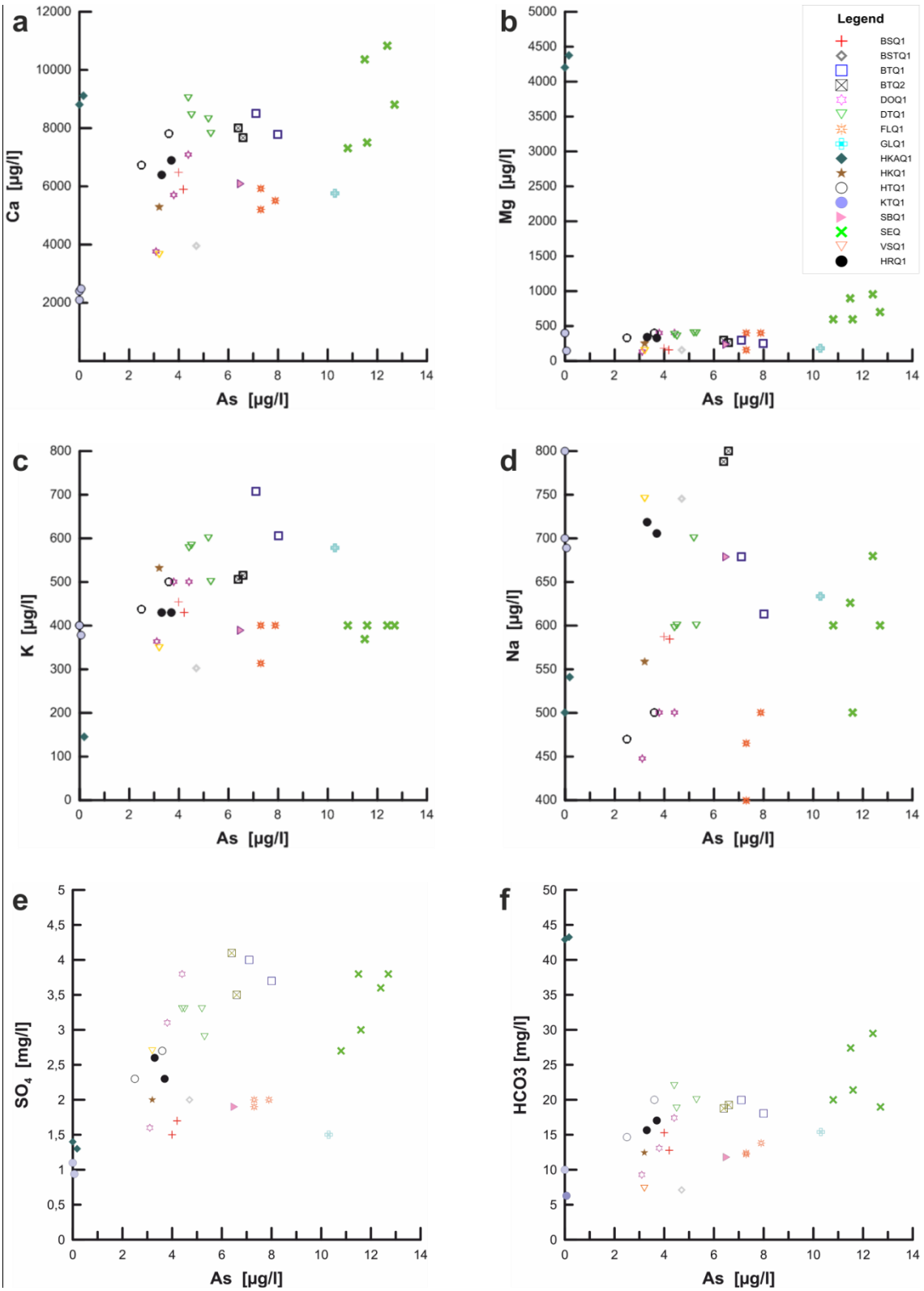

Figure 20: Scatter plot of the major element concentrations of the samples against As concentrations.

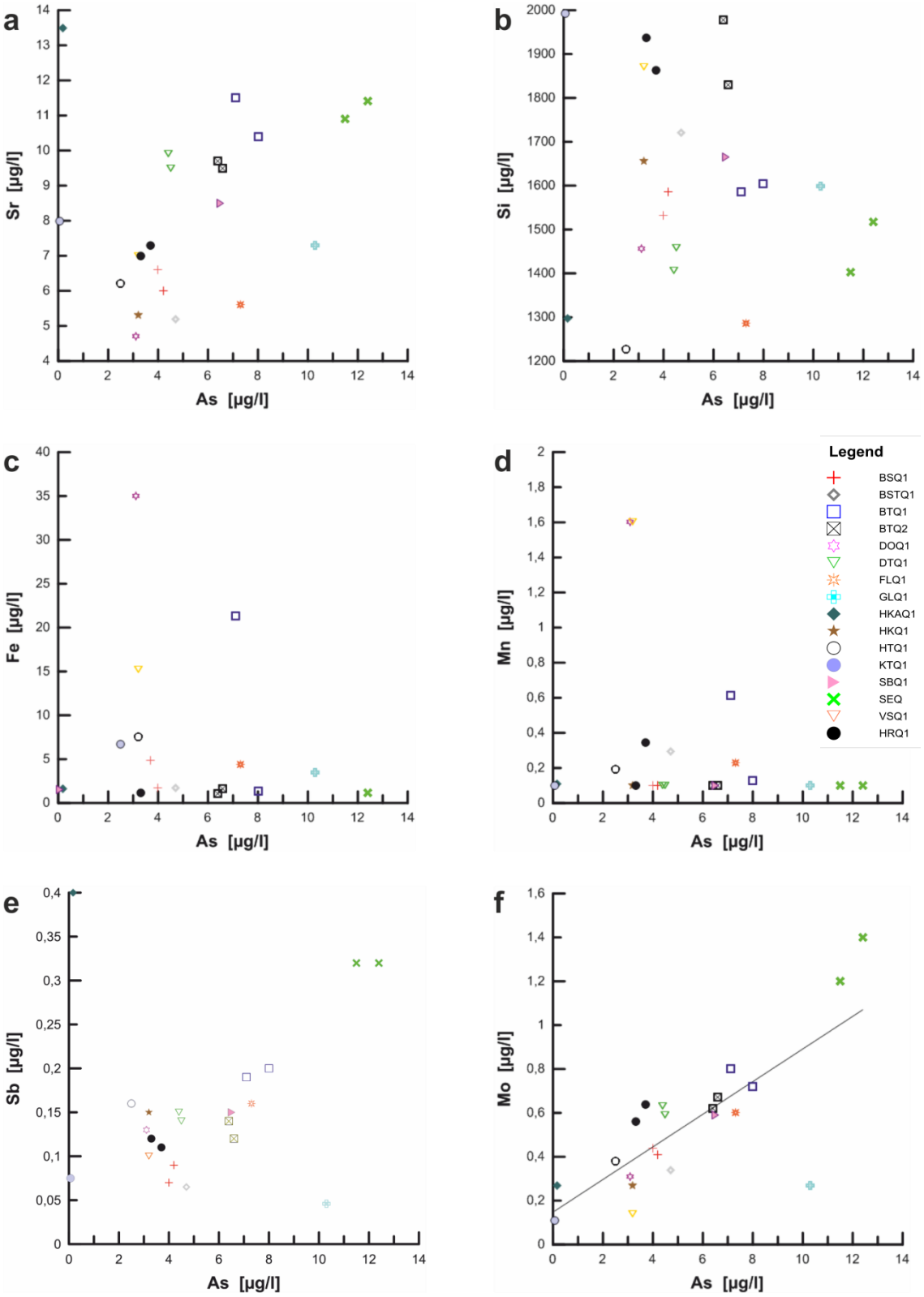

Figure 21: Scatter plot of the minor element concentrations of the samples against As concentrations.

4.1.1 Stable Isotopes

δ^2H, $\delta^{18}O$:

Isotopic data of the investigated springs indicate a Local Meteoric Water Line (LMWL) with slightly higher δ^2H values than the Global Meteoric Water Line (GMWL). Long term measurements of previous projects from the SEQ spring (2009 – 2017) also show a LMWL (Equation and Figure 22). Due to a good correlation between the long-term values of SEQ and the values from the recent investigated springs, they can be merged and seen as one LMWL.

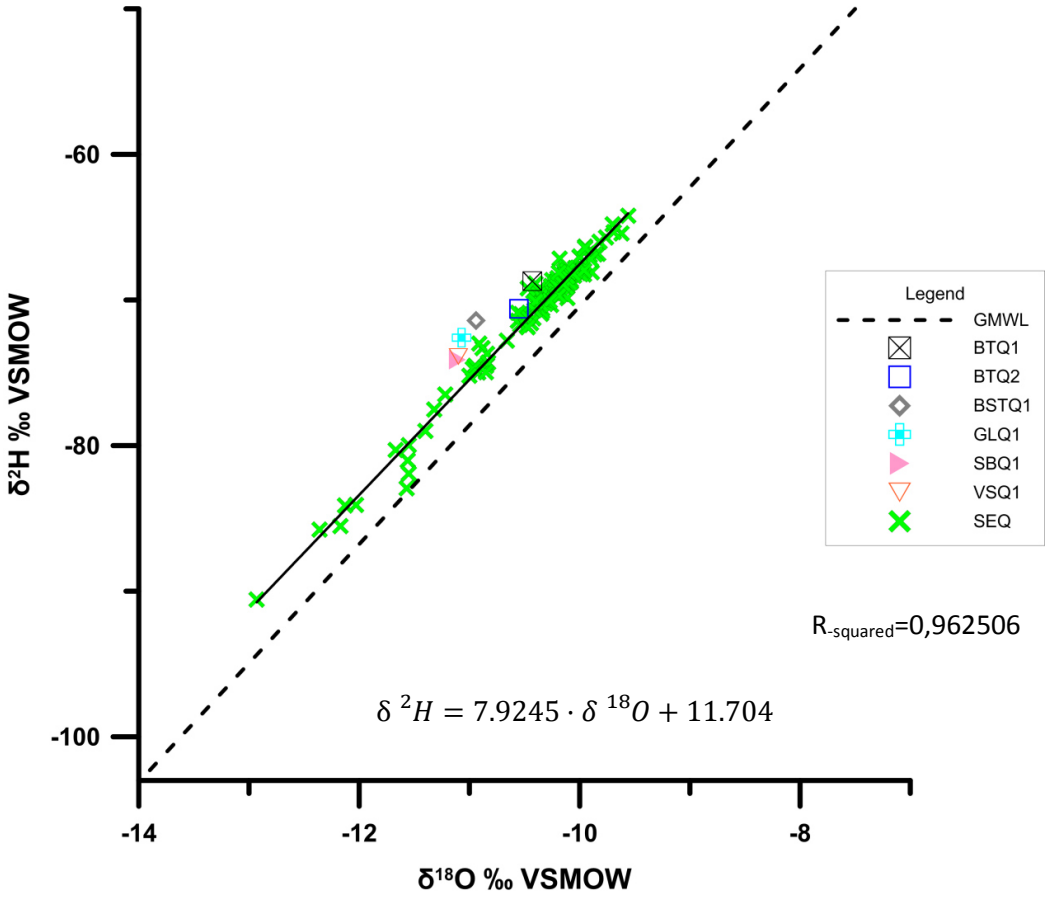

Figure 22: LMWL of all measured springs including SEQ Data from previous projects. The dashed line represents the GMWL ($\delta^2H = 8\ \delta^{18}O + 10$) after Craig 1961. The equation describes the linear relationship of the LMWL including all samples.

$$\delta^2H = 7.7508 \cdot \delta^{18}O + 10.004$$

Equation 7: Linear relationship of the LMWL from the SEQ (data is from previous projects and recent measurements 2009 – 2017).

^{34}S

The measured sulphur isotopes from the spring SEQ reveal a nearly neutral δ ^{34}S (VCDT) value of - 0,2 ‰. The following figures show this measured value in relation to δ ^{34}S literature data of different rocks and deposits. According to Krouse 1988, modern seawater sulphates, ancient marine evaporites and marine dimethylsulfide do not correlate with the measured value. Other sulphate sources after Krouse 1988 indicate a correlation for very different sources, but best for biogenic pyrite (). However a comparison with the work of Weber and Cerny 1997 obviously shows, a correlation of the measured ratio with different sulphide ore deposit ratios in Austria (Weber and Cerny 1997) (Figure 24).

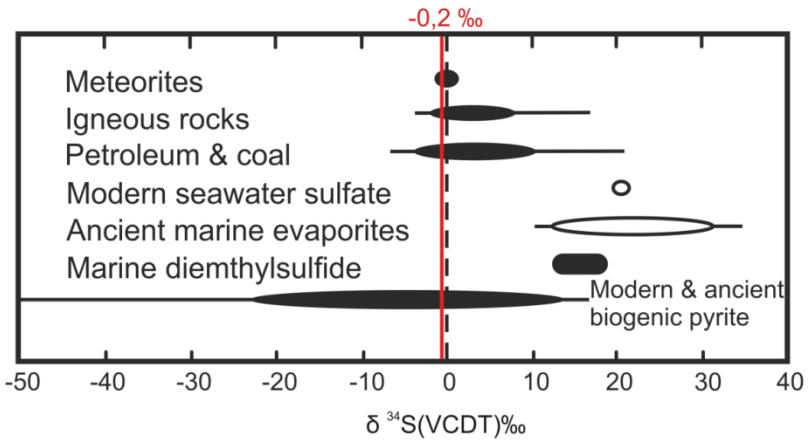

Figure 23: Sulphur isotope ratios of different rocks and the measured sample from SEQ (red line), modified after KROUSE 1988.

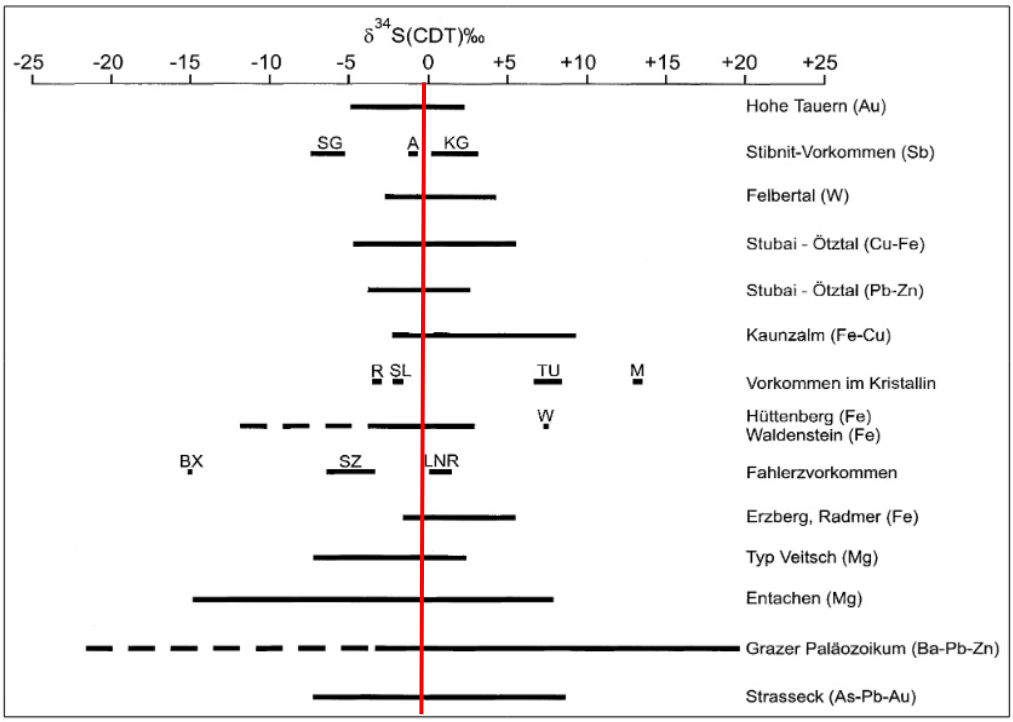

Figure 24: Distribution of sulphur isotope ratios of ore deposits in the eastern Alps and the measured sample from SEQ (red line), SG = Schlaining – Goberling; A = Abfaltersbach; KG = Kreuzeck-Goldeckgruppe; R = Ramingstein; SL = polymetallischer Erzbezirk Schladming; TU = Treffen – Umberg; M = Moosburg; W = Waldenstein; BX = Brixlegg; SZ = Schwaz; LNR = Leogang; Nöckelberg; Röhrerbühel, modified after (Weber and Cerny 1997).

4.2 Petrography

4.2.1 Electron microscopy

The electron microscopy analysis of the concentrated polished sediment sample SEQ revealed different kinds of ore and accessory minerals. The oxides, magnetite and titano-magnetite represent the dominant fractions, in minor quantities also Ilmenite occurs. The minor mineral fraction consists of titanite, zirconite, rutile and garnet (Figure 25). Although the sample was concentrated in heavy minerals the main components in the sample were silicate minerals like feldspar (albite and K-feldspar), mica (biotite and muscovite) and quartz. This indicates a low content of heavy minerals within the sediment sample. No sulphides were detected and no mineral with a significant amount of As.

The following BSE pictures show some microscopy results of the SEQ sedimentary sample:

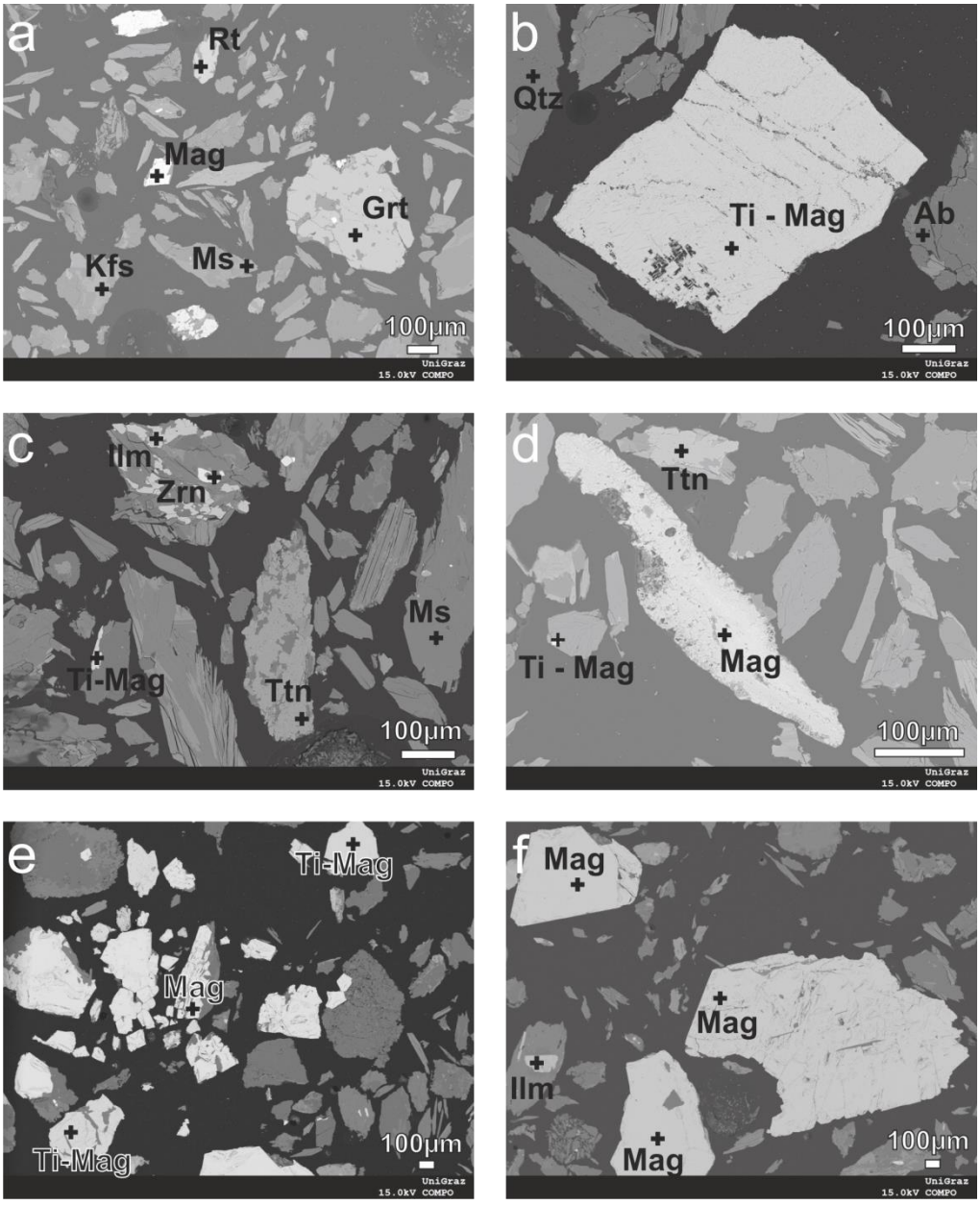

Figure 25: BSE pictures of the enriched sediment sample, main phases with high density (brighter) are mainly ore phases.

Sediment sample whole grains
In addition to the polished sediment sample also selected grains were mounted on an adhesive film. This analysis method revealed additionally to the chemical composition of the grains an insight into the idiomorphically grown crystal structures of the grains.

The analysis shows that magnetite and titano-magnetite with octahedral shape (Figure 26 a, b, c) are the dominant accessories. Additionally, non-idiomorphic shaped silicate minerals with small parts of ores (Figure 26 d), occur. To summarize, the results of the polished sediment samples are confirmed. The main constituents are magnetite and titano-magnetite.

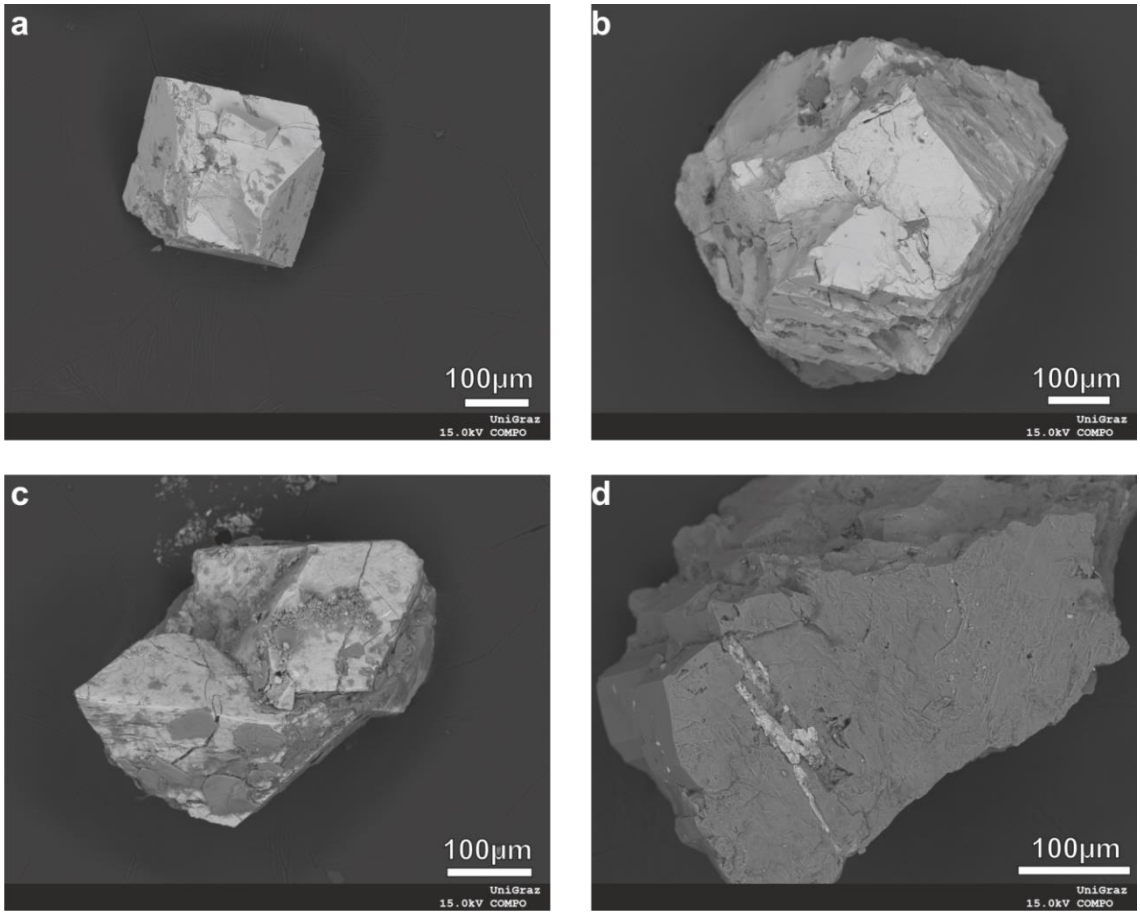

Figure 26**:** BSE pictures of some selected grains out of the enriched sediment sample. The dominant phases are magnetite and titano-magnetite which appear idiomorphic (a, b, c). Picture d represents a silicate mineral with some small ore components.

4.2.2 Geochemistry

Since it is suggested that the rocks within the catchment area reflect the internal composition of the relict rock glacier Schöneben, eight rock samples were taken, to determine their main mineral composition, the geochemical composition and a possible As source.

The samples indicate a SiO_2 composition ranging from intermediate to acidic with a slightly to strong deformation. Orthogenetic metagranites and granite gneisses dominate, however P6 indicate a paragenetic source (Rannach formation). Within these rocks also two samples from a discordant dike were taken, which show a different geochemistry. The fractionation of Rb to Sr after Clark and Černý 1987 indicate that the ratios of the samples are mainly > 0.45 (2.56 - 7.84), except the sample P2 (0.13).

The petrographical classification was applied to compare the rock samples with previously works around the investigation area (Mandl et al. 2018; Pfingstl 2013; Raab 2015). For the classification of the magmatic series different diagrams were used. The results indicate a Calc-Alkaline trend, exceptions are P2 and P7. Most of the samples indicate a peraluminous character, except for P6 (Rannach fm) and P2, which show a metaluminous character.

Plotting the results in the TAS diagram (after (Middlemost 1994) indicates that most of the samples plot in the granite field (P3, P5, P7, P8). Other types are quartz monzonite (P4), granodiorite (P2) and quartzolite (P1, P6) (Figure 29).

The results of this classification confirm the results of previous studies around this area.

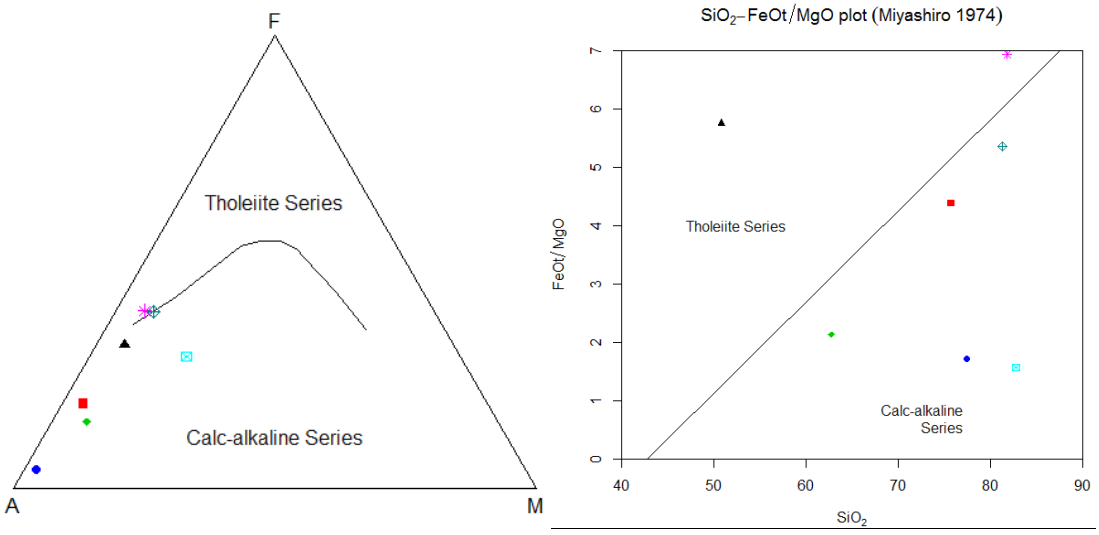

Figure 27: Classification diagrams for magmatic rocks, to differentiate between Tholeiite series and Calc-Alkaline Series. Left: after Irvine and Baragar 1971, Right: after Miyashiro 1974.

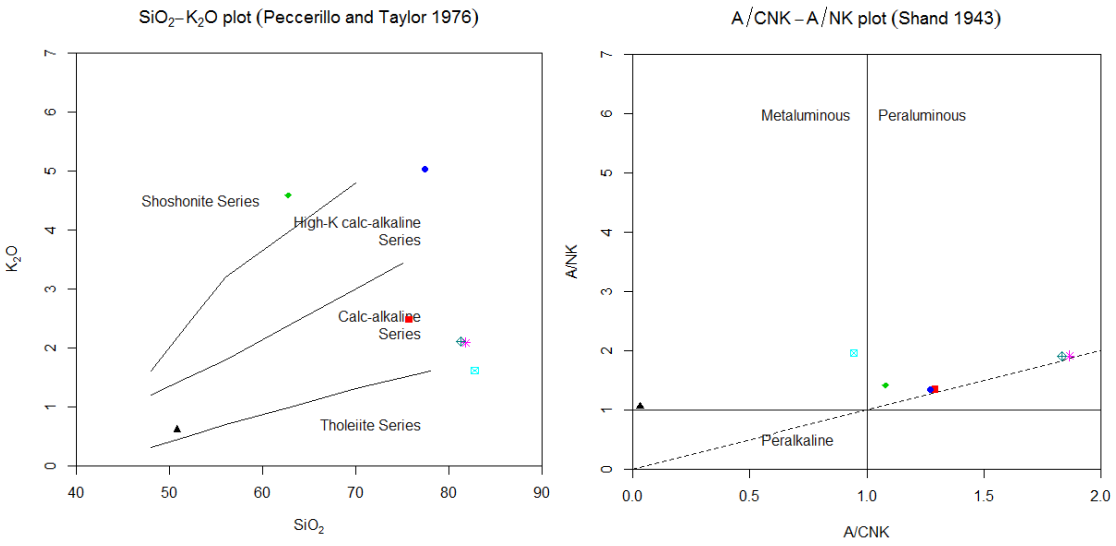

Figure 28: Left: Magmatic classification after Peccerillo and Taylor 1976 . Right: Differentiation between Metaluminous, Peraliuminous and Peralkaline after Shand 1943.

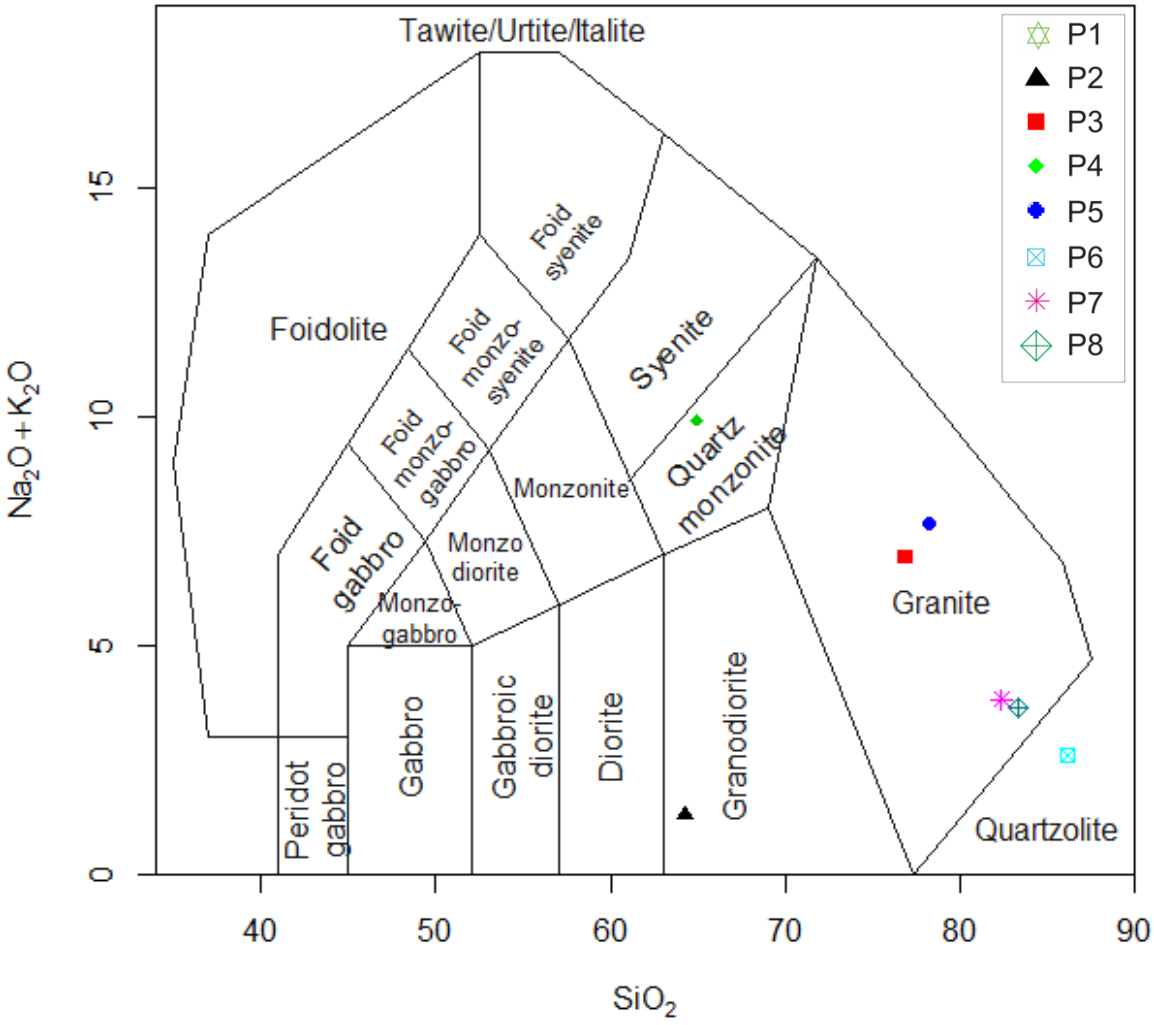

Figure 29: TAS diagram (Middlemost 1994) with the plotted geochemical samples. Since P1 was characterised as a pure quartzite dike rock, it is not plotted within this diagram.

Harker diagrams

Plotting major ions against SiO_2 indicates some significant trends, which are recognisable for Al_2O_3, Na_2O and P_2O_5 (Figure 30). Sample P2 shows a different geochemical composition with the lowest concentrations of ions, except for Ca and FeOt (sum of iron oxides). The minor elements show a similar picture as the major elements, where again P2 indicates a differet behaviour. In this case, it is enriched in Sr, Ba, Sb and As, however for most of the others ions it shows the lowest concentrations (Rb, Co, Cr, Be, Nb, Th). Additionally, P7 is enriched in most of the trace elements in relation to the other samples, especially for rare earth elements Ce and La (Appendix 3). For the other samples trends are visible for Be, Nb and Th (Figure 31). The As content in sample P2 indicates a one to three orders higher concentration then the other samples. P2 is the only sample which contains Sb in a significant amount. Furthermore it is enriched in Sr, Ba, Pb, Cu and depleted in Th, Li, Be, Nb and Ga.

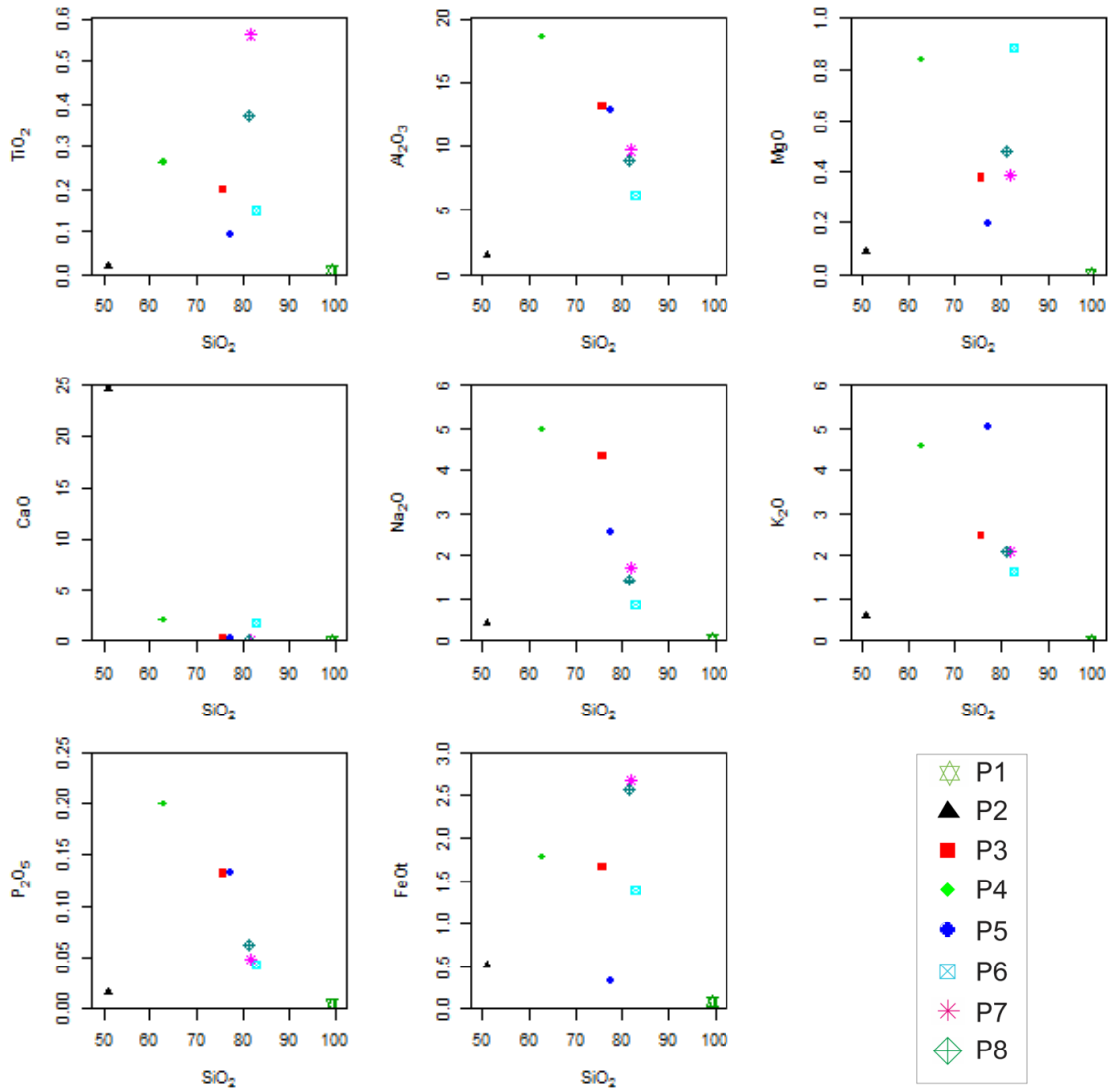

Figure 30: Harker diagrams of the major ions against SiO_2 in mg/kg.

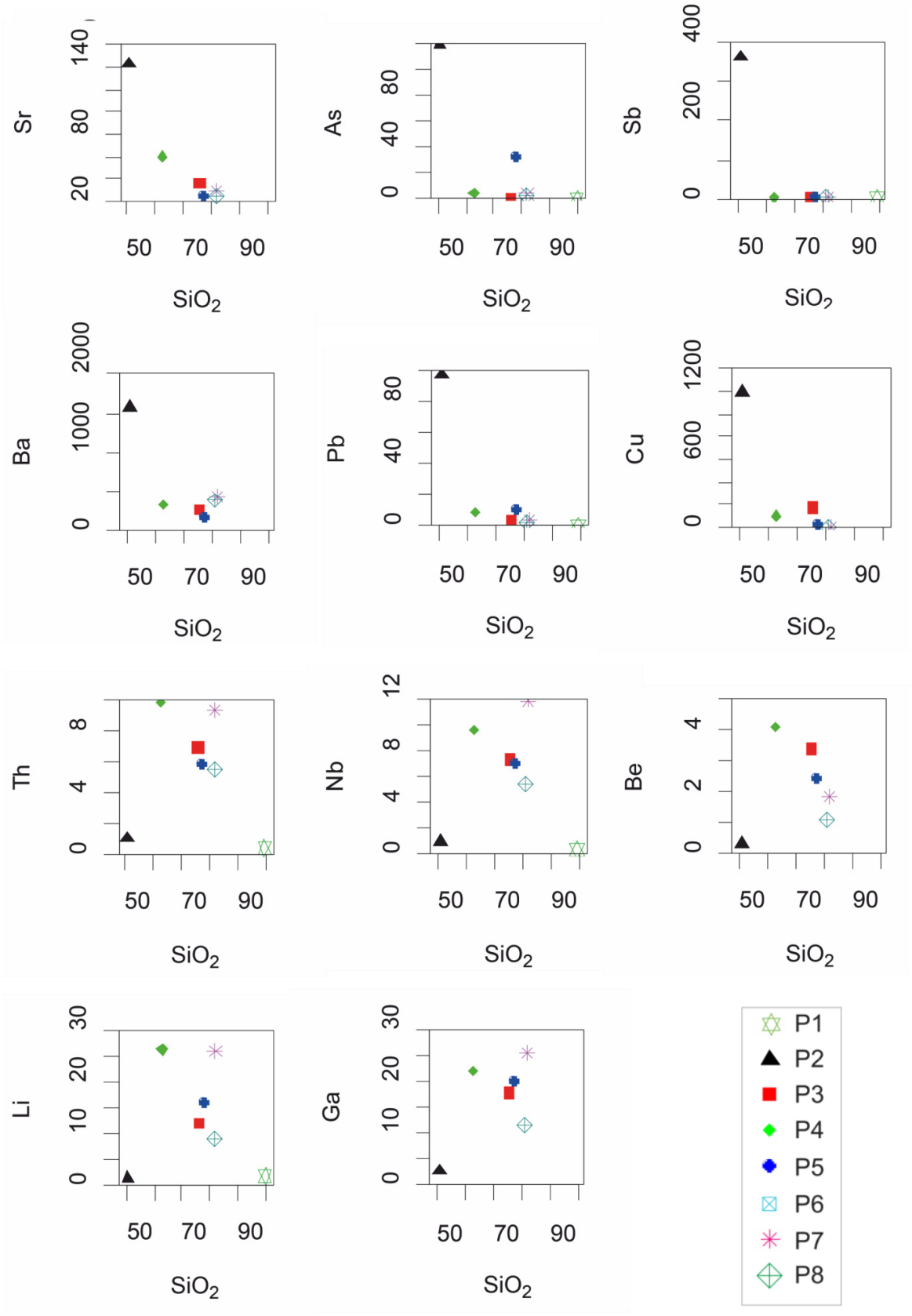

Figure 31: Harker diagrams of the minor ions against SiO_2 in mg/kg.

4.2.3 Mineralogy

The geochemical and mineralogical analysis indicate that the sample P2 has a significant amount of As bearing minerals. Thus, sample P2 was further investigated than the other samples.

P1

This sample was characterised as a quartz dike rock, it has no further relevance for this thesis and therefore a detailed petrography was not applied.

P2

The in situ position of this sample was in the contact zone to a quartz dike (Figure 32). Strong alteration marks on the surface and the HCl test suggested that the sample is a carbonate rock. The white matrix contains mainly blue, sometimes green minerals from millimetres to centimetres size and metallic shining greyish to yellow ores. Further investigations in the laboratory confirmed this, first assumptions. The matrix consists of a carbonate quartz mixture, which contains in lower quantities also feldspar. Occurring ore minerals are mainly Chalcopyrite, Arsenical Tetrahedrite and the green and blue minerals are malachite and azurite. Further accessories are baryt and titanite (according to the qualitative chemical analysis by electron microscopy).

Generally, the sample P2 is a compact holo-crystalline-porphyritic, phanerocrystalline rock. The main crystal shape is hypidiomorph with a fine to middle grain size (0.1 – 5mm). Deformation processes are not visible in the thin sections (Figure 35). Calcite and quartz minerals are in the range of 0.01 to 5 mm size and show no distinct distribution, the smaller fraction creates the matrix. Feldspar minerals are characterised as K-feldspar and altered plagioclase. The ore minerals are also randomly distributed in the matrix and reach seldom millimetre size, mainly they are smaller than 0.5 mm.

Regarding to the TAS diagram (Figure 29) this intermediate acidic rock is characterised as a granodiorit.

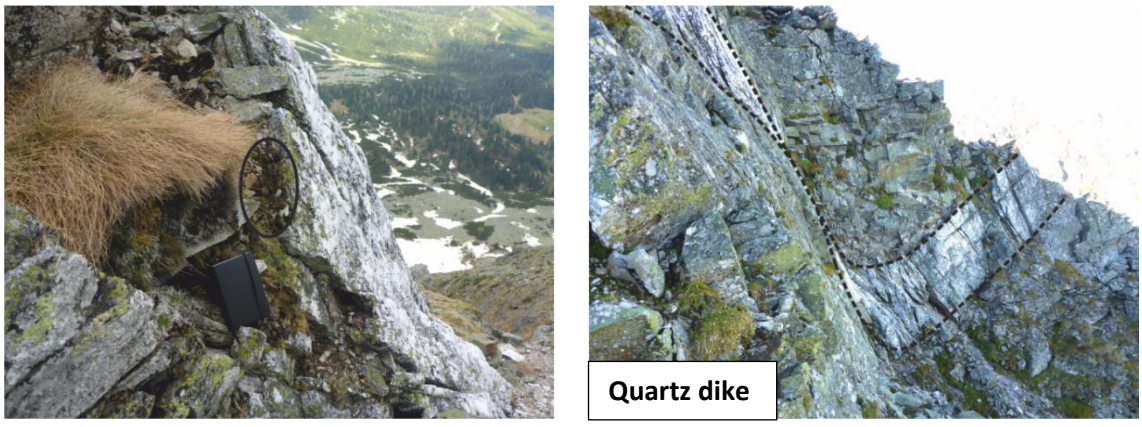

Figure 32: Left: In situ position of the sample P2. The sample was situated in the contact area to a quartz dike. Right: Quartz dike in the catchment area of SEQ, the dashed lines show the borders.

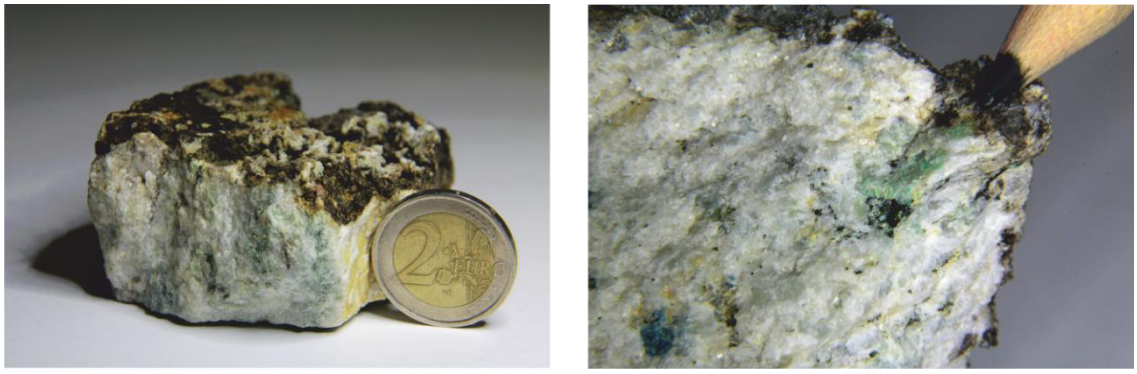

Figure 33: Hand piece of the sample P2. Left: Size relation of the sample P2 with a coin. Right: Malachite (green) and azurite (blue) minerals in relation to a lead pen.

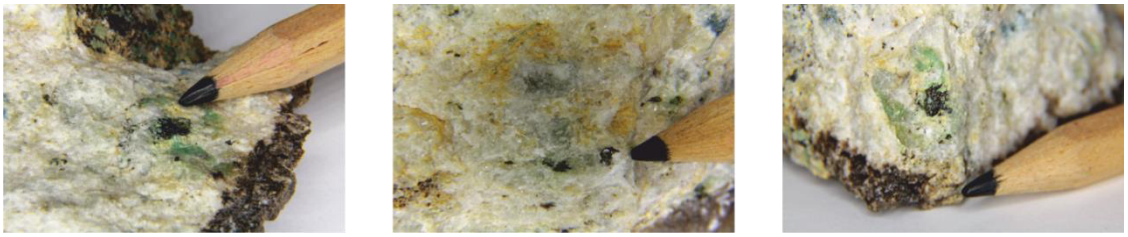

Figure 34: Different pictures of a hand sample with a fresh fracture plane. Grey shiny minerals (probably tetrahedrite) in relation to a lead pen.

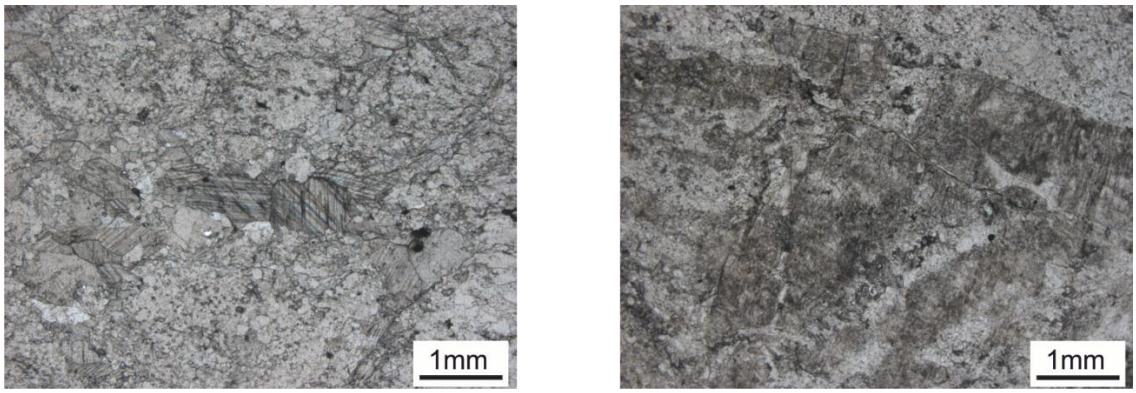

Figure 35: Linear polarised pictures of the sample P2. Left: Calcite crystals in the middle with the obvious cleavage. Right: probably altered feldspar.

Arsenic phases

The main As bearing phase in this sample is the arsenical tetrahedrite ($Cu_6[Cu_4(Fe,Zn)_2](Sb,As)_4S_{13}$), a variety of the tetrahedrite which is a copper antimony sulfosalt (Figure 34). This cubic mineral forms a massive phase which seems to be a "core". It acts like a "core" because in this case all investigated phases indicate a Cu, As and Fe rich alteration margin (Figure 36, b-f) with higher As and Fe but reduced Sb concentrations and no S. The margin can be differentiated into several layers which may indicate different alteration stages (Figure 36, c). They show different geochemical compositions, but no distinct trends. In lower concentrations Ag, Zn, Mo and Bi are

contained in the margin. Table 8 shows an example of the chemical composition of a “core” and points on the margin from the phase. For the values in Table 8 it has to be considered that the geochemical analysis was applied with EDX, which indicates a significant error for the absolute values. For all chemical analysis see Appendix 5.

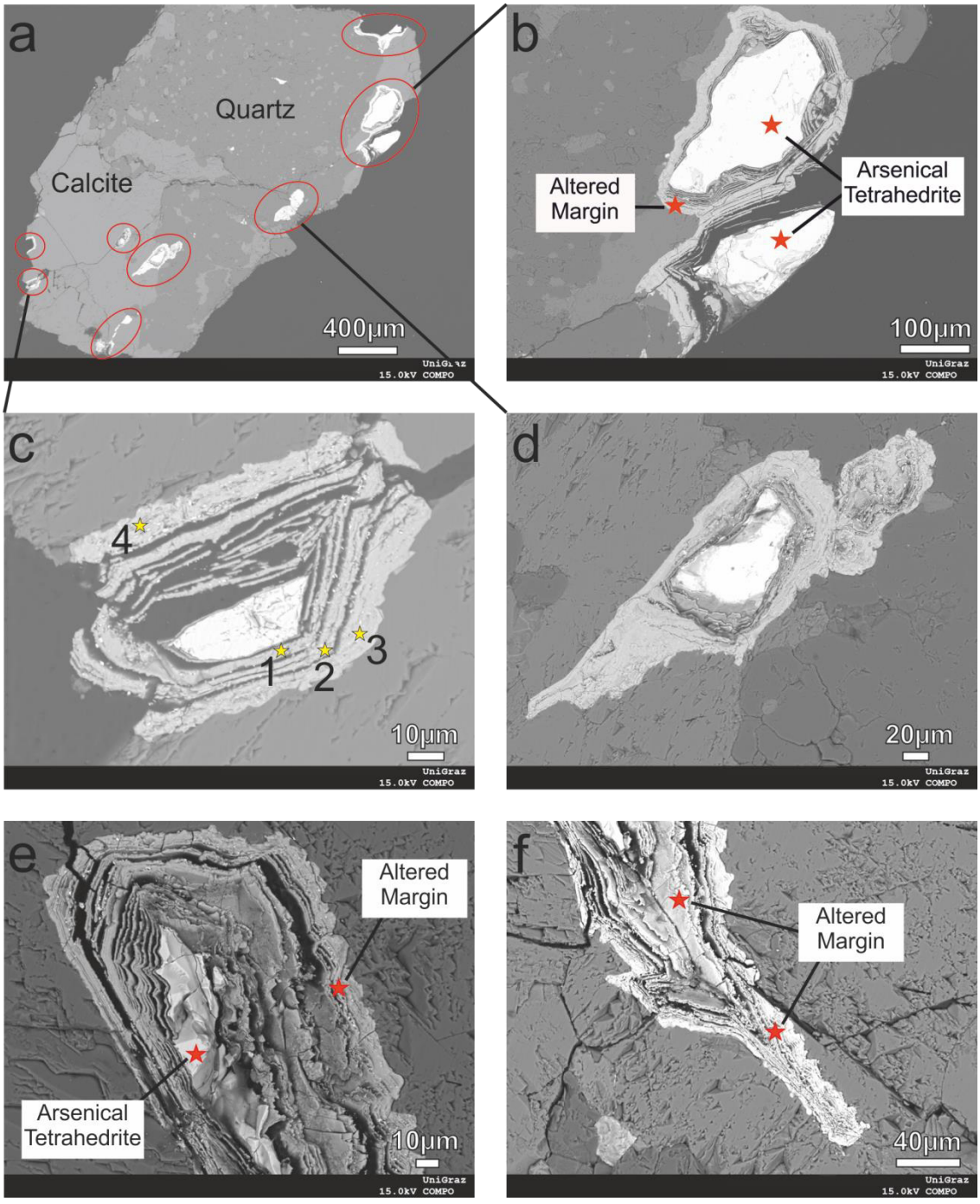

Figure 36: BSE pictures of arsenic bearing ore minerals within the sample P2. The margin itself indicates a differentiation into chemical different layers, which is shown in c and the related Table 8. The numbers 1 – 4 represent measurement points within the margins. Pictures e and f represent one single phase with a clearly visible core and margin structure.

	Fe	Ag	Si	S	Cu	Zn	As	Mo	Sb	Bi	Th
"core"	3.5			29.2	34.7	4.3	3.9		24.5		
1	14.9	3.2	2.7		42.6	2.4	16.3	5.2	6.7	6.1	
2	8.29		2.4		52.8		13.5		23		
3	8.43		2.2		49.3		9.9		25.2		5
4	7.46		2.2		52.9		10.3	4.2	22.9		

Table 8: Example of the chemical analysis from the phase of Figure 36, c, the analysis 1 – 4 represents the margin. This EDX measured compositions just show the relations of the element concentrations, absolute values have a significant error.

Geochemical analysis of this sample revealed in relation to the other samples' higher concentrations of various minor elements and especially high values for Ca, As (119,67 mg/kg), Sb and Cu (Table 9). The bulk As value of P2 is three orders higher than the average As value of the surrounding metagranitoids.

Unit	**[mg/kg]**		**P2**				
SiO_2	234183.46	**Sr**	143.00	**Co**	13.28	**Ho**	1.70
Ca	176485.74	**As**	119.67	**Dy**	9.43	**Tb**	1.54
Al	7441.36	**Ti**	113.87	**Gd**	9.11	**Li**	1.36
K	5005.58	**Zn**	109.70	**Sm**	8.13	**Th**	1.07
Fe	3979.69	**Pb**	97.33	**Yb**	5.82	**Nb**	0.92
Mn	3253.00	**Ni**	38.85	**Pr**	5.51	**Tm**	0.79
Na	3071.29	**Ce**	37.67	**Er**	5.12	**Lu**	0.78
Ba	1588.00	**P**	34.91	**Sc**	4.20	**Cr**	0.49
Cu	1202.00	**Nd**	25.10	**Eu**	2.83	**Be**	0.34
Mg	536.70	**Rb**	18.60	**Ga**	2.80	**Ta**	0.30
Sb	363.38	**La**	15.62	**V**	1.82	**Hf**	0.13
						Mo	0.07

Table 9: Geochemical analysis of the sample P2, the elements are sorted after their concentration. High element concentrations in relation to the other samples are highlighted.

P3

The sample P3 is a compact holo-crystalline-porphyric, phanerocrystalline rock. The main crystal shape is hypidiomorph with a fine to coarse grain size (0.1 – 10 mm) (Figure 37). Main minerals are quartz, feldspar and mica. Accessories are ores (probably magnetite and chalcopyrite). Grain shapes indicates no to very slightly deformation processes. Quartz minerals are in the range of 0.01 to 10 mm size and show no distinct distribution. Feldspar minerals are characterised as altered K-feldspar and plagioclase with a size of 1 – 10 mm in the hand sample they are slightly pink. The main mica mineral is biotite, which occurs mainly within small "dikes". As concentrations are very low with 0.84 mg/kg.

The sample P3 can be classified as a metagranitoid. For detailed geochemical data see Appendix 3.

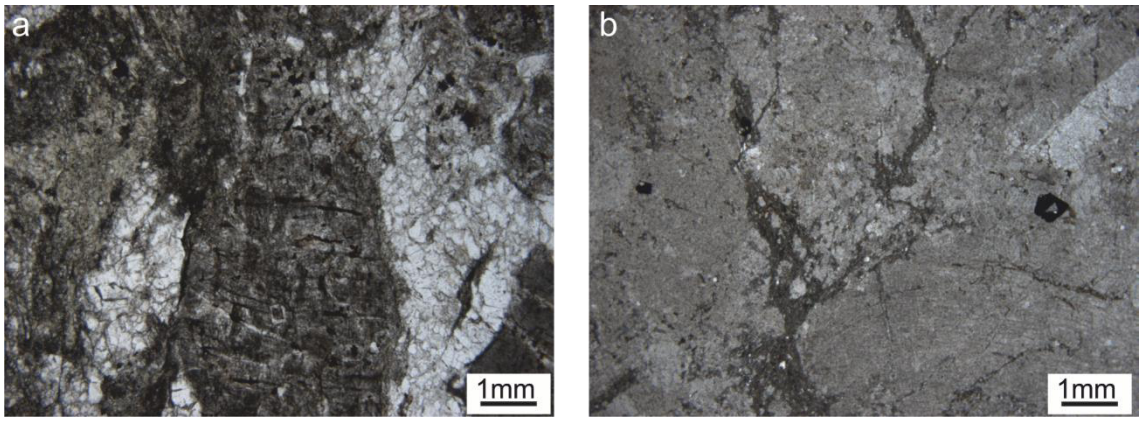

Figure 37: Linear polarised thin sections of the sample P3. a)Tthe white area represents fine grained quartz and the big mineral in the middle feldspar. b) Ore minerals (black) and the "dikes" with biotite.

P4

The sample P4 is a compact holo-crystalline, aphanatic rock. The main crystal shape is hypidiomorph with a fine to coarse grain size (0.1 – 10 mm). Main minerals are quartz, plagioclase, biotite and muscovite. Accessories are ores (magnetite). Grain shapes indicates a slightly to no deformation. Quartz minerals are in the range of 0.01 to 0.5 mm size and show no distinct distribution. Feldspar minerals are characterised as altered, sericitised plagioclase and K-feldspar with a size of 1 – 10 mm. The mica minerals were defined as small grained biotite and muscovite, which occur in small "dikes" and as sericite (Figure 38, a, b).

Arsenic concentrations from the geochemical analysis show a low concentration of 4.05 mg/kg.

According to the geochemical classification this sample represents a quartz monzonite. For detailed geochemical data see Appendix 3.

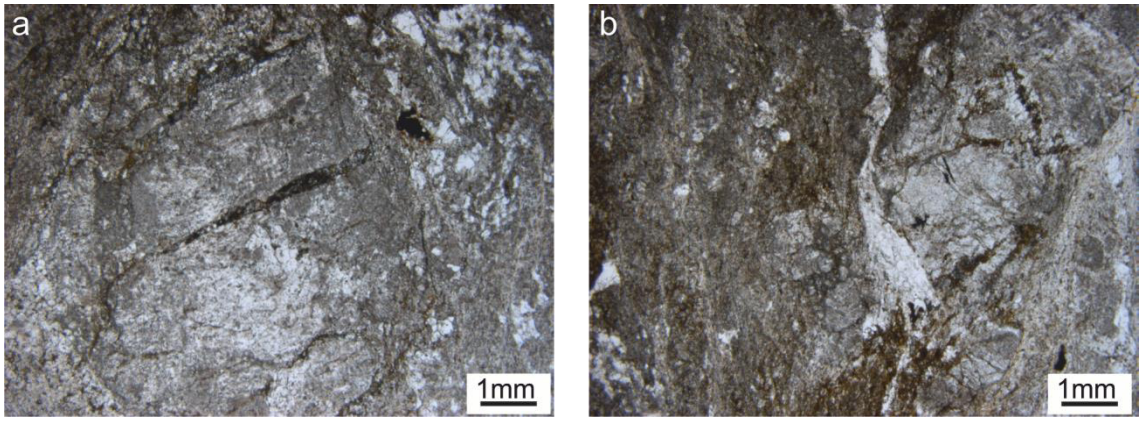

Figure 38: Linear polarised thin sections of the sample P4. a) Altered feldspar grain in the middle, surrounded by muscovite and quartz. b) Altered feldspar grains with biotite and muscovite.

P5

The sample P5 is a compact holo-crystalline, phanerocrystalline rock. The main crystal shape is hypidiomorph with a fine to coarse grain size (0.05 – 8 mm). Main minerals are quartz, feldspar and mica. Grain shapes indicates no deformation processes. Quartz minerals are in the range of 0.01 to 5 mm size and show no distinct distribution. Feldspar minerals are characterised as altered K-feldspar and plagioclase with a size of 1 – 10 mm, in the hand sample they are beige to white. The main mica mineral is biotite, which occurs between the feldspar grains and on alteration planes. Seldom small ore grains (0.5mm) occur as accessories.

Arsenic concentrations from the geochemical analysis indicate a slightly higher concentration of 32.88 mg/kg.

According to the geochemical classification this sample represents metagranite. For detailed geochemical data see Appendix 3.

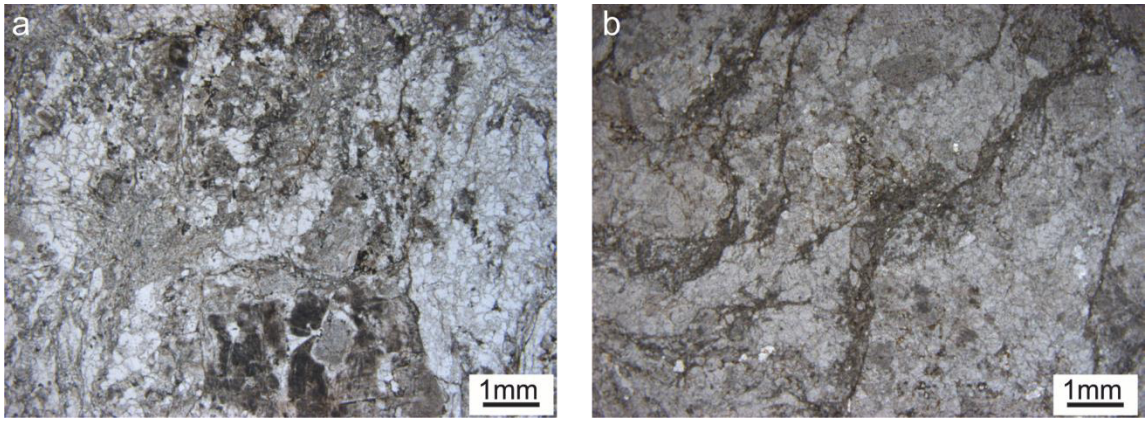

Figure 39: Linear polarised thin sections of the sample P5. a): Altered feldspar grains surrounded by quartz. b): Biotite “dikes”.

P6

The sample P6 is a compact holo-crystalline, phanerocrystalline rock. The main crystal shape is hypidiomorph with a fine to very coarse grain size (0.01 – 40 mm). Main minerals are quartz, feldspar, mica and calcite. Grain shapes indicate a strong deformation with sigma shaped quartz clasts. Quartz minerals are in the range of 0.01 to 40 mm size and indicate an alignment. Feldspar minerals are characterised as plagioclase with a size of 1 – 4 mm. The main mica mineral is muscovite, which is distributed irregular in the matrix with a grain size of < 0.5 mm and occurs also in “dikes”. Calcite minerals indicate a size of 0.5 to 2 mm (Figure 40). The hand sample shows the big quartz clasts, the alignment and parts with red to brown rusty alteration. This sample belongs to the Rannach fm. which is not part of the catchment area of the SEQ.

In the geochemical analysis this sample was not measured in respect to As. According to the geochemical classification this sample represents a Quartzolithe, which is determined as a metasedimentary rock. For detailed geochemical data see Appendix **3**.

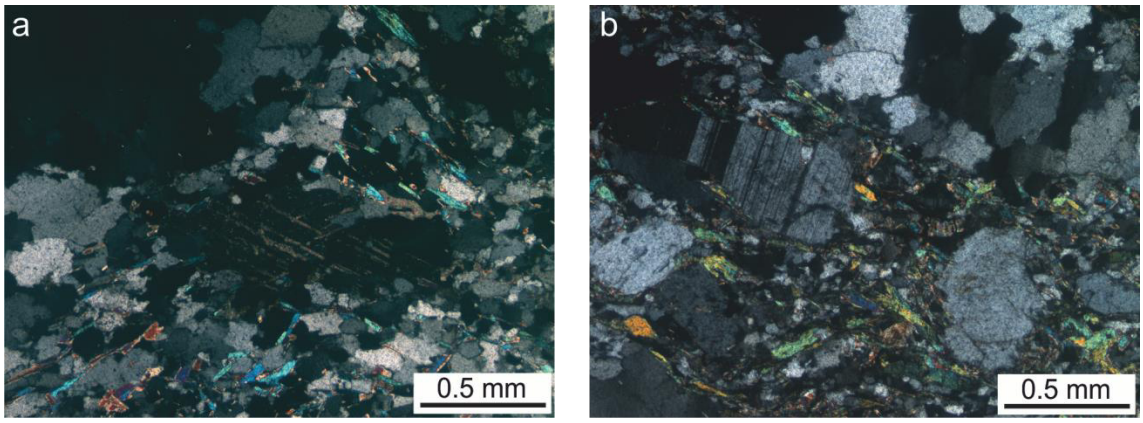

Figure 40: Crossed polarised thin sections of the sample P6. a): Calcite grain surrounded by quartz and muscovite. b): Plagioclase grain (obvious lamella cleavage) within quartz and muscovite.

P7

The sample P7 is a compact holo-crystalline, aphanatic rock. The main crystal shape is hypidiomorph with a fine to coarse grain size (0.05 – 10 mm). Main minerals are quartz, feldspar and mica. The grain shapes indicate deformation and an alignment. Quartz minerals show partially big sigma clasts and recrystallized quartz in an alignment they appear in the size of 0.01 to 10 mm. Feldspar minerals are characterised as plagioclase with a size of 0.5 – 1 mm. The main mica mineral is muscovite, which show a strong alignment (Figure 41, a).

Arsenic concentrations from the geochemical analysis indicate a low concentration of 3.86 mg/kg.

According to the geochemical classification this sample represents gneiss-metagranite. For detailed geochemical data see Appendix 3.

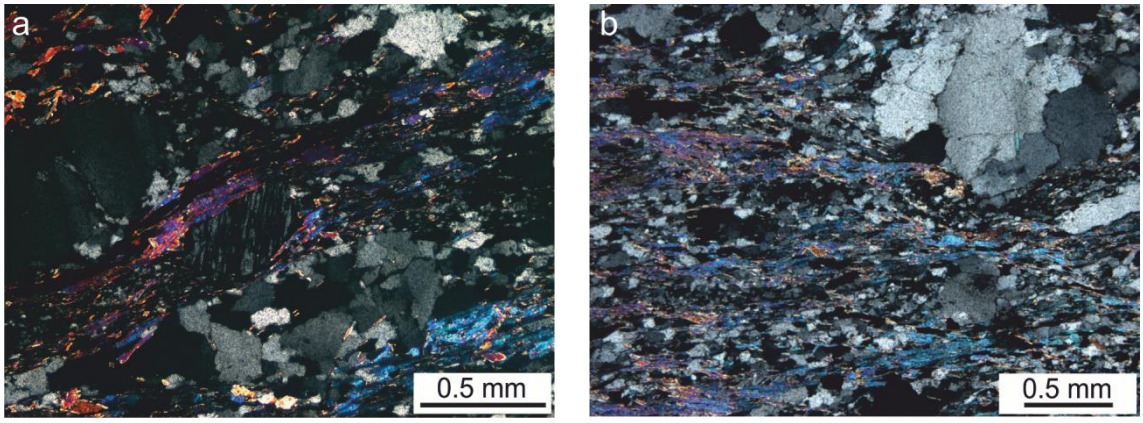

Figure 41: Crossed polarised thin sections of the sample P7. a): Plagioclase grain surrounded by deformed muscovite and quartz. b): Alignment of muscovite between recrystallized quartz.

P8

The sample P8 is a compact holo-crystalline, aphanatic rock. The main crystal shape is hypidiomorph with a fine to coarse grain size (0.05 – 10 mm). Main minerals are quartz, feldspar and mica. The grain shapes indicate deformation and an alignment. Quartz minerals show partially big sigma clasts and recrystallized quartz in an alignment they appear in the size of 0.01 to 10 mm. Feldspar minerals are characterised as plagioclase with a size of 0.5 – 1 mm and K-feldspar. The main mica mineral is muscovite and chlorite, which both show a strong alignment (Figure 42, a, b).

Arsenic concentrations from the geochemical analysis indicate a low concentration of 1.93 mg/kg.

According to the geochemical classification this sample represents gneiss-metagranite. For detailed geochemical data see Appendix 3.

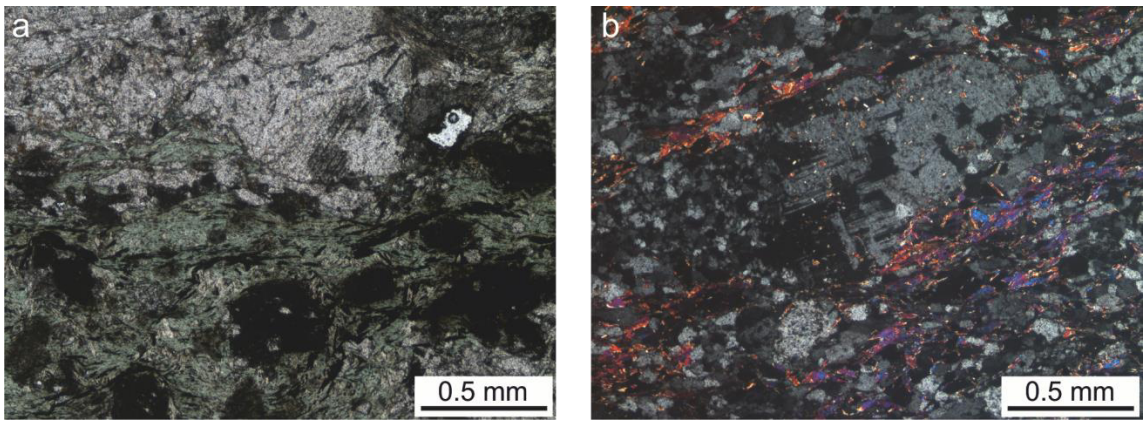

Figure 42: Linear (a) and crossed (b) polarised thin sections of the sample P7. a): Green chloride. b): K-feldspar and aligned muscovite.

P9 (Lose ore material)

Within the catchment area of SEQ near the in situ position of sample P2 fragments of bedrock with a carbonate matrix and high ore content were collected and additionally concentrated in respect to the ores. The investigation of these ores indicates that the main ore mineral is chalcopyrite, which occurs in form of big grains (>1cm) (Figure 43, a,d) and around silicate minerals with smaller grain size (Figure 43, d). Accessories are arsenopyrite (Figure 43, a), tetrahydrite (arsenical, bismuthian) (Figure 43, c) and iron oxides (Figure 43, b,d). The iron oxides occur as margins around the grains and in veins within chalcopyrite or quartz grains. Some of these iron oxide margins contain As (Figure 43, b,c).

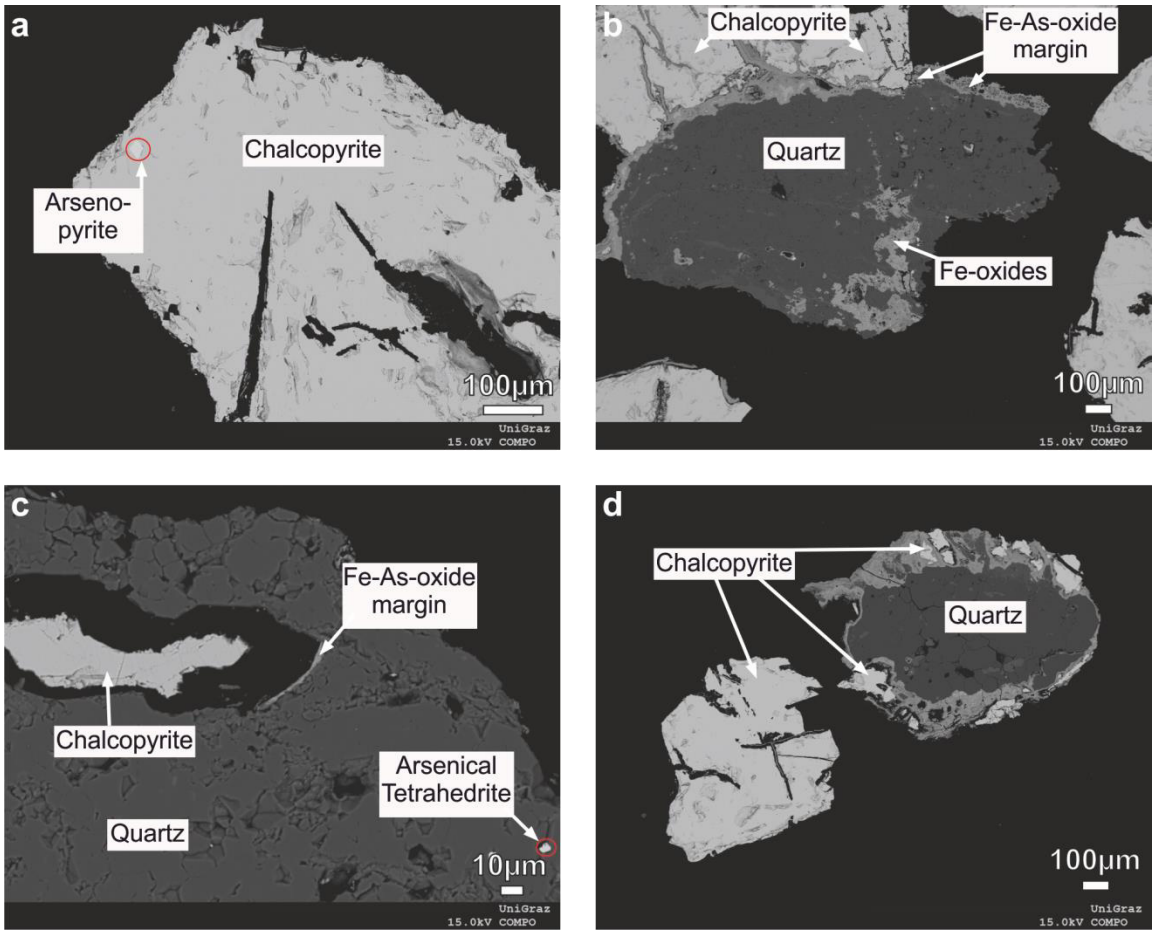

Figure 43: BSE pictures of collected and concentrated ore minerals, the main mineral is chalcopyrite, As occurs in small accessories and partially in iron oxide margins.

4.3 PhreeqC Modelling

The results of the mineralogical, geochemical and hydrogeochemical analysis were used to set up a PhreeqC inverse model for the Schöneben spring water, with the goal to understand the hydrogeochemical processes within this rock glacier and detect counterintuitive processes. Table 11 shows the results of the modelling for two measurements of the SEQ. The negative values (mass leaving solution) represent precipitation or in case of CO_2(g) degassing and the positive values (mass entering solution) dissolution. The inverse modelling resulted in ten possible model versions. Within these models the most probable model in respect to the research question was chosen. Finally, a set of mineral phases was fit together, which was able to produce solution 2 (Table 10).

Final Phases	Formula
Calcite	$CaCO_3$
As-pyrite	$FeAs_{0.004}S_{1.996}$
Biotite	$KMg_3AlSi_3O_{10}(OH)_2$
Chalcopyrite	$CuFeS_2$
Ferrihydrite	$Fe(OH)_3$
Kaolinite	$Al_2Si_2O_5(OH)_4$
Cuprite	Cu_2O
Chalcedony	SiO_2
Gypsum	$CaSO_4{:}2H_2O$
Carbon Dioxide (g)	CO_2

Table 10: Mineral phases, which were included into the final inverse model.

Mineral	Stoichiometry	"Rainwater"/SEQ_4	"Rainwater"/SEQ_5
		mmol/kg	
CO_2(g)	CO_2	-2.19	-2.15
As-pyrite	$FeAs_{0.004}S_{1.996}$	0.04	0.04
Calcite	$CaCO_3$	2.7	2.7
Biotite	$KMg_3AlSi_3O_{10}(OH)_2$	0	0.01
Chalcopyrite	$CuFeS_2$	1.2	1.2
Ferrihydrite	$Fe(OH)_3$	-1.24	-1.24
Plagioclase	$Na_{0.62}Ca_{0.38}Al_{1.38}Si_{2.62}O_8$	4.91E-04	0.04
Kaolinite	$Al_2Si_2O_5(OH)_4$	-2.49E-03	-0.03
Cuprite	Cu_2O	-0.6	-0.6
Chalcedony	SiO_2	-	-0.05
Gypsum	$CaSO_4{:}2H_2O$	-2.47	-2.47

Table 11: Mol transfers of the two invers models SEQ 4 and SEQ 5 from the spring Schöneben.

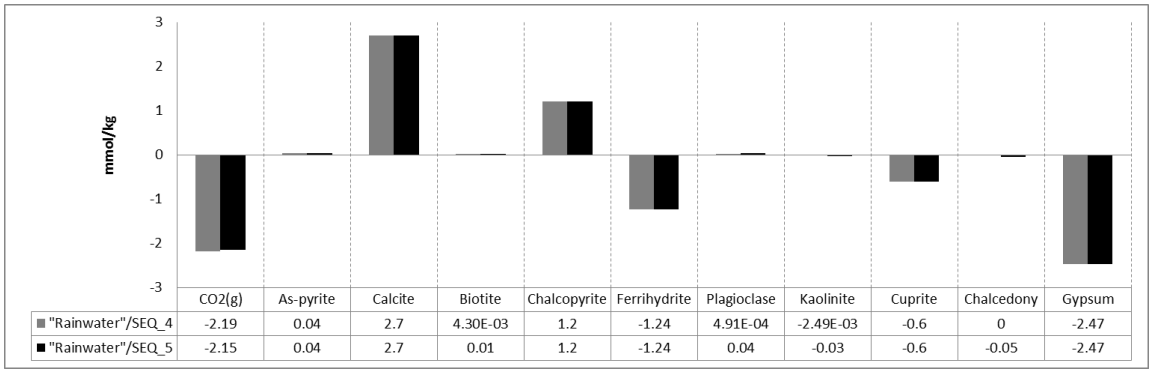

Figure 44: Diagram of mol transfers of the two invers models SEQ 4 and SEQ 5 from the spring Schöneben.

The model includes chalcopyrite and arsenopyrite. Highest dissolution rates indicate calcite, followed by chalcopyrite, less important are arsenopyrite, biotite, plagioclase. “Precipitation” rates are dominated by gypsum, carbon dioxide (degassing) and ferrihydrite, in minor extent also kaolinite and chalcedony precipitates. Counterintuitive are the high surplus of SO_4 which is visible in the high gypsum precipitation.

5 Discussion

Hydrogeochemical analysis of the water samples, regarding As revealed that, a distinct spatial As distribution of the water samples is not obvious. The comparison of the different measured elements of the springs with respect to As, show no explicit correlations, except for Mo (Figure 21, f). Regarding to these observations, trace elements do not reveal one general As source for the different spring waters. Possible reasons for that can be, that various hydrochemical processes superimpose each other, or multiple sources for As exist, or both. The true role of Mo in connection with As is not clear. There is also no evident correlation between the present geological features and the As concentrations. The area of the HPS fits for most of the measured springs with higher As values but cannot be interpret as the final As bearing host rock. That is because within the HPS also several springs with low As concentrations (< 5 µg/l) exist. Furthermore, the second spring with As values higher than 10 µg/l has four different geological units (HPS, GMS, PP and GP) within its catchment area. Due to these results it is assumed that the As contaminations are bound to rocks like P2. This would be a local phenomenon (e.g. occurrence of ores) within the different lithologies of the catchment areas.

During the tectonic evolution of the Seckauer Tauern Range various deformation, metamorphism and metasomatic processes influenced this area. According to the results of the geochemical classification and previous studies the predominant magmatic rocks in this area are products of island arc magmatism. In further developments, different granites (HPS, GP, PP) intruded into one host rock (GMS) (Mandl et al. 2018). Though the As was probably distributed more or less regularly within this granite bodies, the bodies can be seen as the initial source for the As. Regarding the SEQ, its present position is located within the HPS. Geochemical analysis of metagranitoids from the catchment area indicates generally low As concentrations from 0.8 – 3.9 mg/kg, with the exception of sample P5 which shows a higher value of 32.88 mg/kg. With respect to the SEQ these rocks probably represent the initial As source rock, though mineralogical investigations indicate no occurrence of sulphide ores or As-minerals (chapter 4.2.1), which seems likely to act as a source. Therefore, concentrated deposits of As are necessary for the present conditions. These deposits were created in the course of time by metasomatic processes, which were possible due to deformation processes. These deposits exist and occur today as secondary crystallized dikes within the catchment area of the SEQ, the sample P2 represents one of these dikes. In this area low grade deformation predominates but there are also local areas with higher deformation rates. This can be seen in petrographic investigations from rock samples of the SEQ catchment area (chapter 4.2.3). Two samples represent deformed metagranite-gneisses and give a clue for the existence of deformation zones. Such a deformation is most probably a product of alpine or variscian orogeny processes and created cracks within the metagranitoids which provide the space for fluid circulation. Low temperature hydrothermal fluids of mainly CO_2 or SiO_2 character led to alteration (altered feldspar) (chapter 4.2.3, P2). The fluids leached besides the major elements, preferentially Ca (from plagioclase) and heavy metals and sulphide out of the host rock material (HPS) and created one or more discordant quartz dikes with partially associated non-biogenic carbonate and calc-silicate precipitations (Figure 32). Simultaneously, sulphide ore minerals precipitated in this carbonate matrix, this can be seen in the rock sample P2. These ore

minerals can be differentiated into fine grained, distributed and locally concentrated coarse-grained ores (chapter 4.2.3, P9). The electron microscopic investigation revealed chalcopyrite as dominant coarse-grained sulphide phase, however these ores contain only a very small amount of As. In contrary, the fine grained ore is less common, but contains significant amounts of As. Also, the general As concentration of this dike material indicates an enrichment of As (~119 mg/kg) with two orders of magnitude above the average concentration in igneous rocks (1.5 mg/kg). According to the qualitative EDX analysis, the main As bearing mineral can be described as Arsenical tetrahedrite or freibergite (chapter 4.2.3, P2). Additionally, arsenopyrite occurs but is less common in the investigated samples. According to Krouse 1988 and Weber and Cerny 1997, the $d^{34}S$ = -0,2 per mil vs. VCDT isotopic measurements of SO_4 in the spring water can be interpreted as a signature of released SO_4 from sulphide ores. Summarizing, the As contamination source can be traced to discordant carbonate bearing rocks which are associated with quartz dikes. The carbonates contain significant amounts of arsenical tetrahedrite and less common arsenopyrite, which dissolute under oxidizing conditions in water.

5.1 Development of the aquifer system

In the Pleistocene, after the alpine orogeny and the development of the hydrothermally influenced dikes, erosional processes were the main changing factors in this area. Although the Seckauer Tauern Range was only partially glaciated, glaciers formed the landscape of today and led to the development of cols and U-shaped valleys. At this time a lot of moraine material was formed and deposited. In the area around the SRG this process also includes that the dike and carbonate material with ore content was involved in these processes. That means that the grain size of these rocks was reduced by physical erosion and the specific surface increased significantly. The periglacial phase after the Würm glacial age, the so-called “Gschnitzzeit”, represents the time of the active development of RGs in this area (Nagl 1976). Movements of the RG probably led to a further “grinding” of basal situated material, which resulted in an additional decrease of the grain size and an increase of specific surface within. Finally, in the Holocene the active RGs lost their internal ice and stopped their movements. Collapsed structures appeared at the surface (Winkler et al. 2016). Eventually, the RG Schöneben got its present shape and hydrogeological properties (chapter 2.2.3, Figure 45). The base layer is assumed to be the part of the RG where the main dissolution processes of As take place. This assumption is based on the facts that the base layer indicates a high specific surface and high retention time (approx. 7 months). Due to an extended reaction surface and more reaction time between the rock and the water the dissolution rate of As increases significantly. However, the coarse grained and blocky layer (upper layers) is also hydraulically connected with the base layer and indicates short retention times (hours – days) and a low specific surface. Due to this an influence of event water on the As concentration is assumed. A reliable statement made with the available data is not possible, additional measurements are required.

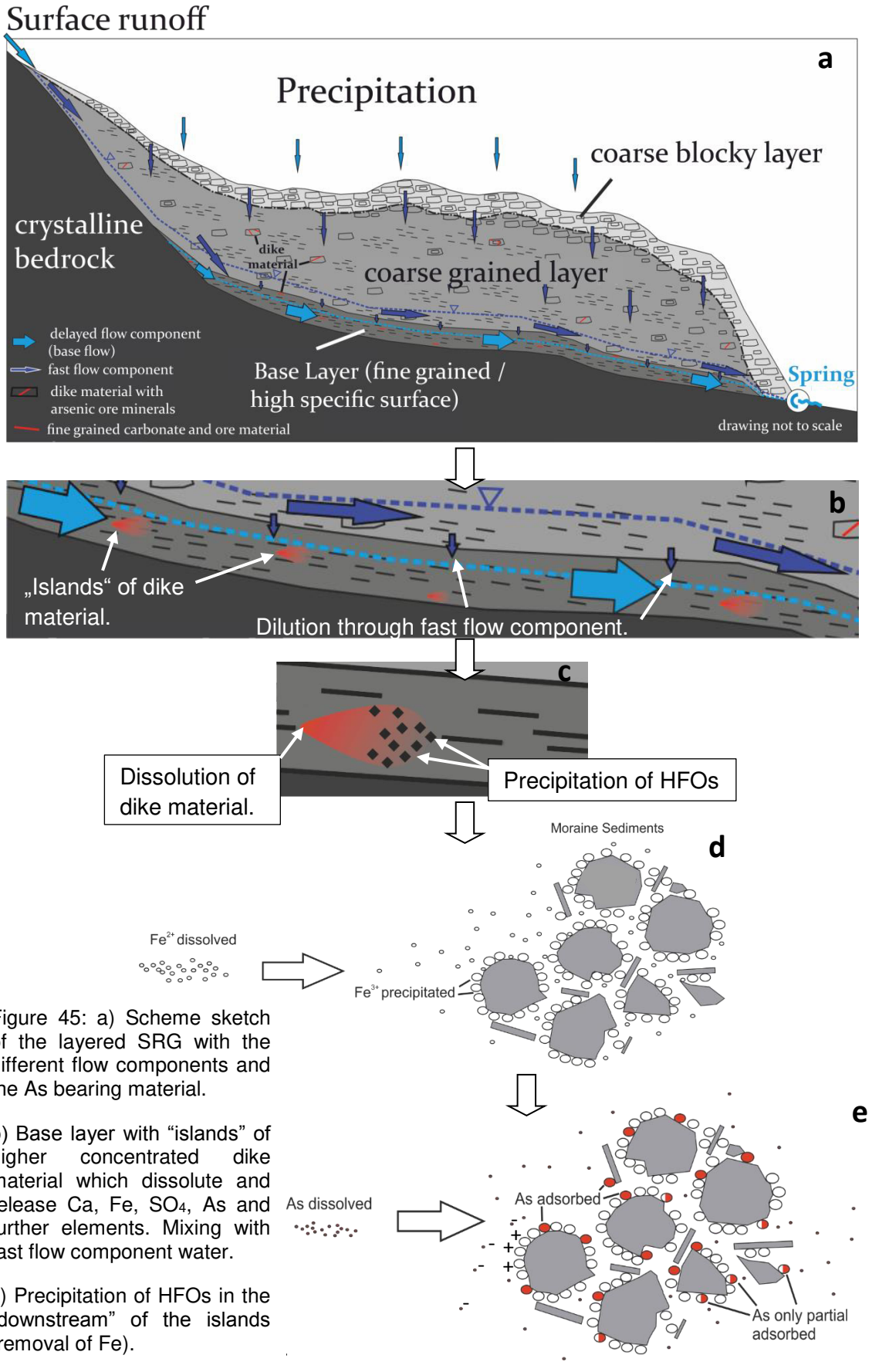

Figure 45: a) Scheme sketch of the layered SRG with the different flow components and the As bearing material.

b) Base layer with “islands” of higher concentrated dike material which dissolute and release Ca, Fe, SO_4, As and further elements. Mixing with fast flow component water.

c) Precipitation of HFOs in the “downstream” of the islands (removal of Fe).

d) Adsorption of negative charged As species on positive charged HFO surface, partially reduced adsorption due to higher pH value.

5.2 Hydrogeochemical way of the spring water (SEQ)

Rain water with a very low mineralization and an annual mean temperature of about 2.1°C (Winkler et al. 2016) reacts with CO_2 in the atmosphere. The catchment area consists of steep metagranitoid slopes which are partially overlaid by talus formations and the RG itself (Figure 8). In the steep areas it is assumed that the rain water shows mainly surface runoff and due to a lack of soil, there is only a negligible amount of soil water interaction. Thus, the main interaction between water and CO_2 happens via the contact with the atmosphere. The infiltration into the RG occurs through water flow from the surrounding talus formations and surface infiltration on the top of the RG. Due to the blocky character of the talus formations and the upper layers of the RG, rain water of the entire catchment area infiltrates very efficiently and fast. Up to this point dissolution processes at the rocks can be neglected due to the short time of the water-rock interaction and the small reaction surface. In the RG the flow components can be split up in a fast flow component "without" reaction throughout the upper layers and a slow flow component with solubilising effect through the base layer. At this point the dissolution processes in the base layer turn significant.

Pathways with similar properties as high hydraulically conductive karst in the upper layers of the RG create an efficient environment to saturate the infiltration water with oxygen (Appendix 2). Finally, this O_2 saturated water reaches the base layer. It is assumed that microbiological activities within the base layer are negligible because of low organic content and low water temperatures (mean annual temp.: 2.2 °C). Thus, water-rock interactions occur in an oxidizing environment. From a petrological point of view, the base layer is dominated by relatively dissolution resistant, but mechanically grinded fine grained metagranitoid rocks and partially carbonate-dike material (chapter 4.2). The sulphide ore bearing carbonates can be distributed more or less regularly within the base layer or appear irregularly as "small islands" of higher concentrations (Figure 45). The latter possibility is assumed for the SEQ. This behaviour can create micro environments within the base layer with different pH values and high saturation indices for mineral phases. Because of the relatively high solubility of the carbonates and ores in comparison to feldspar, mica or quartz in this environment, these minerals have a relatively high influence on the water chemistry. The water type of the SEQ water is a calcium-bicarbonate type (Figure 12, Figure 16), this fits to the theory of carbonate dissolution process, additionally the weathering process is carbonate dominated (Figure 18). Water analysis data of the SEQ indicates the highest Ca values of all samples (Figure 17), which lead to the assumption of a higher amount of carbonate dissolution then in the other samples. Main As bearing minerals are arsenical tetrahedrite, arsenopyrite and according to literature information very likely, although it was not detected, realgar. The predominant aqueous As species is assumed to be arsenate (As(V), $HAsO_4^{2-}$), because of the oxidizing conditions and the pH range of 7.6 – 7.9 (chapter 1.2).

The results of the inverse modelling indicate that the applied principle model with the selected minerals is reasonable (chapter 4.3). However, critical points are adsorption processes, which were not included into the model, but play a key role after the dissolution processes. Arsenate indicates a strong adsorption affinity on Fe-hydroxides (HFOs) around neutral pH (Zhang et al. 2017). This process is possible because the point of zero charge from the HFOs is at pH value of about 8.5 (Suthersan and Payne 2004) and the pH of the groundwater ranges from 7.6 to 7.9. Because the pH is lower than 8.5 the surfaces from the HFOs indicate a positive charge. However, the main arsenic species in the aqueous solution $HAsO_4^{2-}$ is negative charged. Therefore, the

As species will be adsorbed on the HFO surfaces (Figure 45). Due to the oxidation of Fe bearing sulphides, Fe mobilizes and precipitates as HFOs. This assumption is supported by the fact that Fe concentrations within the spring water are below the detection limit and that goethite occurs within the river sediments (Table 7). The most probable Fe-phases are ferrihydrite, lepidocrocite, hematite and goethite (Blowes et al. 2003; Zhang et al. 2017; Smedley and Kinniburgh 2002). Besides HFOs also Al and Mn oxides show an adsorption effect, but they occur in much lower concentrations and the effect is less strong at this pH range. Additionally, alteration/reaction margins around the arsenical tetrahedrite indicate this behaviour. The margin is enriched in Cu, As, Sb with significantly higher As concentrations than the original mineral (Table 8, Figure 36). During the oxidation process the sulphur dissolute and the oxidized margin adsorbs or integrates As. All this oxidized phases show a high adsorption capacity for As (Neidhardt et al. 2018). The amount of adsorbed As cannot be quantified, however it is assumed that only a small surplus of not adsorbed As reaches the spring. The mainly dissolved As remains in the aquifer bound to Fe hydroxides. The role of the dissoluted SO_4 is not fully understood up to now. Because the PhreeqC model showed that the dissolution processes of the sulphides (chalcopyrite, arsenical tetrahedrite and arsenopyrite) are supposed to release significant amounts of SO_4, but this was not verified in the hydrochemical analysis. The inverse model indicates a significant surplus of SO_4 which was buffered by using gypsum as precipitation phase. But in reality, gypsum will not precipitate. Therefore, other mechanisms should lead to this behaviour. Explanations could be the precipitation of barite, with the limiting factor of barium within the system, but the measured Ba concentration within the spring water is too low to confirm this assumption. Another possibility could be the adsorption of SO_4 on HFOs or microbiological degradation, but the environmental conditions are not favourable for the latter process. To prove the last assumption an event-based sampling campaign would be necessary and in general further investigations concerning this question. Furthermore, the pH values don`t seem to be influenced by the SO_4, this can be explained by low concentrations and the dissolution of carbonate, which increases the pH value. Due to this, the measured pH values of the SEQ range around the higher end of a neutral water (7.6 – 7.9) and can show direct at dissolution areas of carbonate most probably even higher values. At such conditions the process of Alkali desorption can also have an influence by reduction of the adsorption rate for As on HFOs and other minerals. This hypothesis should be confirmed with a detailed in situ investigation of the base layer and the internal hydrogeochemical processes.

Other heavy metals do not occur in significant concentrations, the reason for this behaviour is due to the environmental conditions. They are not favourable for heavy metal dissolution and transport, significant lower pH values are needed, or a reductive environment.

Isotopic measurements of ^{2}H and ^{18}O ratios indicate that all measured samples plot as a local meteoric water line, which is typical for alpine environments in this area. Isotopic fractionation processes within the aquifer associated with As concentrations were not assumed. But the results show that evaporation processes do not influence the isotopic signature and therefore not the As concentration.

To sum up, most probably the important water rock interactions take place in an oxidizing environment in the base layer of the RG. Within the catchment area the occurrence of As bearing sulphide minerals is confirmed. In addition, near neutral sulphur isotopic values in the dissolved SO_4 indicate possible sulphide dissolution.

These sulphides occur within a carbonate matrix, which buffers the decrease of pH, due to sulphide dissolution and the release of SO_4. This leads to the assumption that the main dissolution process in the SRG is most probably the sulphide oxidation, with a reduced mobilisation due to As adsorption on HFOs. But a second process, the alkali desorption can prevent some adsorption and lead to an increase of the As concentration in the spring water.

6 Conclusion

Even in low grade mineralized hydrogeochemical environments in the Seckauer Tauern Range, As mobilization can occur, which is shown by low As contaminations in the water of the SEQ and the GLQ. Although As concentrations are low they exceed the guideline value of the WHO (10 µg/l). The contaminations are not linked to, specific geological formations, but they are bound to local phenomena like ore bearing carbonates. The example SEQ indicates sulphide oxidation most probably as the main As mobilizing process, which is possible in the O_2 rich, fine grained base layer of the relict rock glacier. A high specific surface, As rich carbonates and longer retention time creates conditions for the dissolution and transport. Besides that, secondary precipitations like HFOs lead to a decrease of the As concentration within the solution, because these HFOs show a high specific surface and the right charge conditions for adsorption processes. Therefore, most of the As gets adsorbed and "stored" on the HFOs. But an additional process, the alkali desorption is able to decrease the adsorption and increase the concentration of As in the aqueous solution.

Low concentrations of contaminants (As, Pb, …) in aqueous solution, do not indicate the whole contamination risk, due to processes which have led to reduction of As concentration, as especially adsorption. Thus, the real contamination potential is much higher, and a slight change of environmental conditions, e.g. higher air temperatures, can have serious effects on the spring water components:

Higher annual air temperatures can introduce a rise of the vegetation zone in alpine systems:

- ⇨ More vegetation leads to the development of a thicker soil layer which increases soil-water interaction. The high partial pressure of CO_2 in the soil affects the water and results in a decrease of pH, with the result of higher dissolution rates for carbonates and associated contaminants. In addition to that adsorption effects are depending on pH values. A higher contamination risk shall be expected, because in this case As is mainly associated with carbonates.

- ⇨ Increased organic matter content on the surface, might result in higher organic contents washed into the RG. Aerobe bacteria use the organic material and O_2 for energy production. This process can lead to areas with reductive conditions within the base layer. At these conditions Fe hydroxides dissolute and if they had previously adsorbed As, the release of a significant amount of As and heavy metals is possible.

- ⇨ Droughts are able to increase evaporation processes and decrease the mixing and dilution with the fast flow component. Both processes can lead to higher As concentrations within the spring water.

The understanding of this investigated hydrogeochemical system can be used to comprehend and predict the behaviour of As in other similar relict rock glaciers and related systems like talus or different glacial sediment deposits in crystalline rock areas.

By using an interdisciplinary approach of hydrogeochemical and petrological methods processes within the aquifer can be identified. The solutes in spring water tell a story about the geological history, the present hydrogeochemical processes and the geochemical future of such a system. This work helps to understand such processes, their limitations related to As and the importance of the geological history for current processes which are important in our daily life. Due to the climate change the number of relict rock glaciers will increase and therefore, similar cases will occur. Because of their importance as water storage, they will provide an increasing amount of drinking water for future generations and detailed information about their behaviour is of value for a lot of people.

7 References

Alker A. (1972): "Forcherit" vom Ingeringtal. In *Der Aufschluss* (22), pp. 27–28.

Amini, Manouchehr; Abbaspour, Karim C.; Berg, Michael; Winkel, Lenny; Hug, Stephan J.; Hoehn, Eduard et al. (2008): Statistical Modeling of Global Geogenic Arsenic Contamination in Groundwater. In *Environ. Sci. Technol.* 42 (10), pp. 3669–3675. DOI: 10.1021/es702859e.

Anawar, Hossain M.; Akai, Junji; Sakugawa, Hiroshi (2004): Mobilization of arsenic from subsurface sediments by effect of bicarbonate ions in groundwater. In *Chemosphere* 54 (6), pp. 753–762. DOI: 10.1016/j.chemosphere.2003.08.030.

Andreasen, Jens Wenzel; Makovicky, Emil; Lebech, Bente; Møller, Sven Karup (2008): The role of iron in tetrahedrite and tennantite determined by Rietveld refinement of neutron powder diffraction data. In *Phys Chem Minerals* 35 (8), pp. 447–454. DOI: 10.1007/s00269-008-0239-1.

Back (1966): Hydrochemical Facies and Ground-Water Flow Patterns in Northern Part of Atlantic Coastal Plain. In *HYDROLOGY OF AQUIFER SYSTEMS* (Geological survey professional paper 498A).

Blowes, D. W.; Ptacek, C. J.; Jambor, J. L.; Weisener, C. G. (2003): The Geochemistry of Acid Mine Drainage, pp. 149–204. DOI: 10.1016/B0-08-043751-6/09137-4.

Böcher H. (1927): Zur Geologie des Hochreichart und des Zinken in den Seckauer Tauern. In *Mitteilungen des naturwissenschaftlichen Vereines für Steiermark* (63), pp. 136–149.

Brand, Willi A.; Geilmann, Heike; Crosson, Eric R.; Rella, Chris W. (2009): Cavity ring-down spectroscopy versus high-temperature conversion isotope ratio mass spectrometry; a case study on delta(2)H and delta(18)O of pure water samples and alcohol/water mixtures. In *Rapid communications in mass spectrometry : RCM* 23 (12), pp. 1879–1884. DOI: 10.1002/rcm.4083.

Chakraborti, Dipankar; Rahman, Mohammad Mahmudur; Das, Bhaskar; Chatterjee, Amit; Das, Dipankar; Nayak, Biswajit et al. (2017): Groundwater arsenic contamination and its health effects in India. In *Hydrogeol J* 25 (4), pp. 1165–1181. DOI: 10.1007/s10040-017-1556-6.

Clark, G. S.; Černý, P. (1987): Radiogenic 87Sr, its mobility, and the interpretation of Rb,Sr fractionation trends in rare-element granitic pegmatites. In *Geochimica et Cosmochimica Acta* 51 (4), pp. 1011–1018. DOI: 10.1016/0016-7037(87)90112-8.

Clark, Ian D.; Fritz, Peter (1997): Environmental isotopes in hydrogeology. Boca Raton: Lewis Publ.

Craig, H. (1961): Isotopic Variations in Meteoric Waters. In *Science (New York, N.Y.)* 133 (3465), pp. 1702–1703. DOI: 10.1126/science.133.3465.1702.

Cullen, William R.; Reimer, Kenneth J. (1989): Arsenic speciation in the environment. In *Chem. Rev.* 89 (4), pp. 713–764. DOI: 10.1021/cr00094a002.

D.L. Parkhurst and C.A.J. Appelo: Description of Input for PHREEQC Version 3—A Computer Program for Speciation, Batch-Reaction, One-Dimensional Transport, and Inverse Geochemical Calculations.

Dixit, Suvasis; Hering, Janet G. (2003): Comparison of Arsenic(V) and Arsenic(III) Sorption onto Iron Oxide Minerals: Implications for Arsenic Mobility. In *Environ. Sci. Technol.* 37 (18), pp. 4182–4189. DOI: 10.1021/es030309t.

Dzombak, David A.; Morel, François M. M. (1990): Surface complexation modeling. Hydrous ferric oxide. New York: Wiley. Available online at http://www.loc.gov/catdir/description/wiley031/89035596.html.

Fetter, C. W. (Ed.) (1990): Applied hydrogeology. Merill College. 2nd ed.

Frisch, W.; Gawlick, H.-J. (2003): The nappe structure of the central Northern Calcareous Alps and its disintegration during Miocene tectonic extrusion?a contribution to understanding the orogenic evolution of the Eastern Alps. In *International Journal of Earth Sciences* -1 (1), p. 1. DOI: 10.1007/s00531-003-0357-4.

Gao, Xubo; Wang, Yanxin; Hu, Qinhong; Su, Chunli (2011): Effects of anion competitive adsorption on arsenic enrichment in groundwater. In *Journal of Environmental Science and Health, Part A* 46 (5), pp. 471–479. DOI: 10.1080/10934529.2011.551726.

Gasser, From Deta; Gusterhuber, Jürgen; Krische, Oliver; Puhr, Barbara; Scheucher, Lorenz; Wagner, Thomas; Stüwe, Kurt (2009): Geology of Styria: An overview. In *Mitteilungen des naturwissenschaftlichen Vereines für Steiermark* (Bd. 139), pp. 5–36.

GBA (2015): GRUNDWASSERKÖRPER-STAMMDATENBLATT. GK100116_GK.

Gulens; Champ D.R.; Jackson R.E. (1979): Influence of Redox Environments on the Mobility of Arsenic in Ground Water, pp. 81–95. DOI: 10.1021/bk-1979-0093.ch004.

Gupta, Priya; Noone, David; Galewsky, Joseph; Sweeney, Colm; Vaughn, Bruce H. (2009): Demonstration of high-precision continuous measurements of water vapor isotopologues in laboratory and remote field deployments using wavelength-scanned cavity ring-down spectroscopy (WS-CRDS) technology. In *Rapid communications in mass spectrometry : RCM* 23 (16), pp. 2534–2542. DOI: 10.1002/rcm.4100.

Herath, Indika; Vithanage, Meththika; Bundschuh, Jochen; Maity, Jyoti Prakash; Bhattacharya, Prosun (2016): Natural Arsenic in Global Groundwaters: Distribution and Geochemical Triggers for Mobilization. In *Curr Pollution Rep* 2 (1), pp. 68–89. DOI: 10.1007/s40726-016-0028-2.

Islam, Farhana S.; Gault, Andrew G.; Boothman, Christopher; Polya, David A.; Charnock, John M.; Chatterjee, Debashis; Lloyd, Jonathan R. (2004): Role of metal-reducing bacteria in arsenic release from Bengal delta sediments. In *Nature* 430, 68 EP -. DOI: 10.1038/nature02638.

JANOUŠEK, VOJTĚCH; FARROW, C. M.; ERBAN, VOJTĚCH (2006): Interpretation of Whole-rock Geochemical Data in Igneous Geochemistry: Introducing Geochemical Data Toolkit (GCDkit). In *Journal of Petrology* 47 (6), pp. 1255–1259. DOI: 10.1093/petrology/egl013.

KROUSE, H. R. (1988): Sulphur isotopes in our environment. In Peter Fritz (Ed.): Handbook of environmental isotope geochemistry. 1. ed., 2. impr. Amsterdam: Elsevier, pp. 435–471.

Kulkarni, Harshad V.; Mladenov, Natalie; Johannesson, Karen H.; Datta, Saugata (2017): Contrasting dissolved organic matter quality in groundwater in Holocene and Pleistocene aquifers and implications for influencing arsenic mobility. In *Applied Geochemistry* 77, pp. 194–205. DOI: 10.1016/j.apgeochem.2016.06.002.

Lengke, M. F.; Sanpawanitchakit, C.; Tempel, R. N. (2009): THE OXIDATION AND DISSOLUTION OF ARSENIC-BEARING SULFIDES. In *The Canadian Mineralogist* 47 (3), pp. 593–613. DOI: 10.3749/canmin.47.3.593.

Lieb, Gerhard Karl (1991): Eine Gebietsgliederung der Steiermark. In *Mitt. Abt. Bot. Landesmus. Joanneum Graz* (20), pp. 1–30.

Ma, Jian; Sengupta, Mrinal K.; Yuan, Dongxing; Dasgupta, Purnendu K. (2014): Speciation and detection of arsenic in aqueous samples: A review of recent progress in non-atomic spectrometric methods. In *Analytica Chimica Acta* 831, pp. 1–23. DOI: 10.1016/j.aca.2014.04.029.

Malmström, Maria; Banwart, Steven; Lewenhagen, Jeanette; Duro, Lara; Bruno, Jordi (1996): The dissolution of biotite and chlorite at 25°C in the near-neutral pH region. In *Journal of Contaminant Hydrology* 21 (1-4), pp. 201–213. DOI: 10.1016/0169-7722(95)00047-X.

Mandal, B. (2002): Arsenic round the world: a review. In *Talanta* 58 (1), pp. 201–235. DOI: 10.1016/S0039-9140(02)00268-0.

Mandl, Magdalena; Kurz, Walter; Hauzenberger, Christoph; Fritz, Harald; Klötzli, Urs; Schuster, Ralf (2018): Pre-Alpine evolution of the Seckau Complex (Austroalpine basement/Eastern Alps): Constraints from in-situ LA-ICP-MS U Pb zircon geochronology. In *Lithos* 296-299, pp. 412–430. DOI: 10.1016/j.lithos.2017.11.022.

Markl, Gregor (Ed.) (2015): Minerale und Gesteine. Mineralogie - Petrologie - Geochemie. 3. Aufl. Belrin [u.a.]: Springer Spektrum.

Mayo, Alan L.; Muller, Anthony B.; Ralston, Dale R. (1985): Hydrogeochemistry of the Meade thrust allochthon, southeastern Idaho, U.S.A., and its relevance to stratigraphic and structural groundwater flow control. In *Journal of Hydrology* 76 (1-2), pp. 27–61. DOI: 10.1016/0022-1694(85)90089-7.

Metz, Karl (1976): Der geologische Bau der Seckauer und Rottenmanner Tauern. In *Jahrb. Geol. B.-A.* (Bd. 119/H. 2), S. 151—205.

Middlemost, Eric A.K. (1994): Naming materials in the magma/igneous rock system. In *Earth-Science Reviews* 37 (3-4), pp. 215–224. DOI: 10.1016/0012-8252(94)90029-9.

Mielczarski, J. A.; Cases, J. M.; Alnot, M.; Ehrhardt, J. J. (1996): XPS Characterization of Chalcopyrite, Tetrahedrite, and Tennantite Surface Products after Different Conditioning. 2. Amyl Xanthate Solution at pH 10. In *Langmuir* 12 (10), pp. 2531–2543. DOI: 10.1021/la950589t.

Nagl, Hubert (1976): Die Raum - Zeit Verteilung der Blockgletscher in den Niederen Tauern und die eiszeitliche Vergletscherung der Seckauer Tauern. In *Mitt. naturwiss. Ver. Steiermark* (106), pp. 95–118.

Neidhardt, Harald; Winkel, Lenny H.E.; Kaegi, Ralf; Stengel, Caroline; Trang, Pham T.K.; Lan, Vi M. et al. (2018): Insights into arsenic retention dynamics of Pleistocene aquifer sediments by in situ sorption experiments. In *Water Research* 129, pp. 123–132. DOI: 10.1016/j.watres.2017.11.018.

Neubauer, Franz (2002): Evolution of late Neoproterozoic to early Paleozoic tectonic elements in Central and Southeast European Alpine mountain belts: review and synthesis.

Nickson, R. T.; McArthur, J. M.; Ravenscroft, P.; Burgess, W. G.; Ahmed, K. M. (2000): Mechanism of arsenic release to groundwater, Bangladesh and West Bengal (4).

Pauritsch, Marcus; Wagner, Thomas; Winkler, Gerfried; Birk, Steffen (2017): Investigating groundwater flow components in an Alpine relict rock glacier (Austria) using a numerical model. In *Hydrogeol J* 25 (2), pp. 371–383. DOI: 10.1007/s10040-016-1484-x.

Peccerillo, Angelo; Taylor, S. R. (1976): Geochemistry of eocene calc-alkaline volcanic rocks from the Kastamonu area, Northern Turkey. In *Contr. Mineral. and Petrol.* 58 (1), pp. 63–81. DOI: 10.1007/BF00384745.

Pfingstl, Stefan (2013): Tektonische und metamorphe Entwicklung des Seckauer Kristallins. Master Thesis. Karl Franzens University, Graz. Geology.

Pfingstl, Stefan; Kurz, Walter; Schuster, Ralf; Hauzenberger, Christoph (2015): Geochronological constraints on the exhumation of the Austroalpine Seckau Nappe (Eastern Alps). In *AJES* 108 (1), pp. 172–185. DOI: 10.17738/ajes.2015.0011.

Pilger, Harald; Prettenthaler, Franz (Eds.) (2012): Klimaatlas Steiermark. Periode 1971-2000 ; eine anwenderorientierte Klimatographie. With assistance of Otmar Harlfinger. 2., überarb. Aufl. Wien: Verl. der Österr. Akad. der Wiss (Studien zum Klimawandel in Österreich, Bd. 4).

Piper, Arthur M. (1944): A graphic procedure in the geochemical interpretation of water-analyses. In *Trans. AGU* 25 (6), p. 914. DOI: 10.1029/TR025i006p00914.

Raab, Gerald (2015): „Magmatic, Metamorphic and Tectonic Evolution of the Seckau Complex in the Area of the Sonntagskogel Mountain (Triebener Tauern, Province of Styria)". Karl Franzens University, Graz. Geology.

Ravenscroft, Peter; Brammer, Hugh; Richards, Keith (Eds.) (2009): Arsenic pollution. A global synthesis. Oxford: Wiley-Blackwell. Available online at http://www.worldcat.org/oclc/850889189.

Schmid, Stefan M.; Fügenschuh, Bernhard; Kissling, Eduard; Schuster, Ralf (2004): Tectonic map and overall architecture of the Alpine orogen. In *Eclogae geol. Helv.* 97 (1), pp. 93–117. DOI: 10.1007/s00015-004-1113-x.

Schönegger, Michael (2015): Die tektonische und geochemische Entwicklung in den Seckauer Tauern im Bereich des Gaalgrabens Sommertörls (Steiermark). Karl-Franzens-Universität, Graz. Erdwissenschaften.

Schuster, Ralf (Ed.) (2015): Zur Geologie der Ostalpen. Wien: Geologische Bundesanstalt (Abhandlungen der Geologischen Bundesanstalt, Bd. 64). Available online at http://www.worldcat.org/oclc/958146736.

Shand (Ed.) (1943): Eruptive Rocks: Their Genesis, Composition, and Classification, with a Chapter on Meteorites. Revised Second. (2nd) Edition: John Wiley & Sons, Inc.

Sharma, Virender K.; Sohn, Mary (2009): Aquatic arsenic: toxicity, speciation, transformations, and remediation. In *Environment international* 35 (4), pp. 743–759. DOI: 10.1016/j.envint.2009.01.005.

Smedley, P.L; Kinniburgh, D.G (2002): A review of the source, behaviour and distribution of arsenic in natural waters. In *Applied Geochemistry* 17 (5), pp. 517–568. DOI: 10.1016/S0883-2927(02)00018-5.

Suthersan, S. S.; Payne, F. C. (2004): In Situ Remediation Engineering: CRC Press. Available online at https://books.google.at/books?id=MwprDwAAQBAJ.

Thalmann, F. (1989): Geochemischer Atlas der Republik Österreich, 11,000.000. Böhmische Masse und Zentralzone der Ostalpen (Bachsedimente <0,18 mm). Wien: Geologische Bundesanstalt.

Ure, A. M.; Berrow, M. L. (Eds.) (1982): The elemental constituents of soils (2).

Wagner, Thomas; Pauritsch, Marcus; Winkler, Gerfried (2016): Impact of relict rock glaciers on spring and stream flow of alpine watersheds: Examples of the Niedere Tauern Range, Eastern Alps (Austria). In *AJES* 109 (1). DOI: 10.17738/ajes.2016.0006.

Walker, Forest P.; Schreiber, Madeline E.; Rimstidt, J. Donald (2006): Kinetics of arsenopyrite oxidative dissolution by oxygen. In *Geochimica et Cosmochimica Acta* 70 (7), pp. 1668–1676. DOI: 10.1016/j.gca.2005.12.010.

Weber, Leopold; Cerny, Immo (Eds.) (1997): Handbuch der Lagerstätten der Erze, Industrieminerale und Energierohstoffe Österreichs. Erläuterungen zur metallogenetischen Karte von Österreich 1 : 500000 unter Einbeziehung der Industrieminerale und Energierohstoffe ; 37 Tabellen ; [in memoriam emer. Univ. Prof. Dr. mult. Walther Emil Petrascheck. Wien: Geologische Bundesanst (Archiv für Lagerstättenforschung, Bd. 19).

Webster, Jenny G. (1999): The source of arsenic (and other elements) in theMarbel–Matingao river catchment, Mindanao, Philippines. In *Geothermics* 28 (1), pp. 95–111. DOI: 10.1016/S0375-6505(98)00046-7.

Webster, Jenny G.; Nordstrom, D. Kirk (2003): Geothermal Arsenic. The source, transport and fate of arsenic in geothermal systems. In Alan H. Welch, Kenneth G. Stollenwerk (Eds.): Arsenic in Ground Water. Boston, MA: Springer US.

Wechmann (1968): Hydrologie. Oberirdisches Wasser — Unterirdisches Wasser — Hydrometeorologie — Wasserhaushalt. Mit 271 Abb., 38 Taf. München-Wien: R. Oldenbourg 1964 (Lizenzausgabe des Verlages für Bauwesen Berlin) 535 S. DM 64,—. In *Int. Revue ges. Hydrobiol. Hydrogr.* 53 (1), pp. 175–176. DOI: 10.1002/iroh.19680530137.

Wemhöner; Christina Schartner; Harald Loishandl-Weisz; Gerhard Schubert; Albert Schedl (2012): Metalle im Grundwasser in Österreich. With assistance of Christina Schartner, Harald Loishandl-Weisz, Irene Zieritz, Roland Herndler, Johannes Grath, Uta Wemhöner, Martin Kralik, Gerhard Schubert, Rudolf Philippitsch. Edited by Bundesministerium für Land- und Forstwirtschaft, Umwelt und Wasserwirtschaft Referat VII/1a.

Werner, Roland A.; Brand, Willi A. (2001): Referencing strategies and techniques in stable isotope ratio analysis. In *Rapid Commun. Mass Spectrom.* 15 (7), pp. 501–519. DOI: 10.1002/rcm.258.

Winkler, Gerfried; Wagner, Thomas; Pauritsch, Marcus; Birk, Steffen; Kellerer-Pirklbauer, Andreas; Benischke, Ralf et al. (2016): Identification and assessment of groundwater flow and storage components of the relict Schöneben Rock Glacier, Niedere Tauern Range, Eastern Alps (Austria). In *Hydrogeol J* 24 (4), pp. 937–953. DOI: 10.1007/s10040-015-1348-9.

World Health Organization (2011): Guidelines for Drinking-water Quality. Geneva: World Health Organization. Available online at http://gbv.eblib.com/patron/FullRecord.aspx?p=851158.

Yan, Xiu-Ping; Kerrich, Robert; Hendry, M.Jim (2000): Distribution of arsenic(III), arsenic(V) and total inorganic arsenic in porewaters from a thick till and clay-rich aquitard sequence, Saskatchewan, Canada. In *Geochimica et Cosmochimica Acta* 64 (15), pp. 2637–2648. DOI: 10.1016/S0016-7037(00)00380-X.

ZAMG (Ed.) (2004): Klimaatlas Steiermark. Kapitel 4 Niederschlag. With assistance of H. Wakonigg. ZAMG (KLIMAATLAS).

Zhang, Liankai; Qin, Xiaoqun; Tang, Jiansheng; Liu, Wen; Yang, Hui (2017): Review of arsenic geochemical characteristics and its significance on arsenic pollution studies in karst groundwater, Southwest China. In *Applied Geochemistry* 77, pp. 80–88. DOI: 10.1016/j.apgeochem.2016.05.014.

Zobrist, Juerg; Dowdle, Philip R.; Davis, James A.; Oremland, Ronald S. (2000): Mobilization of Arsenite by Dissimilatory Reduction of Adsorbed Arsenate. In *Environ. Sci. Technol.* 34 (22), pp. 4747–4753. DOI: 10.1021/es001068h.

8 Appendix

Appendix 1

Labels and GPS positions of the investigated springs and the taken rock samples.

Spring-ID	Name	Reference system	N	E
BSQ1	Brandstätterkar	WGS 1984	N 47°22.070'	E014°42.314'
BSTQ1	Brandstätterthörl	WGS 1984	N 47°21.470'	E014°41.516'
BTQ1	Bärental Ost	WGS 1984	N 47°21.713'	E014°43.006'
BTQ2	Bärental West	WGS 1984	N 47°22.010'	E014°42.641'
DOQ1	Donnerofen	WGS 1984	N 47°22.280'	E014°36.720'
DTQ1	Dürrtal	WGS 1984	N 47°22.545'	E014°42.442'
FLQ1	Finsterliesingtal	WGS 1984	N 47°23.059'	E014°37.498'
GLQ1	Goldlacke	WGS 1984	N 47°20.303'	E014°45.066'
HKAQ1	Hühnerkaralm	WGS 1984	N 47°24.194'	E014°37.688'
HKQ1	Hirschkarl	WGS 1984	N 47°21.499'	E014°39.392'
HRQ1	Hochreichhartschutzhaus 1	WGS 1984	N 47°22.545'	E014°42.442'
HTQ1	Hölltal	WGS 1984	N 47°21.800'	E014°39.319'
KTQ1	Kettentörl	WGS 1984	N 47°22.369'	E014°35.730'
SBQ1	Siebenbründl	WGS 1984	N 47°20.916'	E014°45.627'
SEQ	Schöneben Alm	WGS 1984	N 47°22.592'	E014°40.501'
VSQ1	Vorwitzsattel	WGS 1984	N 47°20.644'	E014°43.236'

	UTM 33T	
Sample	N	E
P1, P2, P9	5246311	475538
P3	5246125	475639
P4	5246135	475581
P5	5246329	475712
P6	5247233	475948
P7, P8, S1	5247169	475362

Appendix 2

Hydrochemistry of the investigated water samples.

Spring-ID	BSQ1		BSTQ1	BTQ1		BTQ2		GLQ1	HKQ1
Sample-ID	BSQ1_1	BSQ1_2	BSTQ1_1	BTQ1_1	BTQ1_2	BTQ2_1	BTQ2_2	GLQ1_1	HKQ1_1
Ca [µg/l]	5901	6468	3951	7780	8510	7673	8007	5768	5291
Na [µg/l]	585	587	745	613	679	800	788	634	559
Mg [µg/l]	161	175	157	250	292	266	302	176	247
K [µg/l]	430	455	302	606	708	515	506	578	532
Si [µg/l]	1586	1532	1720	1605	1586	1829	1977	1599	1656
B [µg/l]	1.1	1	0.95	1.1	1	1.1	1	0.89	1.2
Al [µg/l]	2.5	2.4	5.1	2.9	16.2	3.7	1.5	1.9	14
Ti [µg/l]									
V [µg/l]		0.053	0.055		0.059		0.034	0.14	
Cr [µg/l]	0.035	0.039	0.041	0.026	0.04	0.03	0.043	0.063	0.043
Mn [µg/l]	0.1	0.1	0.296	0.13	0.611	0.1	0.1	0.1	
Fe [µg/l]		1.7	1.7	1.3	21.3	1.6	1.1	3.5	7.5
Co [µg/l]					0.012				
Cu [µg/l]						0.11			0.15
Zn [µg/l]					2.3				
As [µg/l]	4.2	4	4.7	8	7.1	6.6	6.4	10.3	3.2
Se [µg/l]	0.018	0.021	0.017	0.036	0.035	0.031	0.034	0.025	0.025
Sr [µg/l]	6	6.6	5.2	10.4	11.5	9.5	9.7	7.3	5.3
Mo [µg/l]	0.41	0.44	0.34	0.72	0.8	0.67	0.62	0.27	0.27
Ag [µg/l]	0.1	0.01	0.01	0.1	0.01	0.1	0.01	0.01	0.1
Sb [µg/l]	0.09	0.07	0.065	0.2	0.19	0.12	0.14	0.046	0.15
Ba [µg/l]	0.18	0.18	0.41	1	1.09	0.54	0.77	0.48	0.76
Pb [µg/l]			0.02	0.021	0.048	0.018		0.13	0.02
U [µg/l]	0.46	0.62	0.65	0.83	1	1.1	2.3	0.58	1.2
Cl^- [µg/l]									
NO_2^- [µg/l]									
SO_4^- [µg/l]	1700	1500	2000	3700	4000	3500	4100	1500	2000
NO_3^- [µg/l]	1400	1300	1300	1100	1200	910	1100	860	1100
NH_4 [µg/l]									
HCO_3 [µg/l]	12761.2*	15268.3*	7106.5*	18056*	19971.4*	19251.6*	18769.7*	15402.5*	12444*
W. T. [°C]	4.2	2.3	2.5	4.3	3.9	4.6	4.4	2.6	3.6
W. T. 2 [°C]	4.3	2.4	2.5	4.3	4	4.6	4.4	2.7	3.6
pH	7.208	7.9	7.24	7.084	7.02	7.252	7.44	7.585	7.385
EC [µS/cm]	41.2	39.4	27.5	48.8	51.7	48.5	48.5	35.7	33.9
EC2 [µS/cm]	36.3	37.7	27.1	44.2	49.7	42.6	46.6	32.6	32.8
O_2 [mg/l]	11.11	11.43	10.96	10.55	9.99	10.6	10.87	10.86	11.17
O_2 [%]	101.6	104	101.3	99	92.4	99.7	100.8	100.5	102.3

*values are calculated with PhreeqC

The suffix a at Sample IDs indicates the sampling campaign from previous projects

Spring-ID	DOQ1			DTQ1				HKAQ1	
Sample-ID	DOQ1_1a	DOQ1_2a	DOQ1_3	DTQ1_1a	DTQ1_2a	DTQ1_3	DTQ1_4	HKAQ1_1a	HKAQ1_2
Ca [µg/l]	7100	5700	3776	8300	7800	8437	9041	8800	9126
Na [µg/l]	500	500	448	700	600	600	597	500	541
Mg [µg/l]	400	400	135	400	400	348	371	4200	4378
K [µg/l]	500	500	363	600	500	583	578	400	145
Si [µg/l]			1457			1458	1406		1297
B [µg/l]			0.97			1.1	1		1
Al [µg/l]			51			1.2	1.3		1.5
Ti [µg/l]			0.53						0.1
V [µg/l]									
Cr [µg/l]			0.054			0.038	0.039		0.037
Mn [µg/l]			1.6			0.1	0.1		0.11
Fe [µg/l]			35						1.6
Co [µg/l]			0.032						
Cu [µg/l]			0.49						0.12
Zn [µg/l]			4.6						
As [µg/l]	4.4	3.8	3.1	5.2	5.3	4.5	4.4	0	0.17
Se [µg/l]			0.021			0.035	0.038		0.04
Sr [µg/l]			4.7			9.5	9.9		13.5
Mo [µg/l]			0.31			0.59	0.63		0.27
Ag [µg/l]			0.1			0.1	0.1		0.1
Sb [µg/l]			0.13			0.14	0.15		0.4
Ba [µg/l]			1.2			0.63	0.63		1.2
Pb [µg/l]			0.38						
U [µg/l]			1.5			1.4	1.9		0.34
Cl^- [µg/l]									
NO_2^- [µg/l]	7	19			18				
SO_4^- [µg/l]	3800	3100	1600	3300	2900	3300	3300	1400	1300
NO_3^- [µg/l]	2000	1700	700	2000	1900	1600	1300	2500	1500
NH_4 [µg/l]		12							
HCO_3 [µg/l]	17400	13100	9272*		20000	18794.1*	22014.9*	42900	43261.2*
W. T. [°C]	3.4	5.4	4.4	2.7	2.9	2.9	2.9	3.8	2.6
W. T. 2 [°C]			4.4			2.9			2.5
pH	7.7	7.5	7.342	7.6	7.5	6.95	7.61	7.7	7.915
EC [µS/cm]	43	34	25.5	52	45	51.8	56.6	78	36.3
EC2 [µS/cm]			24.4			48.8	52.9		32.2
O_2 [mg/l]			10.87			11.38	11.38		11.45
O_2 [%]	100	100	101.3	103	100	102	101.6		102

*values are calculated with PhreeqC

The suffix a at the Sample IDs indicates the sampling campaign from previous projects

Spring-ID	FLQ1			HRQ1		HTQ1		VSQ1
Sample-ID	FLQ1_1a	FLQ1_2a	FLQ1_3	HRQ1_1	HRQ1_2	HTQ1_1a	HTQ1_2	VSQ1_1
Ca [µg/l]	5200	5500	5926	6388	6901	7800	6719	3649
Na [µg/l]	400	500	465	719	706	500	470	745
Mg [µg/l]	400	400	157	338	326	400	326	149
K [µg/l]	400	400	313	431	430	500	438	348
Si [µg/l]			1286	1937	1864		1226	1870
B [µg/l]			0.93	1.2	1		0.96	0.89
Al [µg/l]			4	3.9	8.3		11	8.9
Ti [µg/l]				0.1				
V [µg/l]					0.043			0.1
Cr [µg/l]			0.017	0.027	0.026		0.034	0.055
Mn [µg/l]			0.23		0.343		0.19	1.601
Fe [µg/l]			4.4	1.2	4.9		6.7	15.2
Co [µg/l]								
Cu [µg/l]			0.075					
Zn [µg/l]								
As [µg/l]	7.3	7.9	7.3	3.3	3.7	3.6	2.5	3.2
Se [µg/l]			0.018	0.022	0.018		0.025	0.017
Sr [µg/l]			5.6	7	7.3		6.2	7
Mo [µg/l]			0.6	0.56	0.64		0.38	0.14
Ag [µg/l]			0.1	0.1			0.1	0.01
Sb [µg/l]			0.16	0.12	0.11		0.16	0.1
Ba [µg/l]			0.22	0.91	0.88		0.71	0.75
Pb [µg/l]			0.032	0.01	0.031		0.038	
U [µg/l]			1.2	0.84	0.67		1.2	0.84
Cl^- [µg/l]								
NO_2^- [µg/l]	21					18		
SO_4^- [µg/l]	1900	2000	2000	2600	2300	2700	2300	2700
NO_3^- [µg/l]	1900	1500	1300	1100	1200	2100	1500	850
NH_4 [µg/l]	13							
HCO_3 [µg/l]	12200	13800	12389.1*	15664.8*	17037.3*	20000	14658.3*	7344.4*
W. T. [°C]	2.5	7.4	3.2	4.3	4.4	2.1	2.9	2.4
W. T. 2 [°C]			3.2	4.3			3	2.4
pH	7.9	7.5	7.535	7.084	6.684	7.5	7.67	6.782
EC [µS/cm]	29	38	35.7	48.8	41.8	45	42	25.8
EC2 [µS/cm]			34.6	44.2			39.5	25.2
O_2 [mg/l]		11.6	10.87	10.55	11.4		11.17	10.82
O_2 [%]	99	100	101.5	99	103.2	100	102	100.6

*values are calculated with PhreeqC

The suffix a at the Sample IDs indicates the sampling campaign from previous projects

Spring-ID	KTQ1		SBQ1		SEQ				
Sample-ID	KTQ1_1a	KTQ1_2a	KTQ1_3	SBQ1_1	SEQ_1a	SEQ_2a	SEQ_3a	SEQ_4	SEQ_5
Ca [µg/l]	2400	2100	2488	6099	8800	7300	7500	10364	10825
Na [µg/l]	800	700	689	679	600	600	500	626	680
Mg [µg/l]	400	400	145	234	700	600	600	896	954
K [µg/l]	400	400	379	389	400	400	400	369	400
Si [µg/l]			1993	1665				1403	1517
B [µg/l]			0.93	1				1.1	1
Al [µg/l]			5.9					3	3.3
Ti [µg/l]			0.1						
V [µg/l]				0.068					0.018
Cr [µg/l]			0.024	0.031				0.021	0.04
Mn [µg/l]			0.1	0.1				0.1	0.1
Fe [µg/l]			1.5						1.2
Co [µg/l]									
Cu [µg/l]									
Zn [µg/l]									
As [µg/l]	<1	<1	0.065	6.5	12.7	10.8	11.6	11.5	12.4
Se [µg/l]			0.01	0.019				0.027	0.028
Sr [µg/l]			8	8.5				10.9	11.4
Mo [µg/l]			0.11	0.59				1.2	1.4
Ag [µg/l]			0.1	0.01				0.1	0.01
Sb [µg/l]			0.075	0.15				0.32	0.32
Ba [µg/l]			0.59	0.39				0.58	0.59
Pb [µg/l]									
U [µg/l]			0.86	1.6				6.8	6.8
Cl^- [µg/l]				3100					
NO_2^- [µg/l]		19			50	19			
SO_4^- [µg/l]	1700	1100	940	1900	3800	2700	3000	3800	3600
NO_3^- [µg/l]	50	1300	760	600	2000	2200	2000	1400	1400
NH_4 [µg/l]							13		
HCO_3 [µg/l]		10000	6270.8*	11797.4*	18977.1*	20000	21400	27395.1*	29499.6*
W. T. [°C]	3.8	3.7	2.5	3.3	2.3	2.4	2.4	2.5	2.4
W. T. 2 [°C]			2.5					2.5	2.4
pH	7.2	7	7.878	7.181	7.9	7.6	7.6	7.878	7.771
EC [µS/cm]	19	17	64.2	37.4	58	45	49	64.2	65.1
EC2 [µS/cm]		7	54.6	35.1				54.6	62.2
O_2 [mg/l]			11.41	10.64			13.3	11.41	11.6
O_2 [%]	100	104	102.2	100	104	100	100	102.2	102.1

*values are calculated with PhreeqC.

The suffix a at the Sample IDs indicates the sampling campaign from previous projects

Appendix 3

Geochemistry of the investigated rock samples.

Unit	[mg/kg]	P1	P2	P3	P4	P5	P6	P7	P8
Element	Method								
SiO_2	XRF	464192.51	237525.80	353998.15	293345.21	361697.22	386860.59	382326.23	379951.53
Ca	XRF	28.59	176485.74	1422.23	15923.31	1943.96	13421.89	457.40	671.81
K	XRF	116.22	5005.58	20553.59	38110.47	41771.26	13439.52	17324.45	17498.77
Na	XRF	437.70	3071.29	32278.24	37137.41	19036.07	6424.49	12633.84	10675.34
Mg	XRF	<	536.70	2273.45	5059.47	1163.86	5336.87	2333.75	2906.63
Al	XRF	<	7441.36	69740.24	98695.91	68290.07	32882.76	51126.26	46749.30
Fe	XRF	643.46	3979.69	12848.30	13904.42	2566.86	10757.04	20877.62	20073.29
Mn	XRF	7.74	3252.72	77.45	542.12	108.42	836.41	38.72	216.85
Sr	XRF	<	142.50	36.00	59.70	22.50	-	28.50	24.60
Cu	XRF	<	1202.20	170.10	98.40	25.40	-	0.00	0.00
Ti	XRF	59.93	113.87	1186.70	1582.26	539.41	893.02	3368.30	2229.55
Ba	XRF	<	1587.60	249.50	322.00	172.00	-	427.80	373.90
Rb	XRF	<	18.60	113.70	190.80	176.30	-	73.00	74.10
Zn	XRF	<	109.70		21.10		-	21.30	
P	XRF	8.73	34.91	288.04	438.61	290.22	91.65	104.74	137.47
Zr	XRF	<	-	84.50	125.10	43.10	-	133.20	88.30
Pb	ICP-MS	0.71	97.33	4.29	8.49	11.28	-	4.24	1.95
Ga	ICP-MS	<	2.80	17.87	22.15	20.26	-	25.79	11.70
Li	ICP-MS	1.83	1.36	12.00	26.28	16.15	-	26.01	9.10
U	ICP-MS	0.14	1.21	0.97	2.36	1.50	-	2.27	0.95
Th	ICP-MS	0.50	1.07	6.92	9.79	5.86	-	9.29	5.56
Nb	ICP-MS	0.34	0.92	7.34	9.59	6.97	-	11.90	5.41
Be	ICP-MS	<	0.34	3.38	4.07	2.42	-	1.86	1.12
Cs	ICP-MS	<		3.94	3.93	3.39	-	6.33	5.15
Y	ICP-MS	0.12	50.17	13.91	21.78	17.06	-	36.91	13.85
Ni	ICP-MS	0.60	38.85	2.04	1.90	1.69	-	20.75	12.80
Ce	ICP-MS	<	37.67	16.41	14.52	29.23	-	191.43	41.99
Nd	ICP-MS	<	25.10	6.90	7.12	10.71	-	73.30	18.49
La	ICP-MS	<	15.62	5.76	5.28	20.50	-	95.43	19.11
Co	ICP-MS	55.08	13.28	26.38	14.57	27.81	-	42.44	23.11
Dy	ICP-MS	<	9.43	2.39	3.53	3.05	-	6.80	2.61
Gd	ICP-MS	<	9.11	1.90	2.66	2.50	-	8.02	2.98
Sm	ICP-MS	<	8.13	1.80	2.25	2.78	-	10.65	3.35
Yb	ICP-MS	<	5.82	1.60	2.74	1.90	-	3.12	1.19
Pr	ICP-MS	<	5.51	1.72	1.63	3.06	-	21.20	4.76
Er	ICP-MS	<	5.12	1.44	2.22	1.64	-	3.74	1.37
Sc	ICP-MS	0.24	4.20	5.16	6.98	4.82	-	19.31	9.14
Eu	ICP-MS	<	2.83	0.19	0.25	0.42	-	2.66	0.78
V	ICP-MS	<	1.82	12.84	13.99	3.56	-	50.70	61.10
Ho	ICP-MS	<	1.70	0.47	0.71	0.56	-	1.28	0.48
Tb	ICP-MS	<	1.54	0.34	0.51	0.46	-	1.11	0.44
Tm	ICP-MS	<	0.79	0.22	0.36	0.25	-	0.49	0.18
Lu	ICP-MS	<	0.78	0.19	0.39	0.24	-	0.38	0.15
Cr	ICP-MS	0.64	0.49	3.54	4.59	1.69	-	53.19	27.48
Ta	ICP-MS	0.19	0.30	1.38	1.44	1.65	-	1.77	0.85
Hf	ICP-MS	<	0.13	1.26	2.22	1.82	-	2.20	0.98
Mo	ICP-MS	0.07	0.07	0.16	0.10	0.11	-	0.43	0.17
Sb	ICP-MS	1.89	363.38	0.79	1.05	1.42	-	3.45	1.27
As	ICP-MS	0.78	119.67	0.84	4.05	32.88	-	3.86	1.93

<	Below detection limit		-	no measurement	

Appendix 4

PhreeqC Code

```
TITLE Inverse modelling of SEQ_4

SOLUTION 1 Rain water #synthetic
temp 2.5
pH 7 CO2(g) -3.5 #equilibrium with atmosphere
pe 4 O2(g) -0.7 #equilibrium with atmosphere
units mmol/L
Na      0.007
K       0.010
Mg      0.013
Ca      0.033
Cl      0.007   charge
Si      0.006
S(6)    0.033 as SO4
C(4)    0.06

   density   1
   -water    1 # kg

end

SOLUTION 2 SEQ_4
   temp      2.5
   pH        7.878
   pe        4
   redox     pe

units     mg/l
Na        0.626
K         0.369
Mg        0.896
Ca        10.364
S(6)      3.8
Si    1.4 as SiO4
C(4)  22            as HCO3 charge
As    0.0114

   density   1
   -water    1 # kg
save solution 2
end
```

```
INVERSE_MODELING 1
   -solutions      1       2
   -uncertainty    0.025     0.025
   -phases

      CO2(g)
      As-pyrite              dis
      Calcite
      Biotite                dis
      SiO2(am-gel)
      Chalcopyrite           dis
      Ferrihydrite
      Arsenolite     prec
      Plagioclase            dis
      Kaolinite              prec
      Cuprite
      Chalcedony
      Gypsum
      Muscovite
      K-feldspar dis

   -balances
      Ca             0.025   0.025
      As             0.02    0.02
      Na             0.025   0.025
      S(6)           0.05    0.05
   -range            1000
   -tolerance        1e-10
   -mineral_water     false

PHASES

Biotite
        KMg3AlSi3O10(OH)2 + 6H+ + 4H2O = K+ + 3Mg+2 + Al(OH)4- + 3H4SiO4
        log_k 0.0 # No log_k, Inverse modeling only

Plagioclase
        Na0.62Ca0.38Al1.38Si2.62O8 + 5.52 H+ + 2.48H2O =\
        0.62Na+ + 0.38Ca+2 + 1.38Al+3 + 2.62H4SiO4
        log_k 0.0

As-pyrite
        FeAs0.004S1.996 + 1.984H+ + 0.012H2O +  1.98e- = Fe+2 + 0.004H3AsO3 +
1.996HS-
        log_k               0.0

Orpiment
      As2S3 +6.0000 H2O  =  + 2.0000 H2AsO3- + 3.0000 HS- + 5.0000 H+
      log_k        0.0  #-79.4159

K-feldspar
        KAlSi3O8 + 8 H2O = K+ + Al(OH)4- + 3 H4SiO4
        -log_k   0.0 #-20.573

Goethite
      FeOOH +3.0000 H+  =  + 1.0000 Fe+++ + 2.0000 H2O
      log_k        0.0  #0.5345

Muscovite
      KAl3Si3O10(OH)2 + 10H+ = K+ + 3Al+3 + 3H4SiO4
      log_k  0.0 # 12.99

END
```

Appendix 5

Semi quantitative EDX analysis of the sample P2, applied with a microprobe.

P2_1

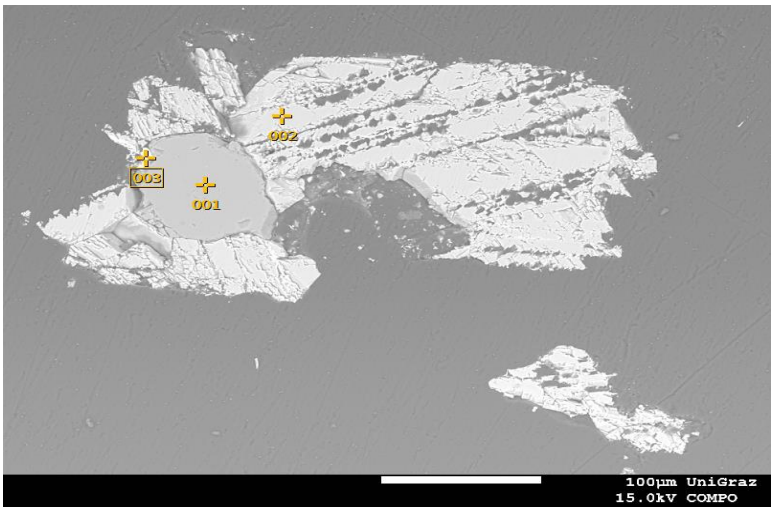

Volt : 15.00 kV

Mag. : x 250

Date : 2018/10/25

Pixel : 1280 x 960

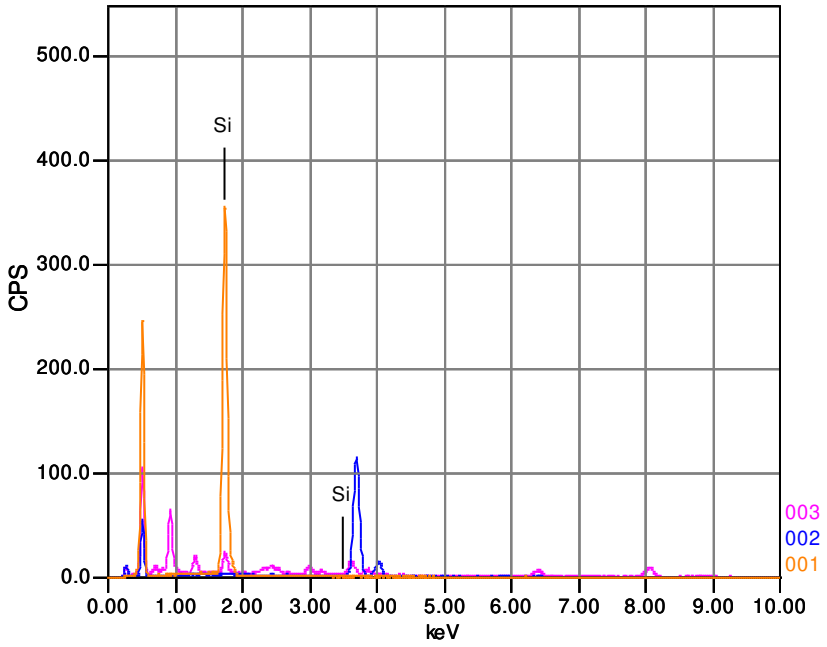

Acquisition Condition

Instrument : 8530F

Volt : 15.00 kV

Current : 10.04 nA

Process Time : T4

Live time : 20.00 sec.

Real Time : 30.88 sec.

DeadTime : 35.00 %

Count Rate : 3090.00 CPS

	CaO	SiO2	MnO	FeO	CuO	As2O3	Ag2O	Sb2O3
001		100.00						
002	98.20		1.80					
003		10.38		12.15	40.22	11.72	7.49	18.04
Average	98.20	55.19	1.80	12.15	40.22	11.72	7.49	18.04
Deviation	0.00	63.37	0.00	0.00	0.00	0.00	0.00	0.00

P2_2

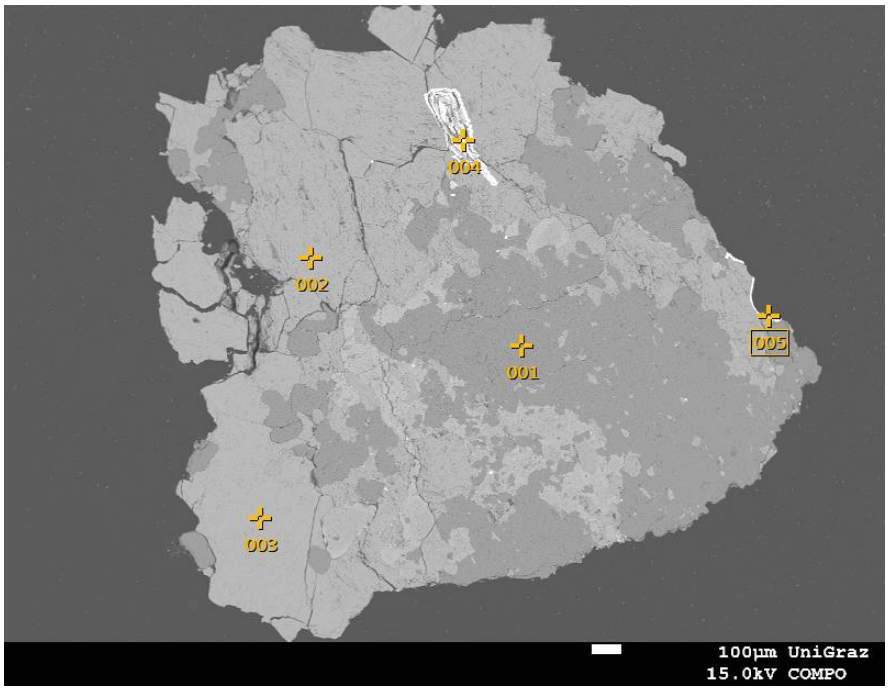

Volt : 15.00 kV

Mag. : x 40

Date : 2018/10/25

Pixel : 1280 x 960

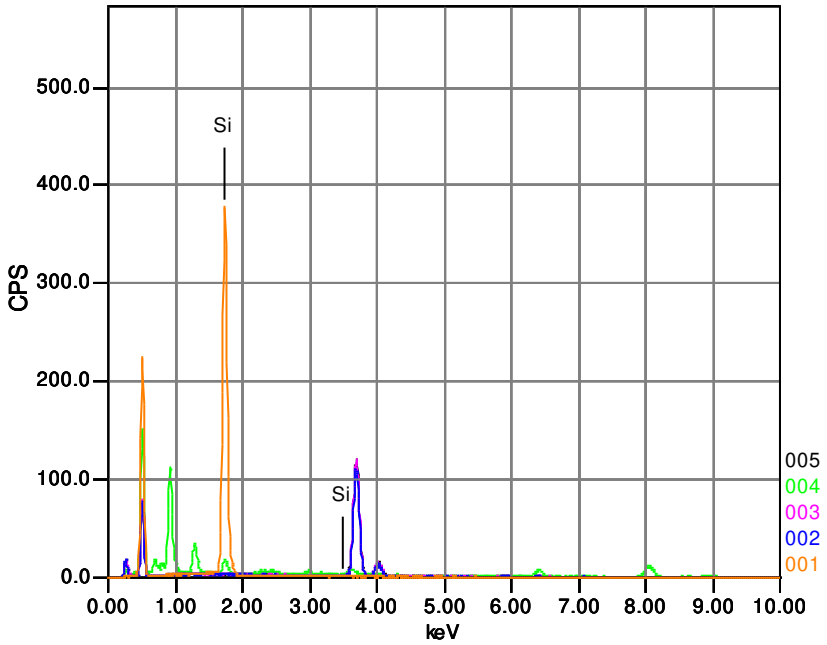

Acquisition Condition

Instrument : 8530F

Volt : 15.00 kV

Current : 10.04 nA

Process Time : T4

Live time : 20.00 sec.

Real Time : 30.65 sec.

DeadTime : 35.00 %

Count Rate : 2277.00 CPS

	CaO	SiO2	MnO	FeO	CuO	As2O3	Ag2O	Sb2O3
001		100.00						
002	98.39		1.61					
003	100.00							
004		7.53		13.30	48.98	20.78	3.28	6.12
005	96.64		1.72	1.64				
Average	98.34	53.77	1.66	7.47	48.98	20.78	3.28	6.12
Deviation	1.68	65.38	0.08	8.25	0.00	0.00	0.00	0.00

P2_4

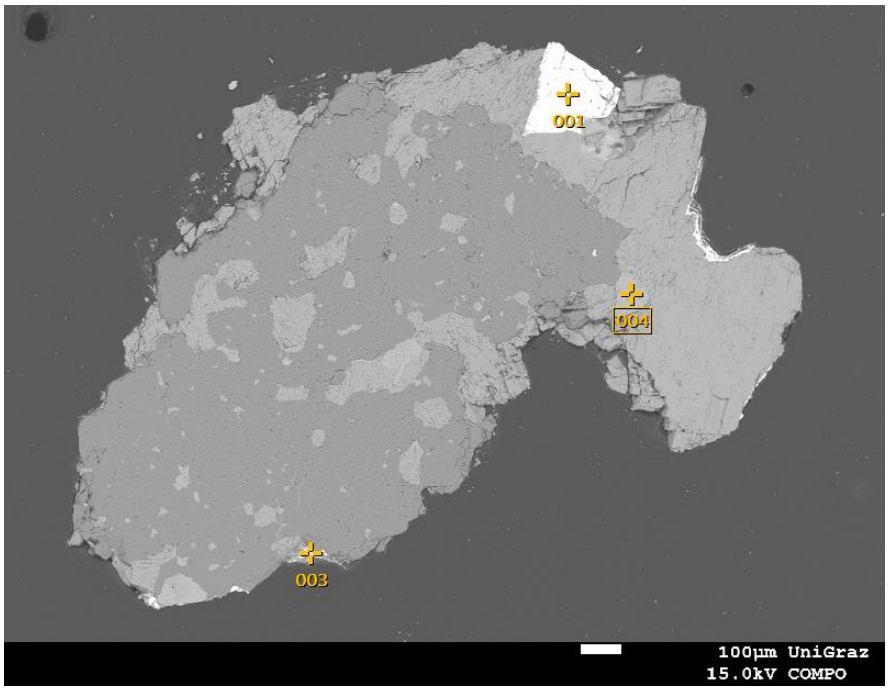

Volt : 15.00 kV

Mag. : x 55

Date : 2018/10/25

Pixel : 1280 x 960

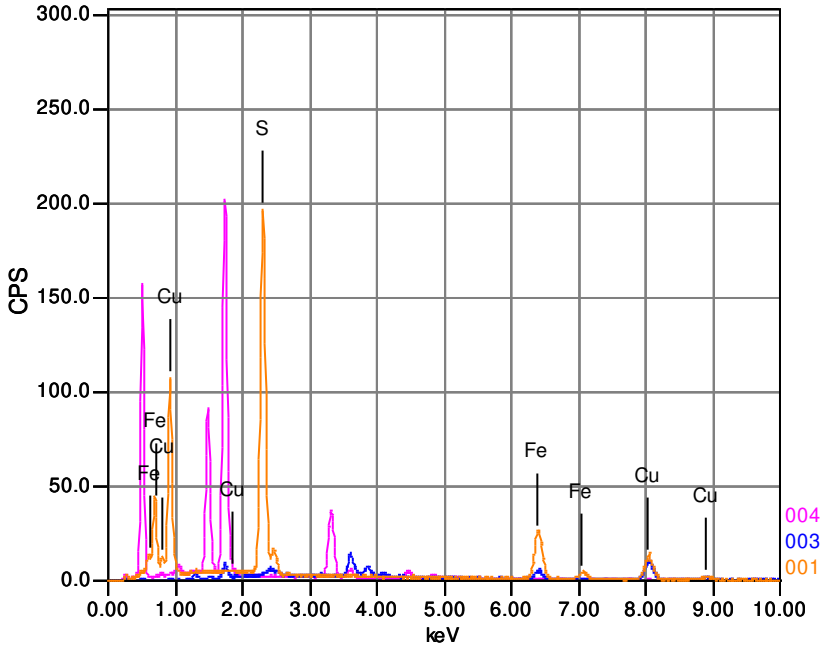

Acquisition Condition

Instrument : 8530F

Volt : 15.00 kV

Current : 10.02 nA

Process Time : T4

Live time : 20.00 sec.

Real Time : 31.11 sec.

DeadTime : 34.00 %

Count Rate : 3392.00 CPS

	Fe	K	Na	Al	Si	S	Cu	As	Sb	Ba
001	28.40					39.94	31.66			
003	11.73				3.07		58.12	3.44	23.64	
004		20.14	1.01	17.59	50.91					10.34
Average	20.06	20.14	1.01	17.59	26.99	39.94	44.89	3.44	23.64	10.34
Deviation	11.79	0.00	0.00	0.00	33.83	0.00	18.71	0.00	0.00	0.00

P2_4_detail

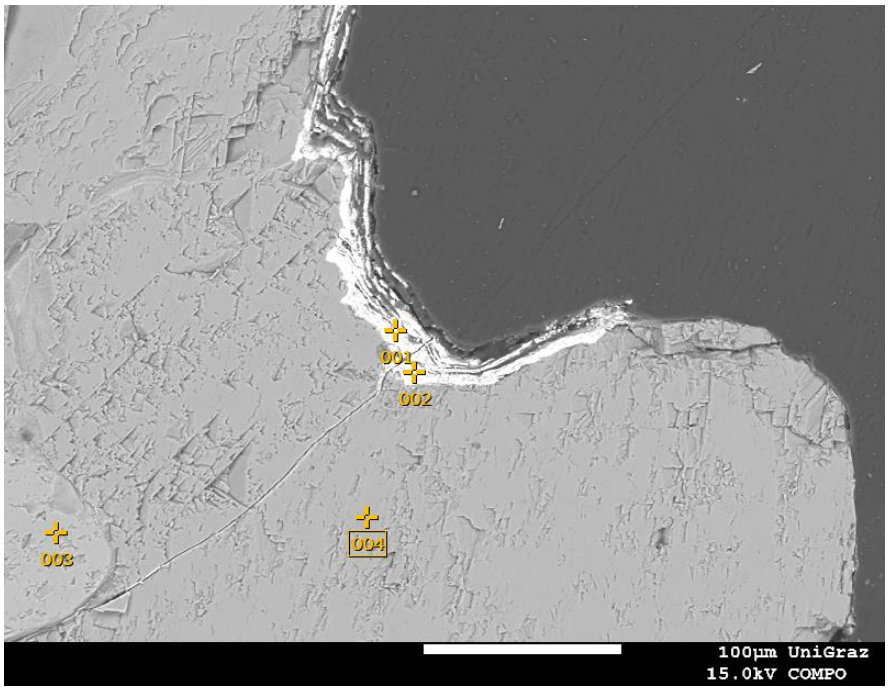

Volt : 15.00 kV

Mag. : x 270

Date : 2018/10/25

Pixel : 1280 x 960

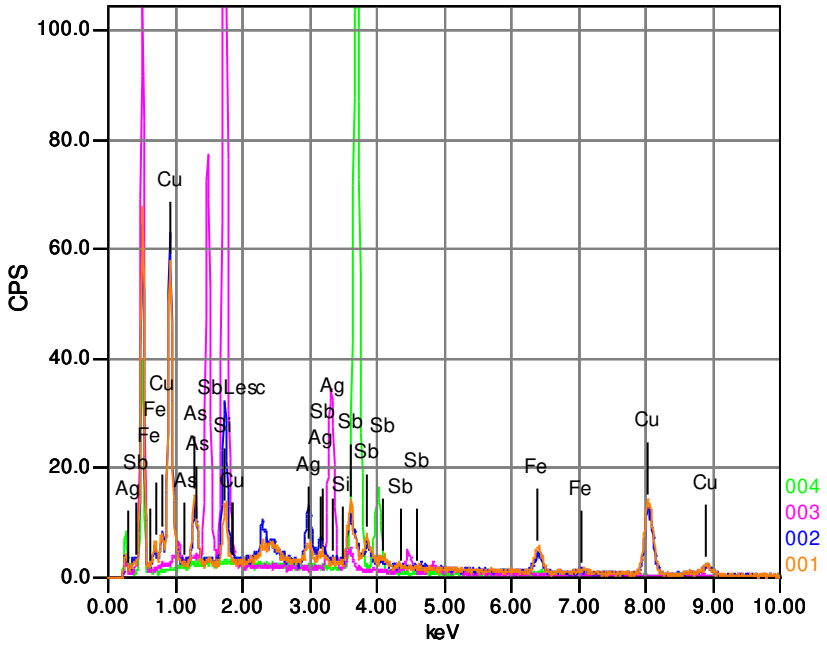

Acquisition Condition

Instrument : 8530F

Volt : 15.00 kV

Current : 10.02 nA

Process Time : T4

Live time : 20.00 sec.

Real Time : 30.48 sec.

DeadTime : 35.00 %

Count Rate : 1488.00 CPS

	Fe	K	Ag	Na	Al	Si	S	Ca	Mn	Cu	As	Sb	Ba
001	8.79		3.78			3.39				58.87	9.94	15.23	
002	5.95		11.56			9.09	1.95			53.42	7.53	10.50	
003		21.52		0.77	16.93	51.06							9.72
004								97.91	2.09				
Average	7.37	21.52	7.67	0.77	16.93	21.18	1.95	97.91	2.09	56.14	8.73	12.87	9.72
Deviation	2.00	0.00	5.50	0.00	0.00	26.03	0.00	0.00	0.00	3.86	1.71	3.34	0.00

P2_5

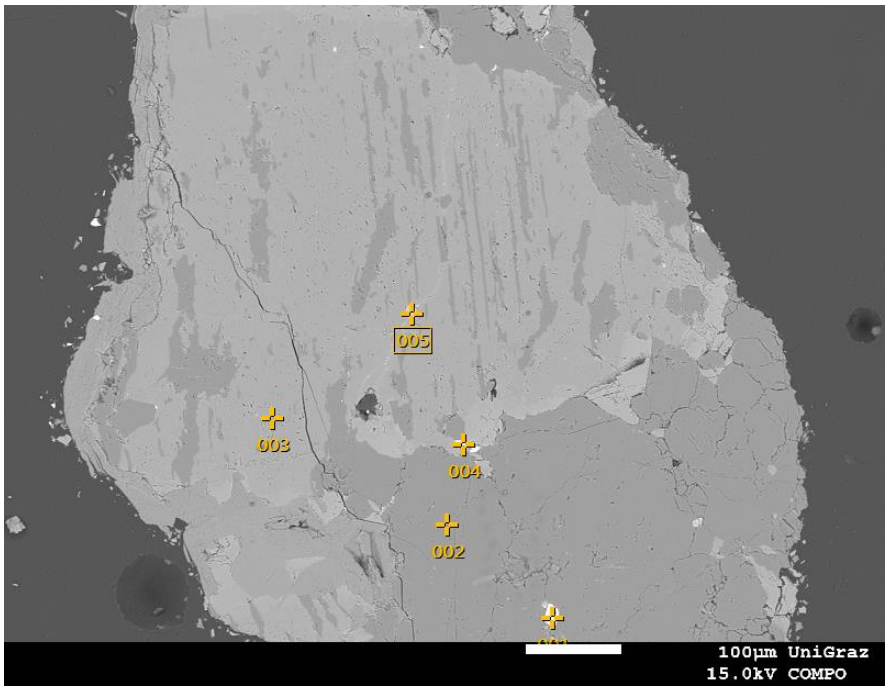

Volt : 15.00 kV

Mag. : x 130

Date : 2018/10/25

Pixel : 1280 x 960

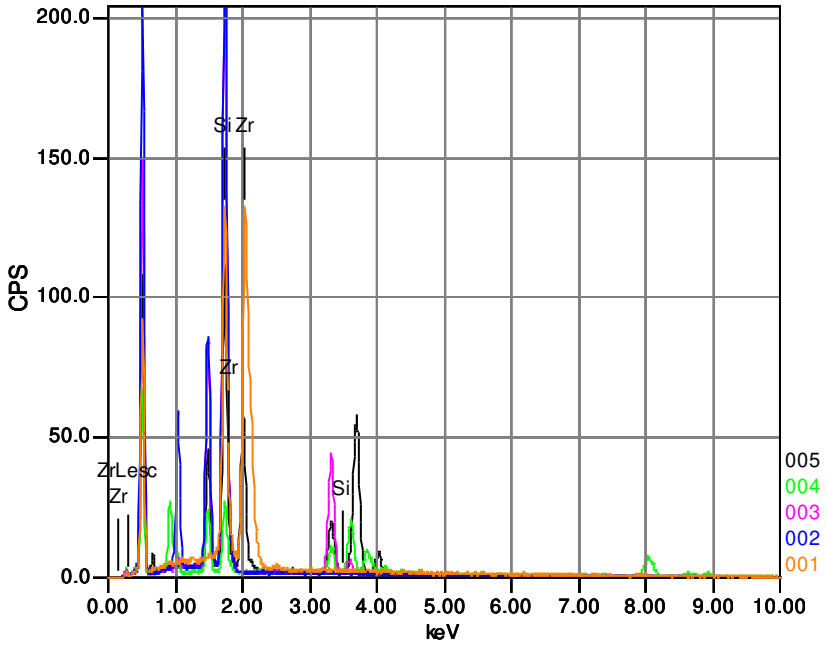

Acquisition Condition

Instrument : 8530F

Volt : 15.00 kV

Current : 10.00 nA

Process Time : T4

Live time : 20.00 sec.

Real Time : 29.92 sec.

DeadTime : 34.00 %

Count Rate : 3279.00 CPS

	P	K	Na	Al	Si	Ca	Cu	Zn	Zr	Sb
001					22.94				77.06	
002			11.59	19.65	68.76					
003		25.67	0.82	16.57	56.94					
004		5.33		8.15	8.82		36.00	8.97		32.73
005	19.90	9.95		8.60	25.34	36.21				
Average	19.90	13.65	6.21	13.24	36.56	36.21	36.00	8.97	77.06	32.73
Deviation	0.00	10.66	7.61	5.76	25.16	0.00	0.00	0.00	0.00	0.00

P2_6

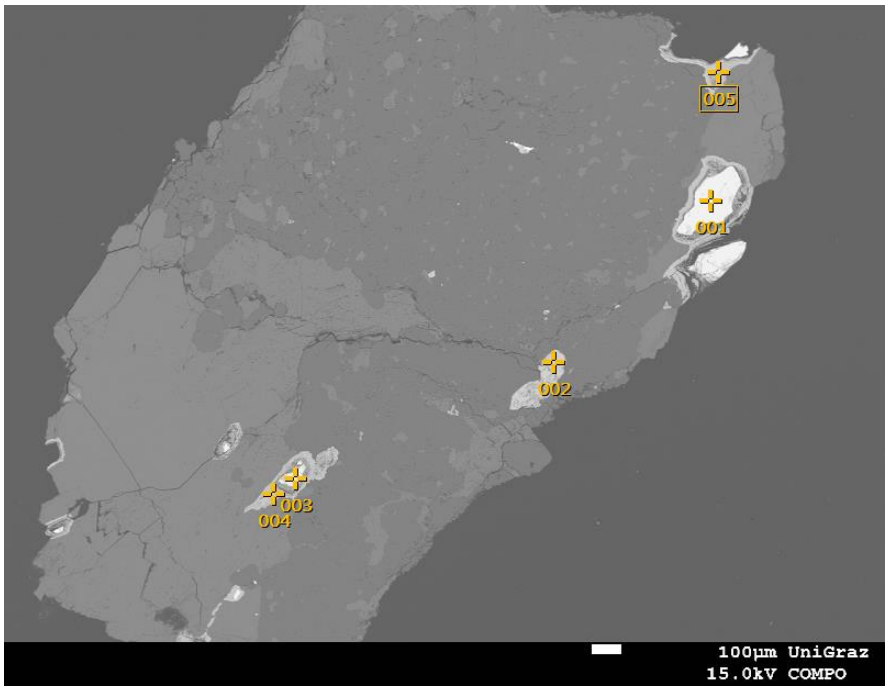

Volt : 15.00 kV

Mag. : x 40

Date : 2018/10/25

Pixel : 1280 x 960

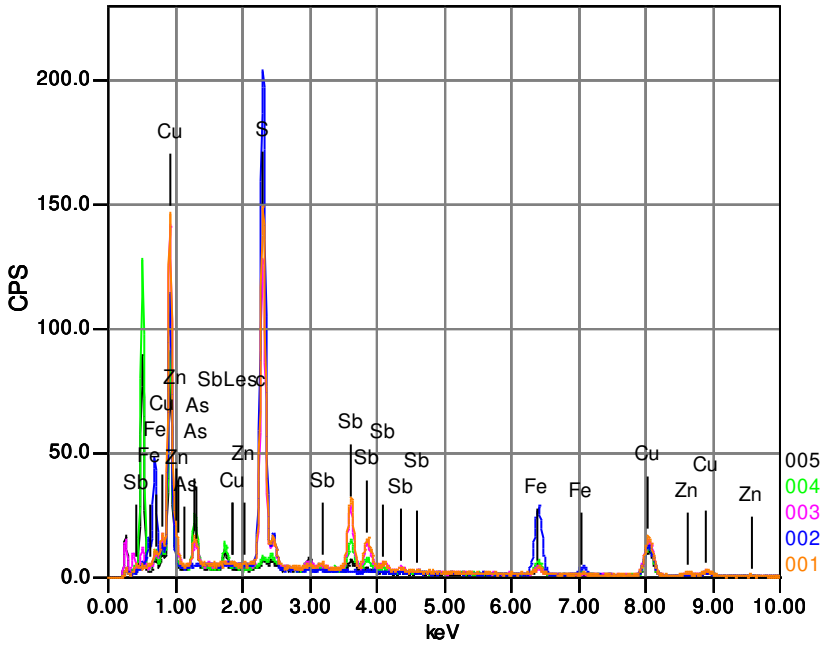

Acquisition Condition

Instrument : 8530F

Volt : 15.00 kV

Current : 10.00 nA

Process Time : T4

Live time : 20.00 sec.

Real Time : 29.65 sec.

DeadTime : 34.00 %

Count Rate : 2641.00 CPS

	Fe	N	Si	S	Cu	Zn	As	Sb
001	2.71			28.77	35.14	4.47	4.49	24.42
002	28.83			40.59	30.58			
003	3.04	6.33		26.72	35.16	2.69	3.45	22.63
004	10.06		3.11		54.14		16.40	16.29
005	9.66		3.08	1.08	61.42		17.56	7.19
Average	10.86	6.33	3.10	24.29	43.29	3.58	10.48	17.63
Deviation	10.64	0.00	0.02	16.63	13.61	1.26	7.54	7.79

P2_6det_2a

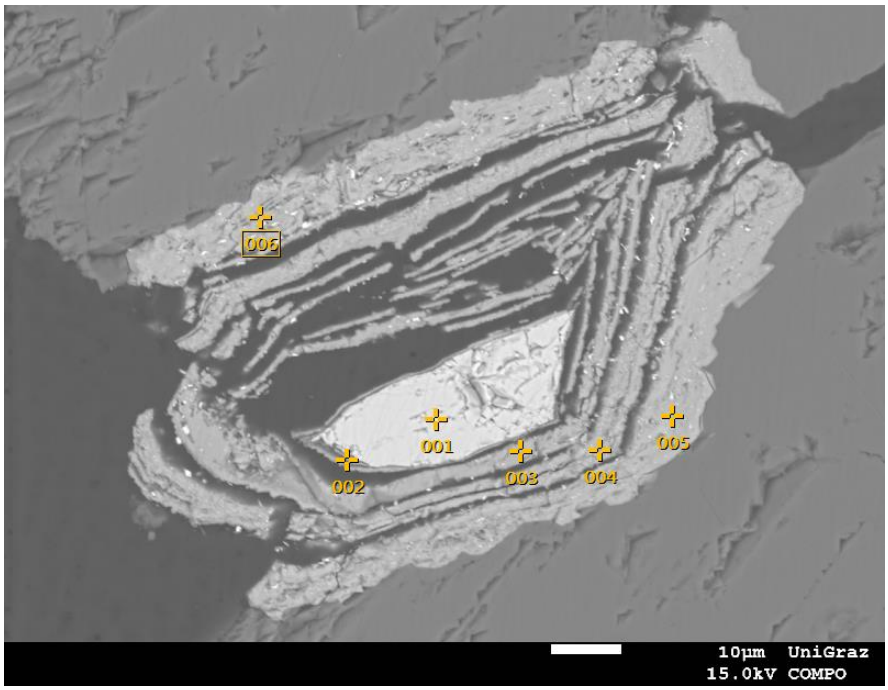

Volt : 15.00 kV

Mag. : x 950

Date : 2018/10/25

Pixel : 1280 x 960

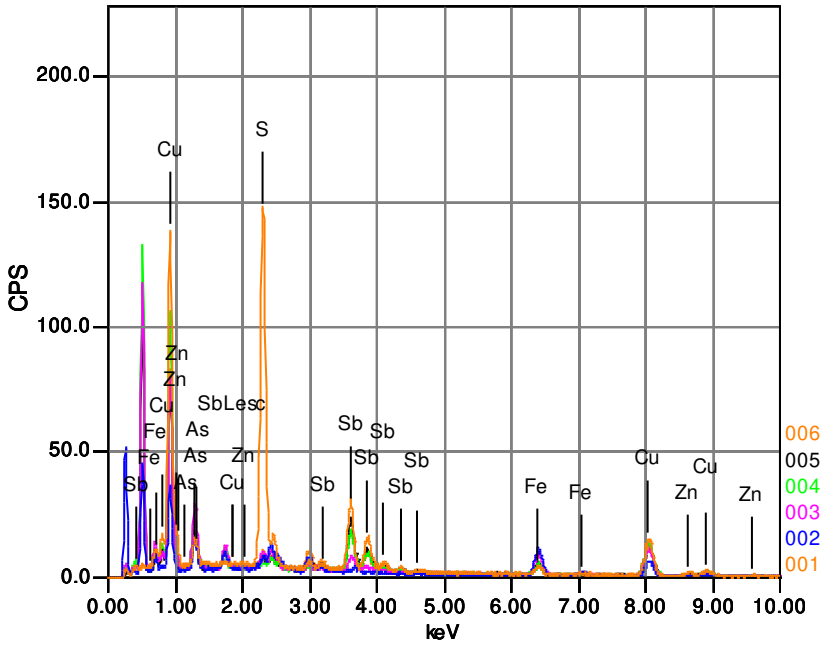

Acquisition Condition

Instrument : 8530F

Volt : 15.00 kV

Current : 10.00 nA

Process Time : T4

Live time : 20.00 sec.

Real Time : 29.78 sec.

DeadTime : 32.00 %

Count Rate : 3038.00 CPS

	Fe	Ag	Si	S	Ca	Cu	Zn	As	Mo	Sb	Bi	Th
001	3.47			29.20		34.66	4.25	3.94		24.47		
002	32.17		3.45		1.75	48.49		14.15				
003	14.87	3.17	2.71			42.60	2.39	16.27	5.23	6.69	6.08	
004	8.29		2.36			52.81		13.53		23.02		
005	8.43		2.15			49.32		9.94		25.20		4.96
006	7.46		2.22			52.93		10.28	4.23	22.87		
Average	12.45	3.17	2.57	29.20	1.75	46.80	3.32	11.35	4.73	20.45	6.08	4.96

P2_6det_3

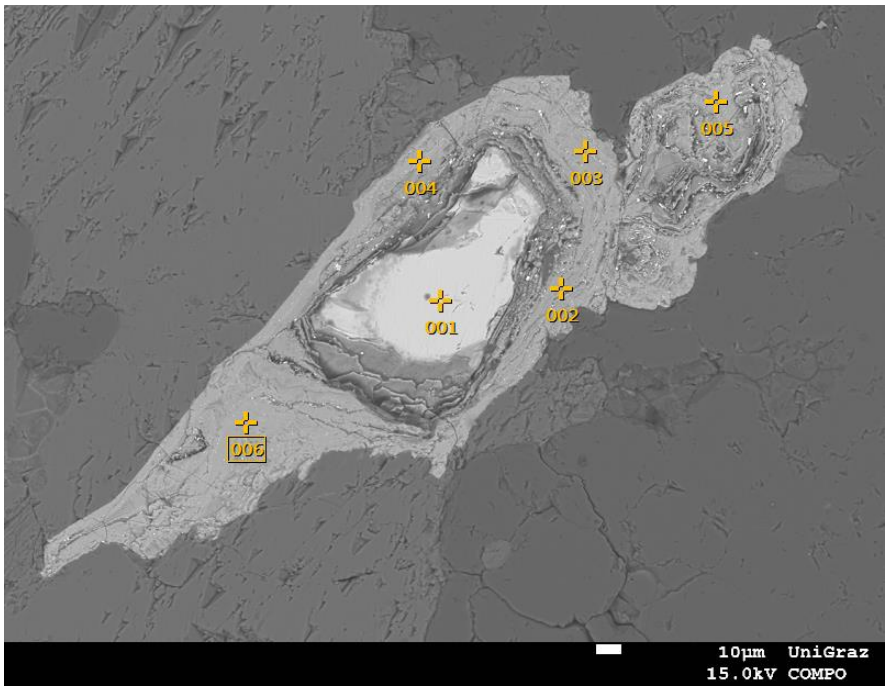

Volt : 15.00 kV

Mag. : x 330

Date : 2018/10/25

Pixel : 1280 x 960

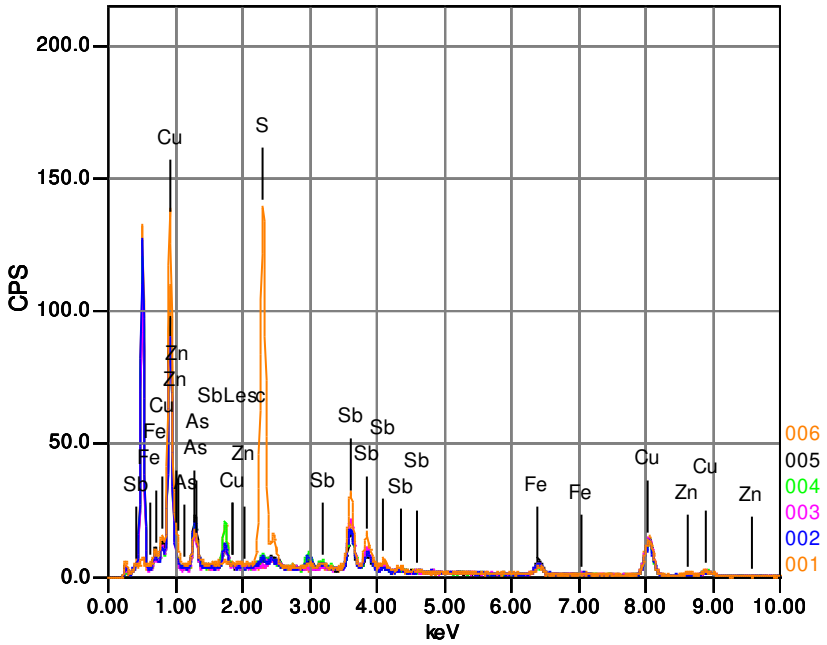

Acquisition Condition

Instrument : 8530F

Volt : 15.00 kV

Current : 10.00 nA

Process Time : T4

Live time : 20.00 sec.

Real Time : 29.83 sec.

DeadTime : 32.00 %

Count Rate : 3223.00 CPS

	Fe	Ag	Si	S	Cu	Zn	As	Sb	Bi
001	3.12			29.21	33.35	3.21	4.50	26.61	
002	7.52		2.81		54.20		12.43	23.04	
003	6.74		2.18		55.06		9.90	26.13	
004	5.77	6.52	4.76		51.81		10.64	20.50	
005	8.49	3.44	2.13		54.05		13.40	18.49	
006	6.13		4.57		54.91		8.31	23.15	2.94
Average	6.30	4.98	3.29	29.21	50.56	3.21	9.86	22.99	2.94

P2_7

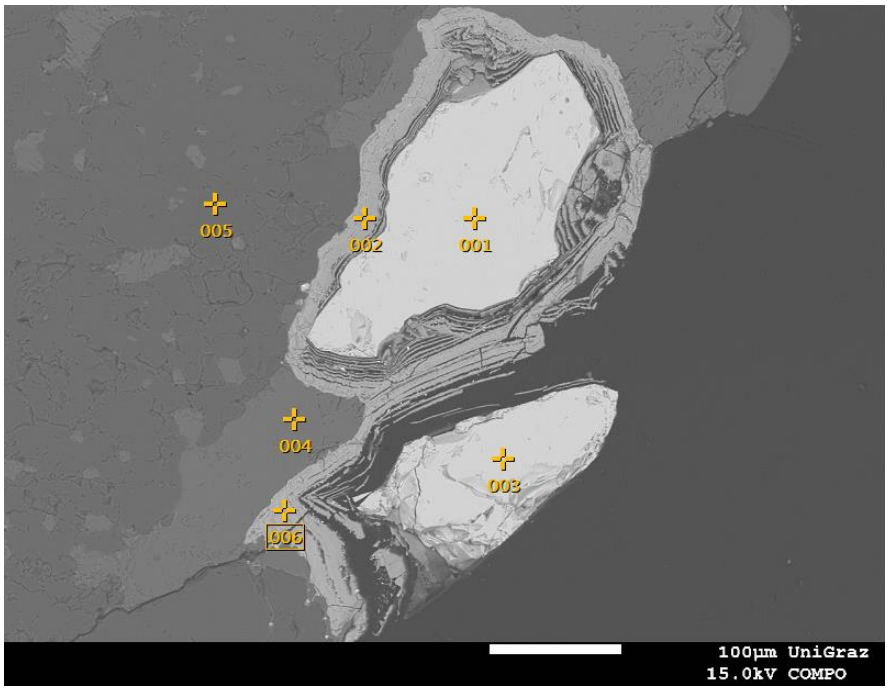

Volt : 15.00 kV

Mag. : x 180

Date : 2018/10/25

Pixel : 1280 x 960

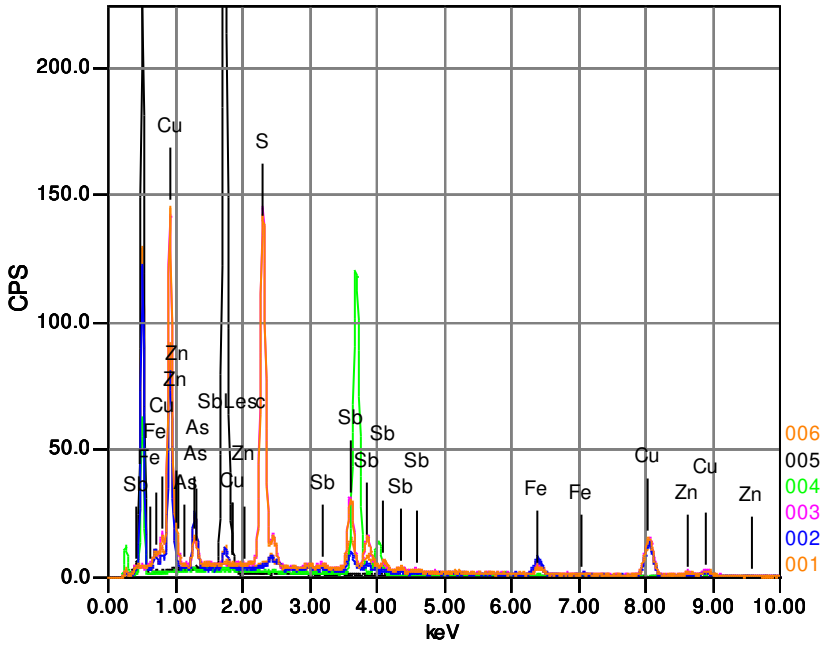

Acquisition Condition

Instrument : 8530F

Volt : 15.00 kV

Current : 10.00 nA

Process Time : T4

Live time : 20.00 sec.

Real Time : 29.71 sec.

DeadTime : 35.00 %

Count Rate : 3120.00 CPS

	Fe	Si	S	Ca	Mn	Cu	Zn	As	Sb
001	2.73		28.92			35.09	3.44	4.63	25.19
002	12.00	2.84				57.87		16.98	10.31
003	3.00		28.10			35.63	4.62	3.91	24.74
004				97.58	2.42				
005		100.00							
006	9.36	2.61				55.34		15.22	17.47
Average	6.77	35.15	28.51	97.58	2.42	45.98	4.03	10.18	19.43

P2_9

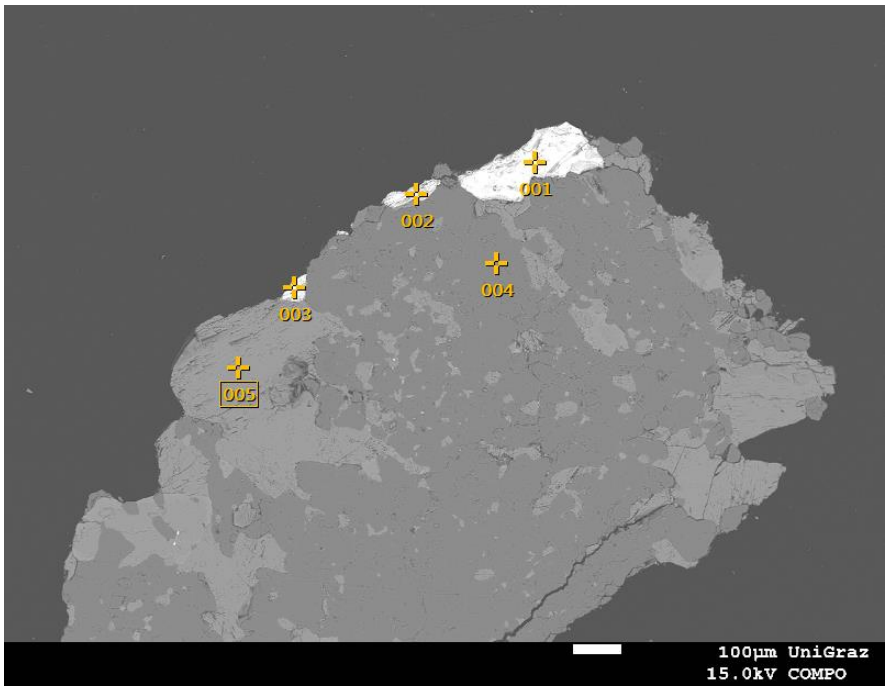

Volt : 15.00 kV

Mag. : x 65

Date : 2018/10/25

Pixel : 1280 x 960

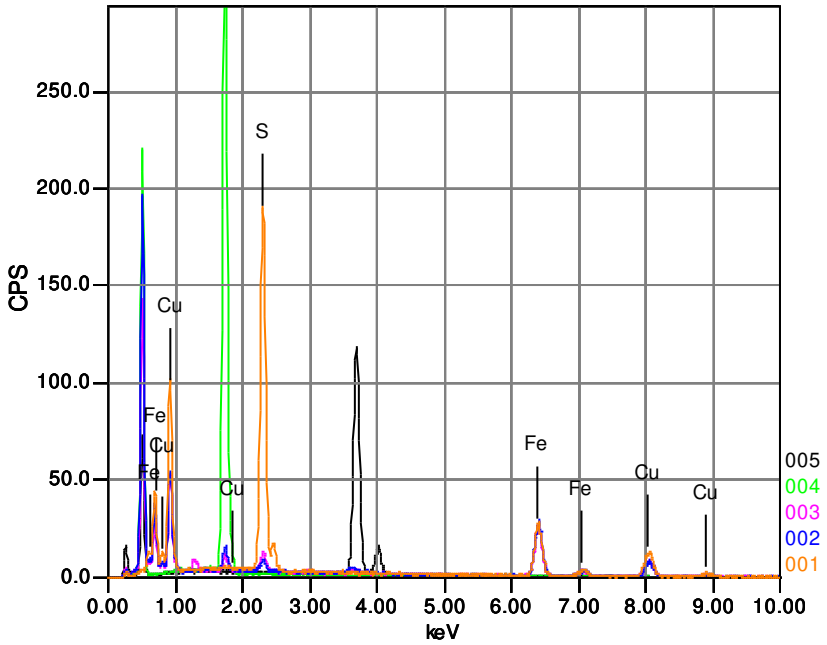

Acquisition Condition

Instrument : 8530F

Volt : 15.00 kV

Current : 10.01 nA

Process Time : T4

Live time : 20.00 sec.

Real Time : 29.49 sec.

DeadTime : 32.00 %

Count Rate : 2392.00 CPS

	Fe	Si	S	Ca	Mn	Cu	As
001	29.00		39.14			31.86	
002	55.81	3.73	2.69			37.78	
003	50.55	2.74	3.55	0.69		37.83	4.64
004		100.00					
005				98.20	1.80		
Average	45.12	35.49	15.12	49.45	1.80	35.82	4.64
Deviation	14.20	55.87	20.80	68.95	0.00	3.43	0.00

P2_10

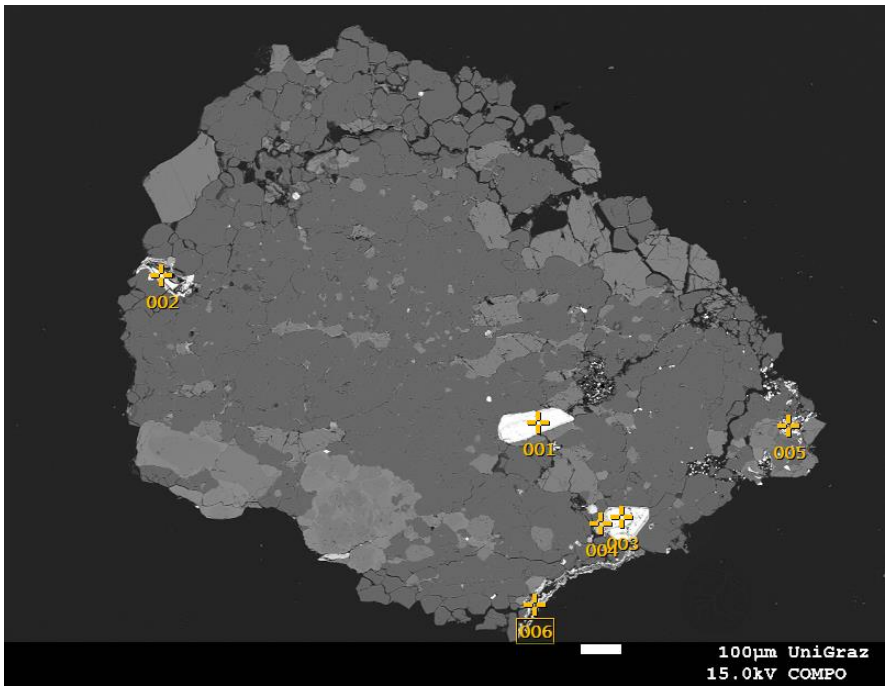

Volt : 15.00 kV

Mag. : x 55

Date : 2018/10/25

Pixel : 1280 x 960

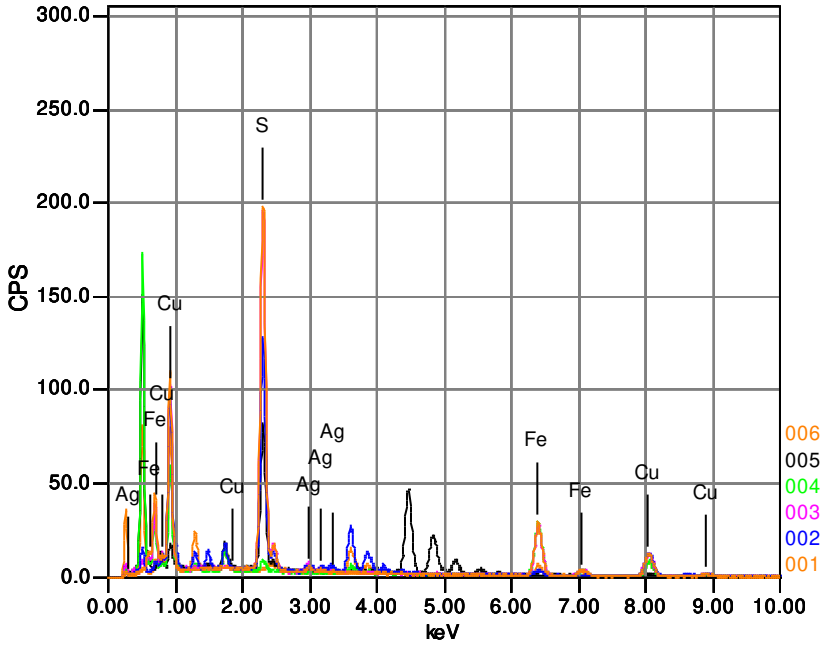

Acquisition Condition

Instrument : 8530F

Volt : 15.00 kV

Current : 10.00 nA

Process Time : T4

Live time : 20.00 sec.

Real Time : 29.63 sec.

DeadTime : 32.00 %

Count Rate : 2924.00 CPS

	Fe	K	Ag	Al	Si	S	Ca	Cu	Zn	As	Sb	Ba
001	28.23		1.94			39.50		30.33				
002	2.99	0.96		1.61	2.52	28.31		32.93	2.93	3.67	24.07	
003	27.96		3.39			38.85		29.80				
004	52.76				3.43	2.28		36.67			4.86	
005					2.58	20.43	0.68	2.85				73.46
006	12.18				3.74			45.55		17.70	20.83	
Average	24.82	0.96	2.67	1.61	3.07	25.87	0.68	29.69	2.93	10.68	16.59	73.46

P2_11

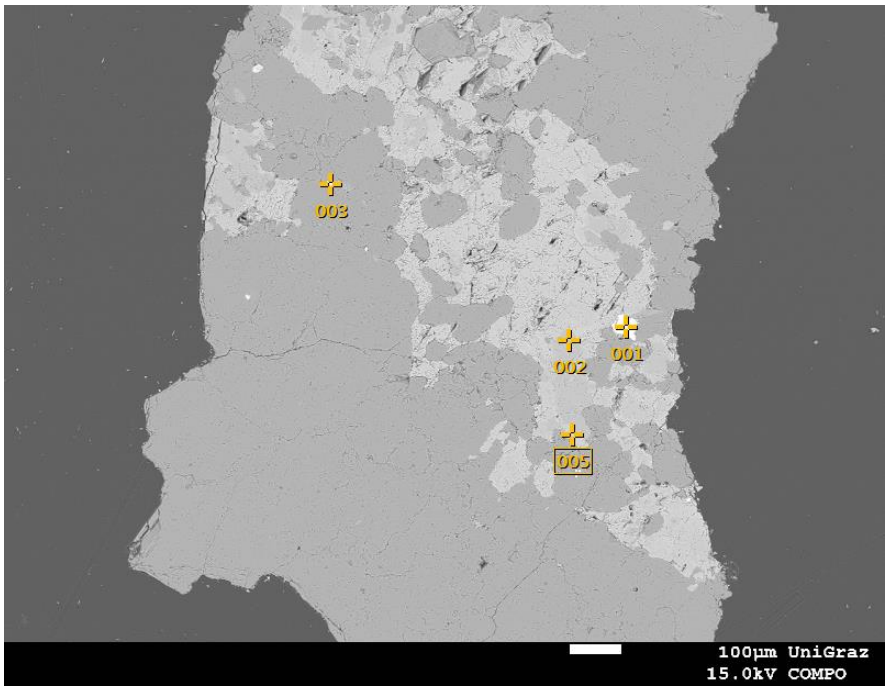

Volt : 15.00 kV

Mag. : x 70

Date : 2018/10/25

Pixel : 1280 x 960

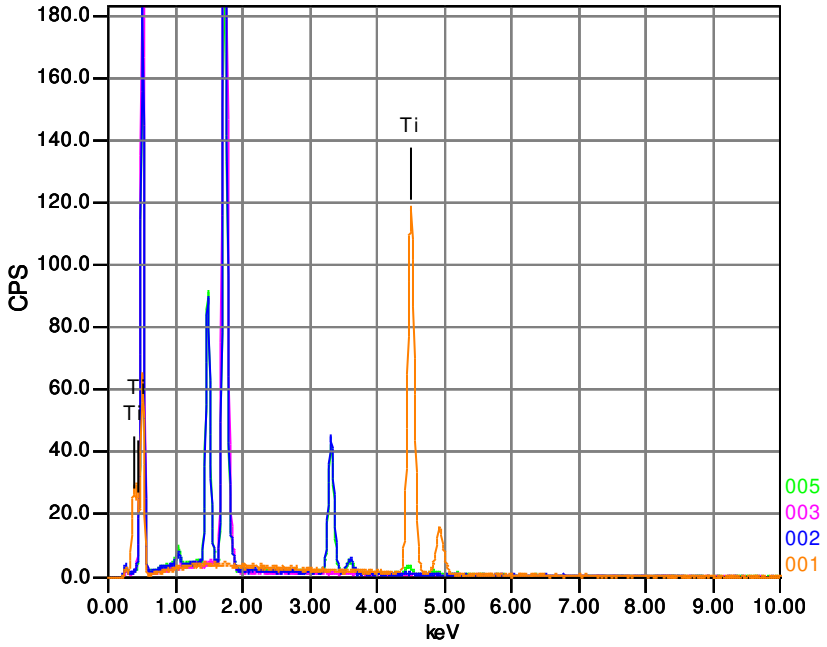

Acquisition Condition

Instrument : 8530F

Volt : 15.00 kV

Current : 10.01 nA

Process Time : T4

Live time : 20.00 sec.

Real Time : 29.97 sec.

DeadTime : 34.00 %

Count Rate : 3826.00 CPS

	K	Na	Al	Si	Ti	Ba
001					100.00	
002	25.45	0.82	16.63	57.10		
003				100.00		
005	22.21	1.22	16.91	52.58		7.08
Average	23.83	1.02	16.77	69.89	100.00	7.08
Deviation	2.29	0.29	0.19	26.17	0.00	0.00